

Using Hyperspectral Remote Sensing for Detecting and Mapping Soil Quality Under Various Land-Uses in Dryland

**Thesis submitted in partial fulfillment
of the requirements for the degree of
“DOCTOR OF PHILOSOPHY”**

by

Nathan

Levi

**Submitted to the Senate of Ben-Gurion University
of the Negev**

**6 December 2022
Beer-Sheva**



Ben-Gurion University of the Negev
Kreitman School of Advanced Graduate Studies

Using Hyperspectral Remote Sensing for Detecting and Mapping Soil Quality Under Various Land-Uses in Dryland

**Thesis submitted in partial fulfillment
of the requirements for the degree of
“DOCTOR OF PHILOSOPHY”**

by


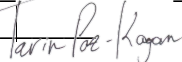
Nathan

Levi

**Submitted to the Senate of Ben-Gurion University
of the Negev**

Approved by the advisor:

Prof. Arnon Karnieli
Dr. Tarin Paz-Kagan

Signature:  _____
Signature:  _____

Prof. Yaron Ziv

Signature:  _____

Approved by the Dean of the Kreitman School of Advanced Graduate Studies

6 December 2022
Beer-Sheva

This work was carried out under the supervision of Dr. Tarin Paz-Kagan, Prof. Arnon Karnieli, and

Prof. Yaron Ziv in Albert Katz International School for Desert Studies, Faculty of Jacob Blaustein
Institutes for Desert Research, Ben-Gurion University of the Negev, Sede Boqer Campus, 8499000,
Israel

Research-Student's Affidavit when Submitting the Doctoral Thesis for Judgment

I _____, whose signature appears below, hereby declare that
(Please mark the appropriate statements):

I have written this Thesis by myself, except for the help and guidance offered by my Thesis Advisors.

The scientific materials included in this Thesis are products of my own research, culled from the period during which I was a research student.

This Thesis incorporates research materials produced in cooperation with others, excluding the technical help, excluding result analysis, commonly applied during such experimental work. Therefore, I attach an additional affidavit stating the contributions made by myself and the other participants in this research, which has been approved by them and submitted with their approval.

This thesis in in Manuscript Format, includes one or more papers in which I am an "equal contributor". I therefore attach an additional affidavit signed by other equal contributor(s) stating their contribution to the paper and their approval that that paper could not be included in another Manuscript Format Thesis.

Date: _____ Student's name: _____ Signature: _____

Table of Contents

Declaration.....	iv
Acknowledgments.....	v
English Abstract	vi

Chapter 1: Using reflectance spectroscopy for detecting land-use effects on soil quality in dryland

1. Introduction	4
2. Material and Methods.....	5
2.1 Study area.....	5
2.2 Soil sampling	7
2.3 Geographic units and laboratory analysis	9
2.4 Spectral measurement and processing.....	9
2.5 <i>Development of soil quality index (SQI)</i>	11
2.6 Correlation and classification of soil and spectroscopy analysis	11
2.7 Statistical analysis of soil properties and SQI.....	11
3. Results.....	13
3.1 Soil properties and analysis.....	13
3.2 Soil quality index (SQI)	15
3.3 Soil properties and SQI correlations with soil spectroscopy.....	20
3.4 Spectral classification of soil samples among LUs and sampling sites.....	21
4. Discussion.....	23
4.1 Soil properties and the Soil quality index	23
4.2 Soil properties and SQI correlation with soil spectroscopy.....	24
4.3 LUs and sampling sites spectral classification.....	26
5. Conclusion	27

Chapter 2: Soil quality index for assessing phosphate mining restoration in a hyper-arid environment.

1. Introduction	28
2. Material	30
2.1 Study area.....	30
2.2 Study area and mining restoration practices.....	32
2.3 Soil sampling and design.....	33
2.4 Selected soil properties	36
2.5 Soil quality index (SQI) development	37
2.6 Statistical analysis	37
3. Results.....	38
3.1 Soil quality indicators.....	38
3.2 Soil quality index (SQI)	40
4. Discussion.....	45
4.1 Indicator selection: a minimum dataset for soil quality measurement.....	44
4.2 Evaluation of restoration practice with time since restoration	45

4.3 Assessment of soil quality index.....	46
5. Conclusion	46

Chapter 3: Airborne imaging spectroscopy for assessing the land-use effect on soil quality in drylands

1. Introduction	50
2. Material and Methods.....	55
2.1 Study area	56
2.2 Research approach and structure	57
2.3 Step 1: soil sampling analysis and SQI development	60
2.4 Step 2: airborne hyperspectral image acquisition and processing	62
2.5 Step 3: IS approach integration of laboratory data.....	66
2.6 Statistical analysis	66
3. Results.....	66
3.1 Soil quality index (SQI) development	66
3.2 Hyperspectral image pre-processing	69
3.3 Spectral classification and correlation of SQI and soil indicators.....	70
3.4 Soil indicators and soil prediction maps	73
3.5 Spectral classification and correlation of SQI and soil indicators.....	74
4. Discussion.....	79
4.1 Soil quality assessment	79
4.2 Spectral discriminant analysis and classification of LU.....	80
4.3 Spectral correlation to soil indicators and the SQI	81
4.4 Soil quality mapping	83
5 Conclusion	86
References	88

Acknowledgments

Nathan Levi was a brilliant student who received his master's degree at the Jacob Blaustein Institute for Desert Research, BGU, Sede Boqer Campus, under Prof. Arnon Karnieli and Dr. Tarin Paz-Kagan. He continued to a combined track doctoral program under the supervision of Prof. Karnieli, Dr. Paz-Kagan, and Prof. Yaron Ziv. Nathan was in the final stages of submitting his Ph.D. when he unexpectedly passed away on September 29, 2022. The dissertation is summarized in three papers published in high-ranking journals, and we submit it on his behalf. We send our deepest and sincerest condolences to his family and friends for their tremendous loss.

Chapter 1: Figure captions

Figure 1: (A) Location of the study area in the Negev desert, Israel; (B) The selected study area with the sampling points of the three land-use categories (agriculture, grazing, and natural reserves), whose locations were selected from a prior stratified random methodology. Full names and numbers of soil samples for all sampling sites are presented in Table 1.

Figure 2: Stratified random survey components of Avdat region: (A) elevation, (B) lithology, (C) land use-land cover (LULC) classification, and the study area's geographical units: north, center, and south.

Figure 3: Examples of scoring curves of the respective transformation functions: (A) more is better, (B) less is better, and (C) optimum.

Figure 4: Boxplot representation of each soil indicator values under different land uses of the entire study area: agriculture, grazing, and natural. Note: available water content (AWC); electrical conductivity (EC); extractable chlorine (Cl); extractable sodium (Na); extractable calcium and magnesium (Ca + Mg); sodium adsorption ratio (SAR); extractable nitrate (NO_3); extractable phosphorus (P); extractable potassium (K); and soil organic matter (SOM).

Figure 5: Scores of soil quality indices (SQIs) and their physical, biological and chemical components for the three land uses, according to the study area's geographical distribution: north, center, and south. Capital letters above the error bars represent significant differences among land uses.

Figure 6: Partial least squares-regression (PLS-R) correlation scatterplots of predicted cross-validation (CV) values versus soil laboratory analysis values for (A) several soil properties and (B) soil quality index (SQI) among the three LUs in Avdat region. RMSEC: root mean square error of calibration; RMSECV: root mean square error of cross-validation; EC: electric conductivity; Cl: chlorine; Na: sodium; Ca + Mg: calcium and magnesium; SAR: sodium adsorption ratio; NO_3 : nitrate; P: phosphorus; SOM: soil organic matter. Each colored shape represents a land-use type: natural ecosystem (blue triangles), agro-pastoral grazing (red squares) and agriculture (green rhombuses).

Figure 7: Partial least squares-discriminant analysis (PLS-DA) classification of initial 2150 bands spectral resolution laboratory spectroscopy for both (A) LUs and (B) sampling sites in Avdat region. Each figure includes a number of latent variables (LV) used, overall accuracy (Acc), and Kappa coefficient (K_c) values for each model. Colored circles indicate 95% confidence level. Full names and numberers of soil samples for all sampling sites are presented in Table 1.

Chapter 2: Figure captions

Figure 1: Schematic map with the location of the Zin phosphate mining field (A); Zin mining field topographic (B); and geological map (C) with the sampling blocks of the three study sites of Gov, Afik, and Hagar (red points).

Figure 2. Scoring functions for data standardization, assigning the appropriate term and mathematical function to each soil property. S_i is the soil property score, x is the parameter value, a is the soil property average, and b is $2\sigma^2$ of the data. Graphs adapted from Karlen et al. (2003). AWC: available water content, SOM: soil organic matter, EC: electrical conductivity, K: potassium, and P: phosphorus.

Figure 3. Predictive power score (PPS) matrix results for all the scored soil properties. Darker shades of blue represent stronger correlations between each pair of variables. The colored frames represent the associated physical, biological, and chemical components of the soil properties. SQI: soil quality

index, AWC: available water content, SOM: soil organic matter, EC: electrical conductivity, K: potassium, P: phosphorus, and Poly: polysaccharides.

Figure 4. Box-whisker plot showing the value distributions and outliers of each of the soil properties in the natural and restored study sites. Red asterisks represent significant differences ($p < 0.05$) between treatments within sites. AWC: available water content, SOM: soil organic matter, EC: electrical conductivity, K: potassium, and P: phosphorus; n refers to the natural area, and r refers to restored.

Figure 5. Spider diagrams showing the differences between the natural and restored plots in unitless scores. AWC: available water content, SOM: soil organic matter, EC: electrical conductivity, K: potassium, and P: phosphorus.

Figure 6. Stack graph of indicator groups for the restoration practice for each site and their combination. An asterisk under the site name represents an overall significant difference between the restoration practices. The asterisks within the colored bars show significant differences between the groups of indicators (i.e., biological, chemical, and physical).

Appendix A. Residuals distribution histograms of the mixed-effect ANOVA tests for the individual scored soil indicators. The red curves represent the normal distribution for each of the indicators. Properties that had their residual normal distribution unmet ($p < 0.05$) were then transformed using the non-parametric rank-transform method (Conover and Iman, 1981). ANOVA: analysis of variance, SW-W: Shapiro-Wilks W-test, AWC: available water content, EC: electrical conductivity, K: potassium, NH_4 : ammonium, NO_3 : nitrate, P: phosphorus, and SOM: soil organic matter.

Appendix B. PCA results for all soil properties from the: (1) Gov, (2) Hagar, and (3) Afik sites compared to their natural sites. Abbreviation: AWC: available water content, EC: electrical conductivity, P: phosphorus, K: potassium, SOM: soil organic matter, and bold numbers refer to high factor loading for each PC.

Chapter 3: Figure captions

Figure 1: (A) Location of Avdat region within the Negev Desert, Israel. (B) Soil sampling sites, their respective land-use class, and the Zin Stream channel positioned over the hyperspectral image. Fully detailed information for all sampling sites is presented in Levi et al. (2020). RHS: runoff harvesting system.

Figure 2: Study flowchart of the three steps for developing the soil quality assessment model for regional-scale imaging spectroscopy (IS) prediction mapping for individual soil properties and the overall soil quality index (SQI) in Avdat region study area.

Figure 3: Predictive power score (PPS) correlation matrix for all the measured soil properties. The colored frames represent the associated physical, biological, and chemical components of the soil indicators. Pairs of soil indicators with high correlations ($\text{PPS} \geq 0.5$) were excluded from further SQI calculation. SQI: soil quality index, AWC: available water content, EC: electrical conductivity, Cl: chlorine, Na: sodium, Ca + Mg: calcium and magnesium, SAR: sodium adsorption ratio, P: phosphorus, K: potassium, NO_3 : nitrate, and SOM: soil organic matter.

Figure 4: Mean overall soil quality index (SQI) scores and their respective physical, biological, and chemical indicators' subgroups for the four land-uses (agriculture, grazing, RHS, and natural) in the Avdat study area. Uppercase letters above the error bars indicate significant differences between the

land-uses of the overall scores. In contrast, lowercase letters within the bars denote the differences between the particular attributes ($p < 0.05$). RHS: runoff-harvesting system.

Figure 5: (A) Normalized difference vegetation index (NDVI); (B) land-use land-cover (LULC) classification map; and (C) final clipped AisaFENIX bare soil image for the Avdat region.

Figure 6: Mean soil spectral signatures of the four land-use practices (agriculture, grazing, RHS, and natural) extracted from the AisaFENIX hyperspectral image for the Avdat study area. RHS: runoff harvesting system.

Figure 7: Partial least squares-discriminant analysis (PLS-DA) classification for the four land-use practices (agriculture, grazing, RHS, and natural) extracted spectra from the AisaFENIX hyperspectral image of the Avdat study area. The figure includes the model's number of latent variables (LV) and the overall accuracy (OA) and Kappa coefficient (Kc) statistics. Colored circles indicate a 95% confidence level. RHS: runoff harvesting system.

Figure 8: Variable importance in projection (VIP) plot of the agriculture (green), grazing (orange), runoff-harvesting system (RHS; purple), and natural (blue) land-uses in the Avdat region. Each bar represents the importance score of a particular hyperspectral image waveband in the partial least squares-discriminant analysis (PLS-DA) spectral classification analysis. The red sections highlight regions with spectral features with significant VIP peaks.

Figure 9: Support vector machine-regression (SVM-R) scatterplots and main results for the correlated soil properties and the overall soil quality index (SQI), between the measured calibration (Cal) and the validation (Val) datasets, and also the results of the upscaled image prediction maps (Pred). RMSE: root mean square error; RPIQ: ratio of performance to interquartile range; RPD: ratio of performance to deviation; AWC: available water content, NO_3^- : nitrate, SOM: soil organic matter, EC: electrical conductivity, SAR: sodium adsorption ratio, P: phosphorus, and K: potassium.

Figure 10: Variable importance in projection (VIP) plot of the physical (blue), biological (pink), and chemical (green) soil properties in the Avdat region. Each bar represents the importance score of a particular hyperspectral image waveband in the support vector machine regression (SVM-R) analysis. The red sections highlight spectral regions with significant VIP peaks. AWC: available water content, EC: electrical conductivity, Cl: chlorine, Na: sodium, Ca + Mg: calcium and magnesium, SAR: sodium adsorption ratio, NO_3^- : nitrate, P: phosphorus, and SQI: soil quality index.

Figure 11: (A) Final upscaled prediction map for the overall soil quality index (SQI) over the Avdat region, affected by various LU features, including (B) grazing LU and highly eroded bright chalky soil around an unrecognized Bedouin village; (C) agricultural fields (on the left edge of the image), stone-wall terraces (on the right), and the Zin Stream (in the center); and (D) a *liman* runoff-harvesting system (RHS) and degraded soil in response to steep and barren topography.

Chapter 1: Table captions

Table 1. Distribution of 121 soil samples among 14 sites across the Avdat region. Each site includes several samples and land-use type (Agriculture, grazing, or natural).

Table 2. The mean values of each soil property along with its respective land-use and geographical unit: (A) Agro-ecosystems; (B) Grazing; and (C) Natural ecosystems, presented each with its standard deviation and significant differences between treatments, represented with small letters (a, b, c).

Table 3. A matrix presenting the measured soil quality properties and their respective Pearson correlation coefficients for the study area. Correlations with high significant differences of $p \leq 0.05$ are marked in bold, whereas strong correlations ($R \geq 0.8$) with very high significant differences of $p \leq 0.01$ were added with (*).

Table 4. Results of the principal component analysis (PCA) of soil in the study area. Chosen principal components (PCs) scores for the model and their ranks were marked bold.

Table 5. Partial least squares-regression (PLS-R) analysis results for the Avdat region. The PLS-R produces distinction of indicative spectral regions for each soil property. For each soil property in the PLS-R model, the number of latent variables (LV), coefficient of determination (R^2), and the ratio of performance to deviation (RPD) are shown. Models with “excellent” ($RPD \geq 2.5$ and $R^2 \geq 0.80$) and “good” ($2 < RPD < 2.5$ and $R^2 \geq 0.70$) are marked in bold. Variable importance in projection (VIP) presents the highly significant wavelengths (nm) for each soil property with either excellent or good prediction value.

Chapter 2: Table captions

Table 1. Soil properties for soil quality assessment in open-pit phosphate mines, their functions, their laboratory chemical analysis methods, and their measurement units.

Table 2. Significant differences (p-values) between sites' restoration and their adjacent natural areas. Bold values are statistically significant ($\alpha < 0.05$)

Table 3. Varimax rotation PCA results of all sites for scoring soil properties from the restored and the natural sites combined. The bolded soil properties refer to the absolute highest loading within 10% of the factor loading. The overall model had a cumulative percentage of 68.1%. AWC: available water content, SOM: soil organic matter, EC: electrical conductivity, K: potassium, and P: phosphorus. Bold numbers refer to the highest factor loading for each soil indicator by its corresponding PC.

Chapter 3: Table captions

Table 1. abbreviations list and acronyms used in the paper.

Table 2: Soil quality properties and their respective affiliation, units of measurement, and analysis methods. A comprehensive review of the applied laboratory survey methods can be found in Levi et al. (2020).

Table 3: Principal component analysis (PCA) results for the scored soil indicators. The highest loading factor within each principal component (PC) for every indicator is marked bold.

Table 4: Support vector machine-regression (SVM-R) analysis and image upscaling of prediction results of Avdat region. For each of the soil properties in the model, the number of support vectors (SVs), the adjusted coefficient of determination for the calibration and validation datasets (R^2_{adjCal} and R^2_{adjVal}), as well as for the F-statistic value and degrees of freedom ($F_{(\text{df})\text{Cal}}$ and $F_{(\text{df})\text{Val}}$), and the root mean square error (RMSE_{Cal} and RMSE_{Val}) were assigned. The ratio of performance to deviation (RPD_{Val}) and the interquartile range (RPIQ_{Val}) for the validation set was also calculated. Properties with significant prediction values ($\text{RPIQ}_{\text{Val}} \geq 3$, $\text{RPD}_{\text{Val}} \geq 2$, and $R^2_{\text{adjVal}} \geq 0.7$) were examined for variable importance in projection (VIP) wavebands, upscaled to the image extent, and were assigned R^2 and RMSE (R^2_{Pred} and $\text{RMSE}_{\text{Pred}}$). Model constraints and optimization parameters' cost (C), epsilon (ϵ), and gamma (γ) are noted.

Abstract: Global population growth has resulted in land-use (LU) changes in many natural ecosystems, causing deteriorated environmental conditions that impact soil quality. This rapid growth in the global population caused many natural ecosystems to be transformed into human-dominated ones. Such LU dynamics require greater resource exploitation, commonly resulting in degraded environmental conditions that are acknowledged in the soil quality. The effects on the soil are even more acute in water-scarce and limited resources environments such as drylands. Therefore, developing appropriate approaches for soil quality and function evaluation is necessary since the soils in those areas are usually undeveloped and retain lower organic matter capacity. The soil quality index (SQI) method for soil quality assessment was well-proved as effective in arid environments with various LU practices. Soil quality differences between LUs can also be observed and measured using the local point-scale and regional scale based on imaging spectroscopy in the near-infrared reflectance spectroscopy (NIRS) method, which includes spectral ranges between 400-2500 nm. Using hyperspectral remote sensing assists in evaluating physical, biological, and chemical soil properties based on spectral differences between both natural soils and interrupted lands by human LU activities (e.g., agriculture, grazing, and mining). In this Ph.D. research, I examined the applicability of the soil quality assessment model in dryland environments that have gone under various anthropogenic influences.

Chapter 1 focused on developing a soil quality assessment index combining 14 soil properties for three different LUs (agriculture grazing and reference natural lands) and geographical units across the study area of the Avdat region in the central Negev Desert, Israel. The research goal was to apply, measure, and evaluate soil properties based solely on the spectral differences between both natural and human-dominated LU practices in the dryland environment of the central Negev Desert, Israel. This goal was achieved through developing and implementing chemometrics techniques generated from soil point spectroscopy. Soil quality index (SQI) values, based on 14 physical, biological, and chemical soil properties, were quantified and compared between LUs and geographical units across the study area. Laboratory spectral measurements of soil samples were applied. Significant differences in SQI values were found between the units. The statistical and mathematical methods for evaluating the soil properties' spectral differences included principal component analysis (PCA), partial least squares-regression (PLS-R), and partial least squares-discriminant analysis (PLS-DA). Correlations between predicted spectral values and measured soil properties and SQI were calculated using PLS-R and evaluated by the coefficient of determination (R^2), the Root Mean Square Error of Calibration, and Cross-Validation (RMSEC and RMSECV), and the ratio of performance to deviation (RPD). The PLS-R produced "excellent" and "good" prediction values for some soil properties, including EC, Cl, Na, Ca + Mg, SAR, NO_3 , P, and SOM. The results of the PLS-R model for SQI

are $R^2 = 0.90$, $RPD = 2.46$, $RMSEC = 0.034$, and $RMSECV = 0.057$. The PLS-DA classification of the laboratory spectroscopy was applied, resulting in high accuracy and kappa coefficient values when comparing LUs. In contrast, comparing the sampling sites resulted in lower overall accuracy ($Acc = 0.82$) and kappa values ($K_c = 0.80$). It is concluded that differentiation between physical, biological, and chemical soil properties, based on their spectral differences, is the key feature in the successful results for recognizing and characterizing various soil processes in an integrative approach. The results prove that soil quality and most soil properties can be successfully monitored and evaluated using NIRS in a comprehensive, non-destructive, time- and cost-efficient method.

Chapter 2 was related to the effects of mining restoration on soil quality. The present study strives to evaluate the impact of restoration practices (i.e., topsoil restoration) on soil quality properties compared to adjacent natural areas in an open-pit phosphate mine in a hyper-arid region of Israel. Mining contributes significantly to economic development, but it entails extensive environmental damage, such as soil degradation and water and air pollution. Mining activity impacts the soil quality, often making it unable to support ecosystem function and structure. The current study aims to apply the soil quality index (SQI) as a methodology for quantifying soil restoration status in an open-pit phosphate mine in Israel's hyper-arid environment. Accordingly, our first goal was to determine whether the topsoil conservation method resembles the adjacent natural area in terms of soil properties and overall soil quality, despite this hyper-arid region's extreme environmental and climatic conditions. Our second goal was to evaluate the restoration success based on the SQI approach as a function of time by comparing the different restoration stages applied in various sites. Therefore, the hypothesis is that the topsoil method in mines would enhance overall SQI and restoration efforts, where the timespan since restoration would also affect the emerging processes due to the poor, slow soil development in such a hyper-arid environment. In this regard, we evaluated an ecological restoration practice that includes topsoil refilling compared to the adjacent undisturbed natural system, using transformed and standardized scorings of 11 physical, biological, and chemical soil properties that were further statistically integrated into overall SQI values. Our results revealed significant differences between the restoration practice areas and the nearby natural areas, with a higher soil quality value in the latter. It is proposed that the topsoil restoration method is mainly affected by soil biological indicators, such as soil organic matter, soil proteins, and polysaccharides related to micro-organic growth, and a lesser extent, by the physical properties (primarily infiltration rate, followed by AWC). The former properties encourage the biocrust establishment, which is essential for soil surface stabilization and affects the water infiltration rate and nutrient availability. The chemical indicators showed no significant differences between most of the sites for the overall

soil quality. In conclusion, soil properties, primarily physio-biological ones, should be selected to quantify and evaluate restoration practices in hyper-arid ecosystems.

Chapter 3 was focused on assessing the effects of human activities (i.e., land uses such as grazing, modern agriculture, and runoff harvesting systems) on soil quality using airborne IS in the Avdat region study area. Thus, the main objective of this study was to assess the effects of human activities (i.e., land-use as grazing, modern agriculture, and runoff harvesting system) on soil quality using imaging spectroscopy (IS) in the arid regions of Israel. Based on the significant impact LUs have on their natural arid soil surroundings, the main goal of this research is to evaluate their effects over the study area using IS applications. Specifically, the objectives include (1) demonstrating the capability of IS for continuous mapping of multiple soil properties and the integrated SQI over the whole study area; (2) examining the combination of both conventional soil chemical laboratory survey and the contribution of the spectral dimension to the regression-based prediction capabilities of IS; and (3) evaluating the effect of LU change on the soil health patterns in arid regions that include agriculture, grazing, and runoff-harvesting systems (RHSs) for agricultural and forestry purposes on the uninterrupted natural land. For this, 12 physical, biological, and chemical soil properties were selected and further integrated into the soil quality index (SQI) as a method to assess the significant effects of LU changes in an arid area in southern Israel. A flight campaign of the AisaFENIX hyperspectral airborne sensor was used to develop an IS prediction model for the SQI on a regional scale. The spectral signatures, extracted from the hyperspectral image itself, were well separable among the four LUs using the partial least squares-discriminant analysis (PLS-DA) classification method (OA = 95.31%, Kc = 0.90). The correlation was performed using multivariate support vector machine-regression (SVM-R) models between the spectral data and the measured soil indicators and the overall SQI. The SVM-R models were significantly correlated for several soil properties, including the overall SQI ($R^2_{adjVal} = 0.87$), with the successful prediction of the regional SQI mapping ($R^2_{adjPred} = 0.78$). Seven individual soil properties, including fractional sand and clay, SOM, pH, EC, SAR, and P, were successfully used for developing prediction maps. Applying IS, and statistically integrative methods for comprehensive soil quality assessments enhances the prediction accuracy for monitoring soil health and evaluating degradation processes in arid environments. This study establishes a precise tool for sustainable and efficient land management and could be an example for future potential IS earth-observing space missions for soil quality assessment studies and applications.

Each chapter was published as a paper in the following journals:

1. Levi N, Karnieli A, and Paz-Kagan T. 2020. Using reflectance spectroscopy for detecting land-use effects on soil quality in dryland. *Soil and Tillage Research*. 199: 104571. (IF= 5.374; Category: soil science; Rank= 6/37 (Q1)). <https://doi.org/10.1016/j.still.2020.104571>
2. Levi N, Hillel N, Zaady E, Rtem G, Ziv, Y, Karnieli, A., and Paz-Kagan T. 2020. Soil quality index for assessing phosphate mining restoration in a hyper-arid environment. *Ecological Indicators*. 125: 107571. (IF= 4.858; Category: Environmental science; Rank= 72/274 (Q1)). <https://doi.org/10.1016/j.ecolind.2021.107571>
3. Levi, N, Karnieli A, and Paz-Kagan, T. (2022). Airborne imaging spectroscopy for assessing the land-use effect on soil quality in drylands. *ISPRS journal of photogrammetry and remote sensing*.186: 34-54. (IF=8.979; Category: geosciences multidisciplinary; Rank: 5/200 (Q1)). <https://doi.org/10.1016/j.isprsjprs.2022.01.018>

Chapter 1: Using reflectance spectroscopy for detecting land-use effects on soil quality in drylands

Levi N, Karnieli A, and Paz-Kagan T. 2020. Using reflectance spectroscopy for detecting land-use effects on soil quality in dryland. *Soil and Tillage Research*. 199: 104571. (IF= 5.374; Category: soil science; Rank= 6/37 (Q1)). <https://doi.org/10.1016/j.still.2020.104571>

1. Introduction

Global population growth over the past few decades has increased the need for food, shelter, and other services and has resulted in the transformation of many natural ecosystems into human-dominated ones (Foley, 2005). Land-use change (LUC) from natural to human-dominated land is a critical aspect of global change (Orenstein and Hamburg, 2009; Phillips et al., 2017) and may cause deteriorated environmental conditions (Metzger et al., 2006; Tschardt et al., 2005). Such LU changes have enabled humans to increase needed resources, but they also potentially reduce the capacity of ecosystems to maintain food production and to regulate climate, soil, and air quality in a sustainable way. LU practices determine soil quality and soil function, which constitute crucial aspects for future sustainable LU management (Crist et al., 2017). Therefore, remediation and maintenance of the soil quality in response to LU is essential (Adeel et al., 2005), especially in drylands, where the soil undergoes degradation processes.

Assessment of soil quality includes the integration of physical, biological, and chemical properties as indicators of the soil's performance (Andrews et al., 2004). These key soil properties are dynamically variable in space and time. Soil quality assessment can be applied to either human-dominated LUs, such as agriculture, where the primary ecosystem service is yield (agricultural productivity), or to natural ecosystems, where the primary ecosystem service could be the continuation of the environmental conditions and biodiversity conservation (Bünemann et al., 2018). The variability of soil indicators makes soil quality assessment a challenging task (Doran and Parkin, 1994). Two approaches for this task are the Soil Management Assessment Framework (SMAF) (Andrews et al., 2004; Viscarra Rossel et al., 2006; Wienhold et al., 2009) and the Cornell Soil Health Test (CSHT) (Idowu et al., 2009; Moebius-Clune et al., 2016). Both approaches are based on selecting a Minimum Data Set (MDS), comprising a minimum number of indicators (soil properties) for defining and quantifying soil performance, while avoiding over-complexity of the soil quality assessment model and maintaining its reproducibility, ease of sampling, and low cost (Andrews et al., 2004; Karlen et al., 1997). According to Bünemann *et al.* (2018), SMAF is a more flexible framework in terms of selecting indicators using standardized protocols. Once the MDS is selected,

the indicators are then transformed into a normalized score that represents the soil quality index (SQI) value (Andrews et al., 2004, 2002; Karlen et al., 1997). Soil quality assessment using the SQI method has been widely demonstrated in the literature, for both agricultural purposes (Mandal et al., 2001; Mukherjee and Lal, 2014; Triantafyllidis and Kontogeorgos, 2018) and ecological monitoring (Blecker et al., 2012; Lima et al., 2016; Paz-Kagan et al., 2016).

SQI requires extensive soil analyses, which remain expensive, as well as time and labor-consuming when using the standard procedures (Paz-Kagan et al., 2014). Therefore, more straightforward, time and cost-efficient, and non-destructive soil quality assessments are required. Near infrared reflectance spectroscopy (NIRS) grants the ability to assess various aspects of soil quality with non-destructive, reproducible, and cost-effective techniques. NIRS is based on hyperspectral data, including the visible (VIS, 400–700 nm), near-infrared (NIR, 700–1100 nm), and shortwave infrared (SWIR, 1100–2500 nm) spectral regions. Studies have shown the advantages of using RS in time-efficiency and the simultaneous analyses of multiple soil properties (Awiti et al., 2008; Cécillon et al., 2009; Romsonthi et al., 2018; Velasquez et al., 2005; Veum et al., 2017). Paz-Kagan *et al.* (2014) demonstrated the use of 14 soil quality indicators in the variability of soil attributes among three different LU types that changed from managed to unmanaged and vice versa. They developed the spectral soil quality index (SSQI) based on the NIRS of physical, biological, and chemical soil analyses. The SSQI integrates all relevant scored SQI indicators and then classifies them according to their soil spectral differences.

Although soil spectroscopy has been demonstrated successfully in many areas, these studies were mostly related to temperate climate regions that were subjected to anthropogenic effects, mainly agricultural systems, and were limited to a few land-use practices. The application of NIRS has not been previously applied in such a hyper-arid environment. This is possibly due to the relatively small-scale human activity and LU changes that generally occur in such scarcely populated regions with extreme climatic conditions. Hence, the main goal of the current research is to assess the effect of LU alteration, with different management practices, on soil quality in a dryland area. The novelty of this research lies in applying the combined SQI and NIRS methods in a water-scarce and nutrient-poor arid area. This objective was accomplished by integrating physical, biological, and chemical analyses, as well as NIRS laboratory-derived data, followed by the SQI method, in the Avdat region, Israel. The research questions include: (1) How do the different management practices (LU) impact soil indicators in an arid area? (2) Which indicators are more sensitive to different management practices?, and (3) Can soil properties and SQI be predicted based on NIRS in arid soils?

2. Material and Methods

2.1 Study area

In this study, the Avdat region, a scarcely populated dryland region in the Negev Desert of Israel, was selected. The area, which extends over 24 km², was chosen since it includes two main human activities, crop cultivation (mainly vines and olives) and the grazing of goats and sheep, that are adjacent to natural park reserves with unique ecological values (Ohana-Levi et al., 2018). The study area (Fig. 1) contains three LU categories, including two types of settlements: agricultural farms (single-family), agro-pastoral grazing land (Bedouin villages), and natural park reserves. The area is defined as arid by the aridity index (UNEP, 1992), which is calculated by the ratio between the annual rainfall (80–100 mm) and the annual potential evaporation (about 1700 mm), in which the precipitation gradient decreases and the evaporation rate increases the further southward from the Mediterranean Sea (Ziv et al., 2014). The average daily temperature ranges from 5°C in the winter to 32°C in the summer (Olsvig-Whittaker et al., 2012). Lithology is dominantly characterized by limestone mixed with dolomite, chalk, and marl. The soil type in the area is homogeneous, consisting mostly of loess soil (Ohana-Levi et al., 2018). Soil development occurs mostly in the upper parts of the watershed, where shallow patches of soil cover exist among steep barren limestone rocks, and in the lower parts, which consist of colluvium embedded with unconsolidated rocks. The soil columns range from 80 cm in the upstream part to several meters in the lower parts (Olsvig-Whittaker, 1983; Yair and Danin, 1980).

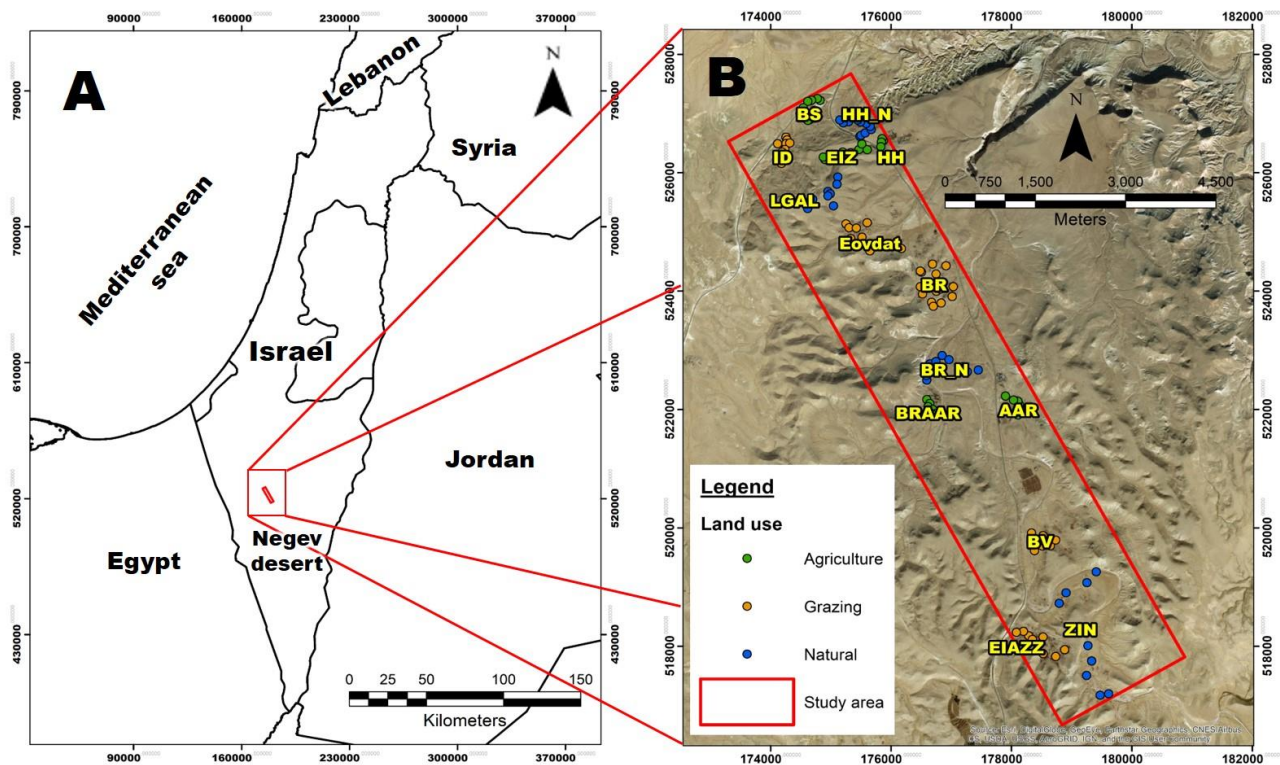


Figure 1: (A) Location of the study area in the Negev Desert, Israel; (B) the selected study area with the sampling points of the three land-use categories (agriculture, grazing, and natural reserves), whose locations were selected from a prior stratified random methodology. Full names and number of soil samples for all sampling sites are presented in Table 1.

Table 1: Distribution of 121 soil samples among 14 sites across the Avdat region. Each site includes several samples, land-use type (agriculture, grazing, or natural), topographic landscape position and means elevation, and soil class based on mean fractional soil texture.

Sampling site	Number of samples	Land-use type	Landscape position and elevation (m)	Soil class and mean fractional Sand, Silt, and Clay (%)
Even Ari farm (AAR)	6	Agriculture	Toeslope (547)	Loam (40.13, 46.2, 13.67)
Borot Ramaliah (BR)	16	Grazing	Toeslope (528)	Sandy Loam (63.1, 23.1, 13.8)
Borot Ramaliah-Even Ari (BRAAR)	6	Agriculture	Toeslope (527)	Loam (51.83, 31.47, 16.7)
Borot Ramaliah natural (BR_N)	9	Natural	Valley, Channel (523)	Sandy Loam (62.7, 23.17, 14.13)
Beit Hashanti (BS)	13	Agriculture	Toeslope, Valley (510)	Sandy Loam (53.17, 27.67, 19.16)
Bedouin village by Even-Ari (BV)	5	Grazing	Toeslope, Valley (559)	Sandy Loam (61.4, 23.6, 15)
El Azazme-Hava stream (EIAZZ)	9	Grazing	Footslope, Toeslope (572)	Sandy Loam (66.4, 17.86, 15.74)
Eyal Israeli farm (EIZ)	8	Agriculture	Footslope (549)	Sandy Loam (58.43, 27.82, 13.75)
Ein Avdat (Eovdat)	9	Grazing	Footslope, Toeslope (541)	Sandy Loam (56.87, 25.52, 17.61)
Havarim stream (HH)	4	Agriculture	Toeslope (553)	Sandy Loam (61.3, 24.7, 14)
Havarim stream natural (HH_N)	10	Natural	Backslope, Footslope (524)	Sandy Loam (60, 30.2, 9.8)
Bedouin village by Beit Hashanti (ID)	8	Grazing	Toeslope (525)	Sandy Loam (62.15, 23.52, 14.33)
Lifa gal viewpoint (LGAL)	8	Natural	Summit (597)	Sandy Loam (58.49, 24.7, 16.81)
Zin stream (ZIN)	10	Natural	Toeslope, Channel (592)	Sandy Loam (59.22, 25.37, 15.41)

2.2 Soil sampling

The sampling area included 14 different sites within the three LUs. Selecting the precise soil sample locations was done by conducting a prior stratified random methodology (SRM, Fig. 2) that was based on three different inputs: (1) elevation based on a digital elevation model; (2) soil type based on a pedology map, with the spatial distribution of soil texture from the official Survey of Israel data; and (3) LU categories based on the classification of a Landsat 8 image acquired on 13 August 2016, with an overall accuracy of 99.8% (Ohana-Levi et al., 2018). The SRM allows the selection of random soil samples based on the variation of the different data sources (Kothari, 2004).

2.3 Geographic units and laboratory analysis

Since the study area stretches over a broad and elongated cross-section approximately 11 km in length (Fig. 1), with different elevations and climatic attributes, soil indicator values may present some significant differences within the study area more related to the environmental gradient than to LU management practices. For example, elevation gradually increases southwards (Fig. 2A), whereas the northern and central parts share a relatively flatter surface around the Zin's downstream basin. Lithology differs as well (Fig. 2B), in which smoother loess soils reside around the stream path. Evapotranspiration, combining precipitation and temperature as environmental factors, shows significant differences between all three parts, in which the mean annual rates are 1671, 1694, and 1717 mm for the northern, center, and southern sections, respectively. Therefore, the statistical analysis was divided into three geographical units to minimize the environmental effect and to evaluate the management practices' effects on soil quality.

Soil samples from the different management practices were collected and transferred to the laboratory for physical, biological, and chemical soil analysis and laboratory spectroscopy. A total number of 121 soil samples were collected in April 2017 from 14 different sites scattered across the landscape. These are presented in Table 1 with their respective LU, landscape position, height, soil class, and texture. The soil samples were collected from the upper topsoil at a depth of 0–15 cm, mostly from lower topographical locations around toe-slopes and stream basins, where the soil column is more developed. Each soil sample was assigned an accurate location using a portable GPS device. The soil samples were packed into paper bags, then transferred and stored unopened at room temperature until analysis and laboratory survey.

The analytic methods included 14 analyses based on the SMAF protocol (Wienhold et al., 2009): physical: soil texture (fractional clay, silt, and sand) for assessing the soil structure and fragmentation, and the available water content (AWC), related to the plant available water storage capacity; biological: soil organic matter (SOM), related to energy and nutrient storage and carbon sequestration, and extractable nitrate (NO_3^-) in the soil, related to nitrogen-containing life building blocks and nitrogen release; and chemical: pH, electrical conductivity (EC), extractable chlorine (Cl), extractable sodium (Na), extractable calcium and magnesium (Ca + Mg), and the sodium adsorption ratio (SAR), which act as indicators for soil salinization conditions, and extractable phosphorus (P) and extractable potassium (K), which are essential nutrients, available in the soil, for plant growth and health.

The measurement of AWC was conducted by oven-drying the soil samples at 105°C to a constant weight, followed by measuring the weight differences (Carter and Gregorich, 2006). Soil organic matter (SOM) was measured by the organic carbon-furnace method after oven-drying soil

samples at 105°C for 3 h (to remove any CaCO₃) and weighing the soil samples, followed by burning the dry soil in a furnace for 2 h at 500°C and re-weighing the soil samples (Casida et al., 1964). Soil nitrogen (N) was measured as extractable nitrate (NO₃⁻) by potassium chloride extractions (Norman and Stucki, 1981). Soil nutrient values (NO₃⁻, P, K, Na, Ca, Mg) were extracted by shaking an ammonium acetate plus acetic acid solution with pH 4.8, which was then filtered through paper, and analyzed using an inductively coupled plasma emission spectrometer (ICP) (Brady and Weil, 1999). The samples' pH values were measured by composing a 2:1 part water-soil suspension and determined using the pH electrode probe of a Lignin pH robot. Finally, the soil EC was examined on a well-stirred 1:1 soil-water suspension (20 ml each), using an EC meter.

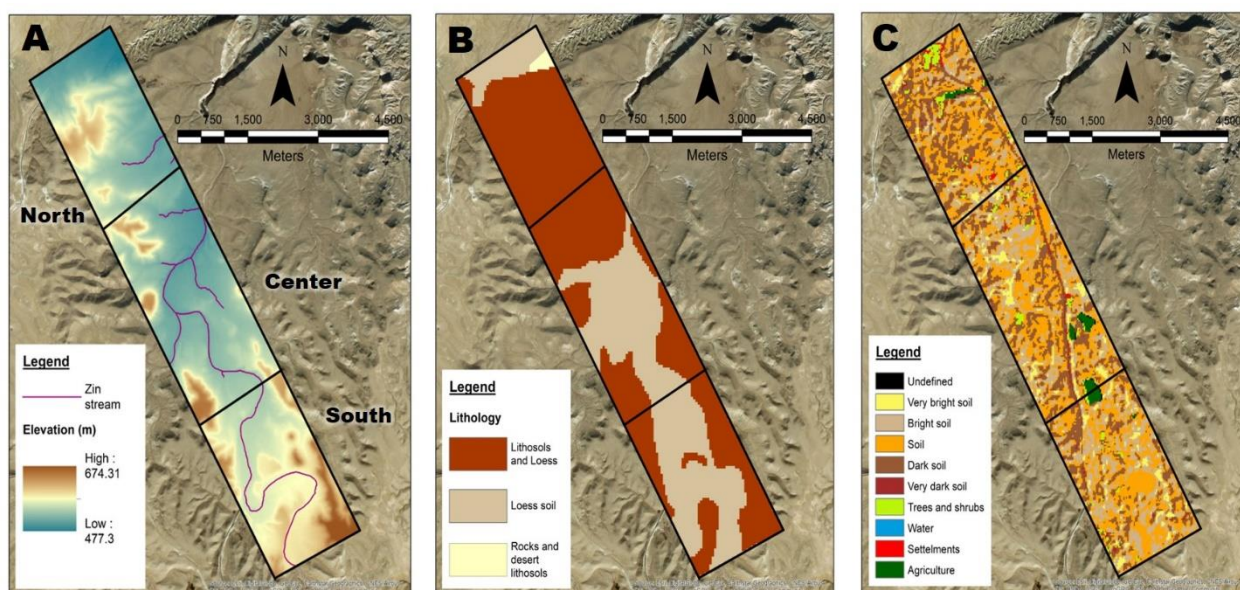


Figure 2: Stratified random survey components of Avdat region: (A) elevation, (B) lithology, (C) land use-land cover (LULC) classification, and the study area's geographical units: north, center, and south.

2.4 Spectral measurement and processing

The spectral measurements of all 121 soil samples were performed in laboratory conditions. The soil samples were sieved through a 2-mm sieve to remove aggregation and stones and were spectrally measured using the portable Analytical Spectral Devices (ASD) Field Spec® Pro spectrometer. The ASD spectral range is 350–2500 nm with a 25° field of view. The spectrometer was recalibrated using a standard white reference panel (Spectralon Labsphere Inc., North Sutton, NH, USA). Samples were scanned under illumination from four directions, while the spectrometer sensor was set above the sample at the height of 18.5 cm. The idea behind this step is to diminish the effects of micro-topography shadowing (bidirectional illumination effects). The mean value of every four readings was used as the representative sample signature that was then averaged to one spectral reading. The spectral resolution of the obtained data was 1 nm for the entire spectral range.

2.5 Development of soil quality index (SQI)

Soil quality indices combine all relevant indicators for soil condition interpretation within a proportional score. Transforming the indicators is necessary in order to standardize each indicator on a comparable scale. All indicators from the laboratory analysis were transformed and standardized into unitless scores (S_i), ranging from 0 to 1, which were then given a proportional weight and summed. These scores represented each of the indicator's explanatory contributions to the soil conditions according to management practices and LU, where natural ecosystem measurements were set as a reference for the other two LUs. AWC, SOM, and NO_3^- are essential soil quality indicators; therefore, the maximum presence of all indicates higher soil quality.

On the other hand, high abundances of EC, Cl, Na, and Ca + Mg soil properties may indicate a condition in which the soil is under the salinization process, which means lower soil quality and functionality. Therefore, the aim is to observe lower soil salinity values. The remaining soil indicator values (pH, SAR, P, and K) are likely to vary between each LU treatment, where either very high values (e.g., excessive fertilizing) or low ones may harm the soil's quality. Hence, an equal amount needs to be obtained. The sampling sites were grouped according to their geographical locations (i.e., northern, central, and southern), and their overall SQI values and physical, biological, and chemical components were calculated separately.

Eqs. 1–3 and Fig. 3 show the scoring functions, including their respective typical curves, according to the above adjustments and transformations, and based on previous literature (Moebius-Clune et al., 2016; Paz-Kagan et al., 2014; Seybold et al., 1997; Wienhold et al., 2009). Three functions can be defined: (1) the “more is better” scoring curve with positively graduating slopes that characterize AWC, SOM, and NO_3^- ; (2) the “less is better” curve for negatively depressing slopes, which represents EC, Cl, Na, and Ca + Mg; and (3) the “optimum” curve that centers around a mean value, which characterizes pH, SAR, P, and K. The transformations of the original values were calculated using the following functions (Masto et al., 2007):

$$S_{i_{more}} = \frac{1}{1 + b^{-b(x-a)}} \quad (1)$$

$$S_{i_{less}} = \frac{1}{1 + e^{b(x-a)}} \quad (2)$$

$$S_{i_{optimum}} = 1 \times e^{-\frac{(x-a)^2}{b}} \quad (3)$$

where x is the soil property value, a is the value's least square deviation from the mean, and b is the slope of mean according to its standard deviation ($2d^2$). Soil indicator performances with scores from 1.0–0.8 are considered to be very high scores, 0.8–0.6 are high, 0.6–0.4 are medium, 0.4–0.2 are low, and 0.2–0.0 are very low scores.

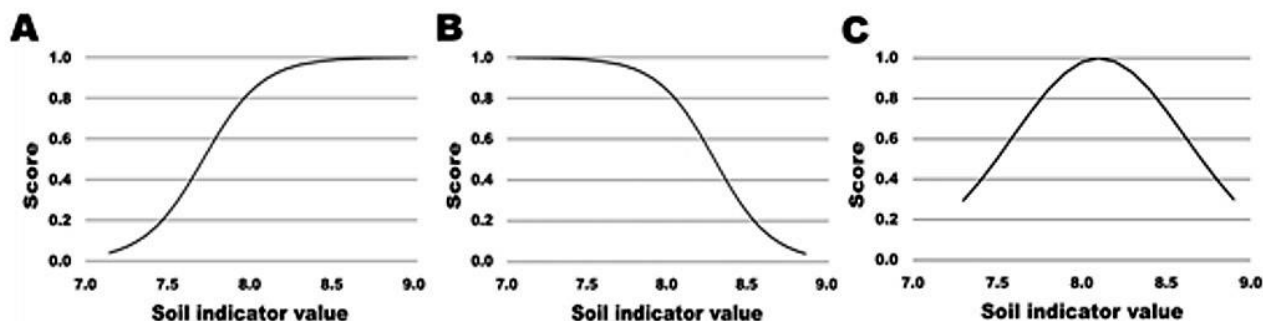


Figure 3: Examples of scoring curves of the respective transformation functions: (A) more is better, (B) less is better, and (C) optimum.

Once the original values were rescaled by their respective functions, a principal component analysis (PCA) was performed for further interpretation. The PCA is a statistical method that aims to reduce the number of dimensions within a dataset (Jolliffe et al., 2016). It transforms correlated variables into a smaller number of significantly different uncorrelated dimensions (variables) called principal components (PC), where the chosen number of PCs account for most of the variability of the data (Hotelling, 1933). The low co-variability among PCs helps to separate the data into statistically distinct groups. For this reason, the correlations between variables were calculated. Soil variables that were highly correlated were removed from the data to prevent redundancy in the model (Jolliffe et al., 2016). PCs with a higher proportion of variance than 5% were examined. The scored soil properties were calculated into an additive value of the essential weighted indicators for each LU, which is the ultimate soil quality index (SQI) Eq.4:

$$SQI = \sum_{i=1}^n PW_i \times S_i' \quad (4)$$

where PW_i is the PCA weighing factor and S_i' is one of the scoring functions, depending on the soil property. This final index value is considered as a total rank of the soil quality, with regard to the examined management practices and LU under study.

2.6 Correlation and classification of soil and spectroscopy analysis

The correlation between the laboratory soil measurements and their spectral data was performed using a partial least squares-regression (PLS-R) cross-validation procedure. PLS-R is a predictive

technique for quantitative spectral analysis (Paz-Kagan et al., 2014; Viscarra Rossel et al., 2006). Its main advantage derives from its ability to use multiple predictor variables to create predictive models with high collinearity. PLS-R uses covariance between the spectra (predictor: X) and the soil laboratory analysis, as well as the SQI (response variables: Y). The focus was placed the abovementioned soil indicators and their correlations with their spectral data. Each soil indicator correlates differently with its spectral data, and each has more significant wavelengths with which it corresponds. This is due to the fact that characteristic wavelengths differ between each soil indicator and management practice according to the relationship their physical and chemical structures maintain with the electromagnetic radiation, which can be measured in a comparative spectral analysis (Ben-Dor et al., 2009; Cécillon et al., 2009).

Pre-processing transformations (PPTs) were applied and tested on the spectral signatures in an attempt to improve their prediction ability through the regression process. Such PPTs include mean and maximum normalization and baseline offset effects corrections (Tekin et al., 2014), first and second derivatives of the reflectance values (Fystro, 2002; Shepherd and Walsh, 2002), the second-order polynomial Savitzky–Golay smoothing algorithm with 11 smoothing points (Savitzky and Golay, 1964), and generalized least squares weighting (GLSW) (Martens et al., 2003). The best predictive fitted values were found with the combination of two PPTs: (1) autoscale and (2) GLSW with a single adjustable parameter, α , which was set to 0.02 (Paz-Kagan et al., 2015; Rozenstein et al., 2015) (See Appendix A). To measure the relative importance of each wavelength, variable importance in projection (VIP) scores were derived from the PLS-R to determine the significant effect of each wavelength defined by each soil indicator. Evaluations of the prediction rate for the regressions between the predicted and observed soil indicators were made by calculating the Root Mean Square Error of Calibration and Cross Validation (RMSEC and RMSECV) and the coefficient of determination (R^2) values. Therefore, the data needed to be divided into a calibration dataset (75% of the data) and a randomly chosen validation dataset (25% of the data), which was used as the model prediction accuracy. In addition, to standardize the prediction correlations comparably, the ratio of performance to deviation (RPD) was calculated as $RPD = SD/RMSECV$. Chang *et al.* (2001) proposed the RPD's graduated ranking of the prediction models, in which models with $RPD \geq 2.5$ and $R^2 \geq 0.80$ are considered "excellent," $2 < RPD \leq 2.5$ and $R^2 \geq 0.70$ are considered "good," $1.5 < RPD \leq 2$ and $R^2 \geq 0.60$ are considered "moderate," and $RPD \leq 1.5$ and $R^2 < 0.60$ are considered "poor". However, Mcbratney and Minasny (2016) have warned about the use of both measures as the only indices of the prediction model, since they share a strong relationship and ultimately present the same concept. Thus, RPD and R^2 cannot be used as assessment tools for goodness of fit on their own. Instead, both measures should be presented and compared along with the RMSEC and

RMSECV of the prediction models to compare the models' prediction intervals.

Assessment and quantification of the differences in the spectral variation in soil quality between LUs were conducted using partial least-squares discriminant analysis (PLS-DA). The PLS-DA categorizes the continuous predictor variable (X: soil indicators) into separate classes according to their variance between each group of samples. The outcome of the PLS-DA is a scatterplot in which each sample is classified into one of the predetermined classes (LU or sampling site), in addition to a statistical evaluation of significant differences between classes.

2.7 Statistical analysis of soil properties and SQI

We applied a one-way analysis of variance (ANOVA) for each soil indicator and SQI under each particular LU. The distinction between each pair of LUs made by their separation of means was examined using a Tukey Honest Significance Difference (HSD) post hoc test, for which $p \leq 0.05$ indicates a significant difference. In cases where ANOVA assumptions of the variables were not met for the original data, a logarithmic transformation was applied, followed by a reexamination of the assumptions. If the indicators' assumptions were still violated, a non-parametric Kruskal-Wallis test was conducted, following by a pairwise Wilcoxon rank-sum test to examine significant differences between pairs of LUs for each soil property. Statistical calculations and analyses were performed using the R-Studio version 1.0.143 software (RStudio Inc., Boston, MA, USA).

3. Results

3.1 Soil property analysis

The laboratory analysis of the soil is shown in Table 2, presenting the mean values of the soil properties and their standard deviations (SDs), according to their LU and geographical unit. To remove the minimum number of outliers from the dataset, by excluding only the extreme values, we applied the median absolute deviation (MAD) approach that excludes observations higher or lower than three SDs around the variable's median value (Leys et al., 2013). Using the MAD method on the data resulted in the removal of very few outliers, not exceeding 5% removal for any of the soil properties; for some soil properties, no outliers were removed. Fig. 4 shows the comparative analysis of soil properties for the whole study area, without the geographical subdivision. In this case, only small significant differences were noticed between LUs. The soil texture analysis resulted in the classification of almost all the sampling sites as the sandy-loam soil type (Table1), according to the USDA soil texture triangle (Groenendyk et al., 2015), with a few soil samples classified as loam. Similar results were found when comparing LUs across geographical units (Table 2). One-way ANOVA tests for the original values showed that AWC and pH had no assumptions violated, and both showed no significant differences between LUs. Following this, the transformed data resulted in

SAR and SOM properties having no assumptions violated and presenting some significant differences between LUs, according to the Tukey HDS test, in which for both indicators, the natural ecosystem LU showed lower values than the other two LUs with significant differences. For most soil properties, the agro-ecosystems and grazing LUs showed significantly higher values than those of the natural ecosystem, notably EC, Cl, Na, and Ca + Mg, which may indicate soil salinity levels.

Furthermore, the natural ecosystem showed significantly lower soil nutrient values (NO₃, P, and K) than the grazing and agro-ecosystem LUs, which implies the presence of higher biotic activity (due to cropping and herding) in the soil of the latter two LUs. Nevertheless, the geographical subdivision emphasizes variations even better, where significant differences were shown between LUs for almost all soil indicators (Table 2). A significant difference was noticed between the agro-ecosystem sites (located only in the northern and central areas), for which much higher values were measured in the northern fields than in the central ones for both salinity (EC, Cl, Na, Ca + Mg, and SAR) and soil nutrient (NO₃, P, and K) indicators. The same soil properties, as well as the SOM, showed significantly higher values for the grazing and agro-ecosystem LUs than the natural ecosystem one. Moreover, significantly higher AWC was found in the central agricultural LU than in the other LUs.

Table 2: The mean values of each soil property along with its respective land-use and geographical unit: (A) agro-ecosystems; (B) grazing; and (C) natural ecosystems, each presented with its standard deviation and significant differences between treatments, represented with small letters (a, b, c).

Soil Properties	Location	Agro-ecosystems	Grazing	Natural ecosystems
AWC (%)	North	35.04 ± 4.06 ^a	39.6 ± 6.55 ^a	37.07 ± 3.27 ^a
	Center	40.83 ± 4.58 ^a	35.96 ± 5.48 ^b	34.24 ± 5.53 ^b
	South	-	38.95 ± 7.72 ^a	33.71 ± 5.43 ^a
pH	North	7.99 ± 0.39 ^a	8.1 ± 0.40 ^a	8.08 ± 0.26 ^a
	Center	8.3 ± 0.13 ^a	7.96 ± 0.41 ^b	8.01 ± 0.24 ^b
	South	-	8.05 ± 0.27 ^b	8.55 ± 0.28 ^a
EC (dS/m)	North	25.85 ± 29.64 ^a	13.58 ± 24.31 ^a	5.82 ± 7.33 ^b
	Center	0.75 ± 0.15 ^c	16.8 ± 19.54 ^a	3.21 ± 3.26 ^b
	South	-	18.54 ± 22.1 ^a	9.22 ± 18.81 ^b
Cl (mg/l)	North	296.75 ± 358.69 ^a	147.89 ± 309.15 ^a	45.83 ± 81.66 ^b
	Center	1.45 ± 0.71 ^c	171.05 ± 228.55 ^a	23.65 ± 27.21 ^b
	South	-	190 ± 275.17 ^a	88.78 ± 201.25 ^b
Na (mg/l)	North	103.32 ± 150.45 ^a	79.66 ± 162.33 ^a	29.86 ± 44.46 ^b
	Center	1.21 ± 0.78 ^c	103.78 ± 145.91 ^a	21.2 ± 26.04 ^b
	South	-	104.11 ± 150.63 ^a	79.74 ± 177.49 ^a
Ca + Mg (mg/l)	North	139.75 ± 162.02 ^a	56.02 ± 81.62 ^b	34.8 ± 44.21 ^b
	Center	5.45 ± 1.7 ^b	84.3 ± 99.9 ^a	9.46 ± 8.05 ^b

	South	-	67.37 ± 74.96 ^a	28.22 ± 51.86 ^b
SAR	North	4.9 ± 4.01 ^b	13.46 ± 12.71 ^a	3.37 ± 2.18 ^b
	Center	8.33 ± 3.1 ^a	6.48 ± 5.73 ^a	2.86 ± 1.45 ^b
	South	-	22.06 ± 18.64 ^a	6.52 ± 10.28 ^b
NO ₃ (mg/kg)	North	143.37 ± 154.91 ^a	93.51 ± 111.76 ^a	34.58 ± 41.21 ^b
	Center	14.82 ± 7.63 ^c	94.62 ± 109.98 ^a	26.92 ± 30.64 ^b
	South	-	219.34 ± 193.783 ^a	100.07 ± 220.28 ^b
P (mg/kg)	North	13.62 ± 10.19 ^b	56.52 ± 52.91 ^a	9.53 ± 3.14 ^b
	Center	17.87 ± 3.91 ^b	31.68 ± 48.5 ^a	13.55 ± 8.62 ^b
	South	-	66.86 ± 51.62 ^a	13.57 ± 5.37 ^b
K (ml/kg)	North	2.1 ± 4.03 ^b	6.41 ± 11.34 ^a	0.5 ± 0.33 ^c
	Center	0.48 ± 0.25 ^b	3.1 ± 5.17 ^a	0.42 ± 0.15 ^b
	South	-	15.11 ± 17.71 ^a	0.99 ± 1.41 ^b
SOM (%)	North	3.17 ± 1.35 ^a	3.18 ± 1.48 ^a	1.61 ± 0.8 ^b
	Center	2.44 ± 0.47 ^a	2.59 ± 0.7 ^a	1.94 ± 0.3 ^b
	South	-	2.62 ± 1.61 ^a	1.35 ± 0.51 ^b
Sand (%)	North	56.15 ± 9.06 ^a	59.35 ± 7.31 ^a	59.32 ± 11.7 ^a
	Center	45.98 ± 11.31 ^b	63.1 ± 8.19 ^a	62.7 ± 6.01 ^a
	South	-	64.61 ± 7.03 ^a	59.22 ± 16.46 ^a
Silt (%)	North	27.24 ± 8.74 ^a	24.58 ± 6.44 ^a	27.75 ± 10.51 ^a
	Center	38.83 ± 11.52 ^a	23.1 ± 10.08 ^b	22.86 ± 3.73 ^b
	South	-	19.9 ± 5.45 ^a	25.37 ± 14.89 ^a
Clay (%)	North	16.6 ± 6.22 ^a	16.06 ± 3.8 ^a	12.91 ± 6.4 ^a
	Center	15.18 ± 3.72 ^a	13.8 ± 4.66 ^a	14.43 ± 5.3 ^a
	South	-	15.47 ± 3.41 ^a	15.41 ± 6.4 ^a

Note: AWC: available water content; EC: electric conductivity; Cl: chlorine; Na: sodium; Ca + Mg: calcium and magnesium; SAR: sodium adsorption ratio; NO₃: nitrate; P: phosphorus; K: potassium SOM: soil organic matter; significant differences between land uses are marked with small letters, in which values in each column with the same letter do not differ significantly when $p < \alpha$ (0.05), using ANOVA and Kruskal-Wallis analyses followed by Tukey and Wilcoxon tests. A: high values; b: medium values; c: low values.

Pearson correlation coefficients (r) for the given soil indicators were calculated and are presented in Table 3. To understand the relations and to consider the more powerful correlations between properties, significant correlations ($r \geq 0.5$) are marked in bold, and strong correlations ($r > \pm 0.8$) are marked in bold and with an asterisk (*). Multivariate correlations were also generated to avoid redundancy of properties. Very strong correlations were found between EC and Cl, Na, and Ca + Mg ($r = 0.99, r = 0.95$ and $r = 0.93$; $p < 0.01$, respectively), between Cl, Na, and Ca + Mg ($r = 0.94$ and 0.93 ; $p < 0.01$, respectively), between Na and Ca + Mg ($r = 0.86$; $p < 0.01$), and between sand and silt ($r = -0.88$; $p < 0.01$).

3.2 Soil quality index (SQI)

The SQI for each soil sample and their respective physical, biological, and chemical components was developed using the scores of the transformed soil properties' values. The soil texture variables (fractional sand, silt, and clay) and Cl, Na, and Ca + Mg (which are essential indicators for soil salinity) were excluded from the SQI and PCA calculations due to high collinearity and possible model redundancy (Jolliffe et al., 2016). The PCA results showed that only three PCs had eigenvalues greater than 1 that explained 72.70% of the total cumulative variance of the original data (Table 4). PC1 accounts for 35.83% of the total variance and includes the pH, EC, and NO₃ soil properties. For PC2, the contributory variance was 22.29%, and includes the AWC and P indicators. The third PC3, with a response to 14.58% of the variation, contains SAR, K, and SOM soil indicators within 10% of the highest loading values.

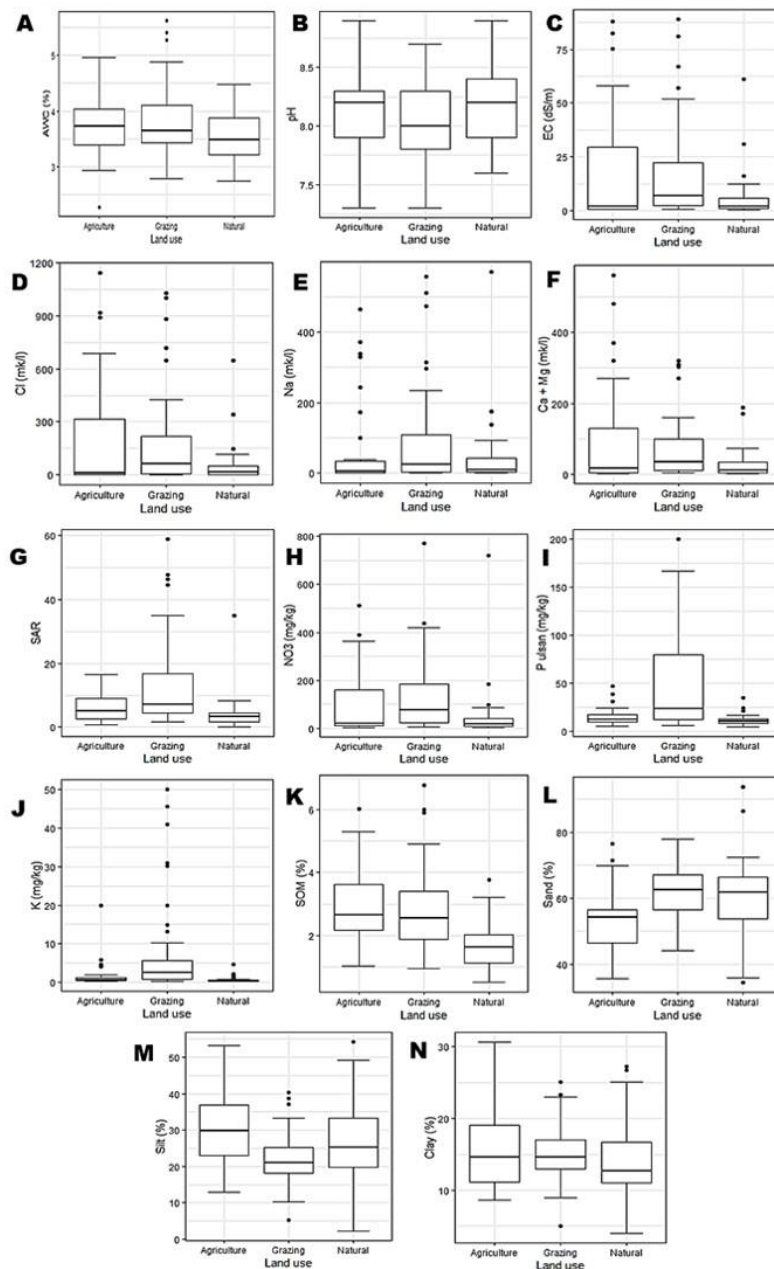


Figure 4: Boxplot representation of each soil indicator value under different land uses of the entire study area: agriculture, grazing, and natural. Note: available water content (AWC); electrical conductivity (EC); extractable chlorine (Cl); extractable sodium (Na); extractable calcium and magnesium (Ca + Mg); sodium adsorption ratio (SAR); extractable nitrate (NO₃); extractable phosphorus (P); extractable potassium (K); and soil organic matter (SOM).

Table 3: A matrix presenting the measured soil quality properties and their respective Pearson correlation coefficients for the study area. Correlations with highly significant differences of $p \leq 0.05$ are marked in bold, whereas strong correlations ($R \geq 0.8$) with very highly significant differences of $p \leq 0.01$ were marked with (*).

	AWC (%)	pH	EC (dS/m)	Cl (mg/l)	Na (mg/l)	Ca + Mg (mg/l)	SAR	NO ₃ (mg/kg)	P (mg/kg)	K (mg/kg)	SOM (%)	Sand (%)	Silt (%)	Clay (%)	
AWC (%)	1.00														
pH	0.09	1.00													
EC (dS/m)	-0.20	-0.55	1.00												
Cl (mg/l)	-0.16	-0.55	0.99*	1.00											
Na (mg/l)	-0.23	-0.42	0.95*	0.94*	1.00										
Ca + Mg (mg/l)	-0.19	-0.56	0.93*	0.93*	0.86*	1.00									
SAR	0.44	-0.14	0.14	0.14	0.11	0.04	1.00								
NO ₃ (mg/kg)	-0.09	-0.41	0.76	0.71	0.74	0.67	0.31	1.00							
P (mg/kg)	0.29	-0.24	0.06	0.05	0.01	0.001	0.41	0.19	1.00						
mg/kg (K)	0.12	-0.3	0.27	0.24	0.26	0.2	0.47	0.55	0.46	1.00					
SOM (%)	0.42	-0.38	0.53	0.54	0.36	0.48	0.39	0.39	0.38	0.33	1.00				
Sand (%)	-0.02	-0.1	0.001	-0.02	0.02	-0.06	0.17	0.03	0.17	0.14	-0.06	1.00			
Silt (%)	0.08	0.12	-0.05	-0.04	-0.13	0.01	-0.16	-0.13	-0.17	-0.16	-0.03	-0.88*	1.00		
Clay (%)	-0.12	-0.03	0.11	0.12	0.22	0.1	-0.02	0.18	-0.02	0.03	0.19	-0.34	-0.15	1.00	

Note: AWC: available water content; EC: electric conductivity; Cl: chlorine; Na: sodium; Ca + Mg: calcium and magnesium; SAR: sodium adsorption ratio; NO₃: nitrate; P: phosphorus; K: potassium SOM: soil organic matter.

The SQI scores and their physical, biological, and chemical components for all three LUs are shown in Fig. 5. The mean overall SQI scores in the northern part are SQI = 0.65, 0.61, and 0.66 for the agricultural, grazing, and natural LUs, respectively. None of the three LUs were found to be significantly different from each other ($\chi^2_{(2)} = 1.53$, $p = 0.46$). Both the biological (representing the SOM and NO₃ soil properties) and the chemical components of the SQI for the natural area differed significantly from the rest, with lower SOM and NO₃ components and higher values for the chemical properties. In the central part, the mean overall SQI scores were SQI = 0.72, 0.65, and 0.63 for the agricultural area, grazing, and natural LUs, respectively, with significant differences between all LUs for both overall SQIs and their components ($\chi^2_{(2)} = 15.67$, $p < 0.05$). The remaining southern part resulted in mean overall SQI scores of SQI = 0.61 and 0.59 for the grazing and natural LUs, respectively, with no significant differences. Within the southern SQI's components, only the biological showed significant differences.

Table 4: Results of the principal component analysis (PCA) of soil in the study area. Chosen principal components' (PCs) scores for the model and their ranks are marked bold.

	Scores PC1	Scores PC2	Scores PC3
Eigenvalue	2.86	1.78	1.16
Variance (%)	35.83	22.29	14.58
Cumulative variance (%)	35.83	58.12	72.70
AWC (%)	0.06	0.55	0.42
pH	0.38	0.15	-0.23
EC (dS/m)	-0.46	-0.34	0.17
SAR	-0.19	0.41	-0.43
NO ₃ (mg/kg)	-0.50	-0.18	-0.20
P (mg/kg)	-0.25	0.51	-0.008
K (mg/kg)	-0.39	0.20	-0.40
SOM (%)	-0.34	0.16	0.57

Note: AWC: available water content; EC: electric conductivity; SAR: sodium adsorption ratio; NO₃: nitrate; P: phosphorus; K: potassium SOM: soil organic matter.

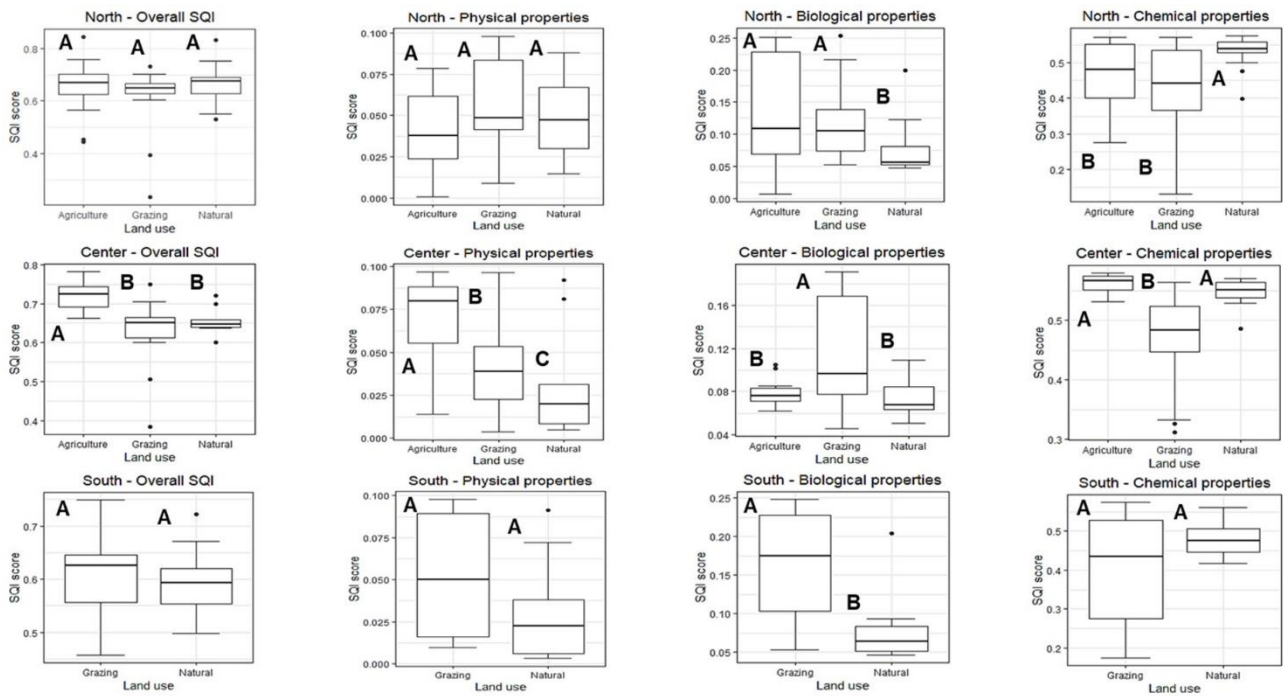


Figure 5: Scores of soil quality indices (SQIs) and their physical, biological, and chemical components for the three land uses, according to the study area's geographical distribution: north, center and south. Capital letters above the error bars represent significant differences between land uses.

3.3 Soil properties and SQI correlations with soil spectroscopy

The results of the PLS-R analysis are presented in Table 5. The results also include several latent variables (LV), coefficient of determination (R^2), RMSEC, RMSECV, RPD, and significant VIP bands used for each soil property included in the model. Soil properties with excellent ($RPD \geq 2.5$ and $R^2 \geq 0.80$) and good ($2 < RPD \leq 2.5$ and $R^2 \geq 0.70$) prediction scores are marked in bold and underlined in Table 5 and presented in Fig. 6, and include EC, Cl, Na, Ca + Mg, SAR, NO_3^- , P, and SOM. Fig. 6 also presents each soil property and SQI soil-laboratory versus soil-spectroscopy regression scatterplots, including their respective RMSEC, RMSECV, R^2 , LVs, and RPD values. The overall SQI resulted in a good prediction value ($R^2 = 0.903$, $RPD = 2.46$, $RMSEC = 0.034$, and $RMSECV = 0.057$). The significant diagnostic wavebands were calculated and identified by the VIP for each soil property and SQI value. For example, significant scores for the highly correlated soil salinity properties (EC, Cl, Na, Ca + Mg, and SAR) were found within the range of bands with strong peaks at 1363, 1896–1899, 1982–1984, 2266–2270, and 2346 nm. Sensitivity bands for biological properties, such as SOM, were found across the VIS-NIR-SWIR regions, with significant peaks at 590–739, 853, 1364, 1899, 2014, 2203, and 2317 nm. For NO_3^- , the wavebands centered mostly within the SWIR region, peaking at 652, 1361, 1420, 1773, 1901, 1974, and 2346 nm. The SQI, combining attributes from multiple soil indicators, found strong sensitivity at 1434, 1749, 1841, 1901, 1988, and 2343 nm.

3.4 Spectral classification of soil samples across LUs and sampling sites

The classification of the soil samples' spectral signatures across varied LUs and sampling sites is shown in Fig. 7, as well as the number of LVs, overall accuracy, and Kappa coefficient values. The PLS-DA classification across different LUs (Fig. 7A) resulted in high overall accuracy and Kappa coefficient values for both grouping methods. The separation between sampling sites (Fig. 7B) resulted in lower classification values, with an overall accuracy of 0.823, and a Kappa value of 0.802. In terms of classification capabilities, the PLS-DA is an accurate quantitative and qualitative approach for predicting variability between different LUs, and between sites to a slightly lesser extent.

Table 5: Partial least squares-regression (PLS-R) analysis results for the Avdat region. The PLS-R distinguishes between the indicative spectral regions for each soil property. For each soil property in the PLS-R model, the number of latent variables (LV), the coefficient of determination (R^2), the root mean squares error of calibration and cross-validation (RMSEC and RMSECV) of the predicted model, and the ratio of performance to deviation (RPD) are shown. Models with “excellent” ($RPD \geq 2.5$ and $R^2 \geq 0.80$) and “good” ($2 < RPD < 2.5$ and $R^2 \geq 0.70$) values are marked in bold. Variable importance in projection (VIP) presents the highly significant wavelengths (nm) for each soil property with either excellent or good prediction value.

Soil properties	LV	R^2	RPD	RMSEC	RMSECV	VIP
AWC (%)	2	0.795	1.71	0.243	0.33	
pH	3	0.976	1.58	0.053	0.231	
EC (dS/m)	2	0.958	3.83	4.146	5.579	1363, 1898, 1982
Cl (mg/l)	2	0.960	3.66	50.987	70.82	1836, 1899, 1983
Na (mg/l)	3	0.949	2.88	25.709	45.299	672, 1363, 1896, 1984, 2346
Ca + Mg (mg/l)	2	0.951	3.22	22.351	31.644	1744, 1897, 2003
SAR	2	0.906	3.19	2.204	3.243	671, 1369, 1875, 2056, 2141, 2196, 2270, 2344
NO ₃ (mg/kg)	2	0.854	2.20	54.288	63.879	652, 1361, 1420, 1773, 1901, 1974, 2346
P (mg/kg)	2	0.866	2.19	10.864	16.352	450, 597, 1040, 1363, 1415, 1660, 1808, 1884, 1915, 2130, 2254, 2345
SOM (%)	4	0.905	2.14	0.338	0.581	590-739, 853, 1364, 1899, 2014, 2203, 2317
Sand (%)	5	0.882	1.53	3.383	7.053	
Silt (%)	4	0.856	1.74	3.638	5.923	
Clay (%)	2	0.915	1.49	1.409	3.518	
Overall SQI	3	0.903	2.46	0.034	0.057	1434, 1749, 1841, 1901, 1988, 2343

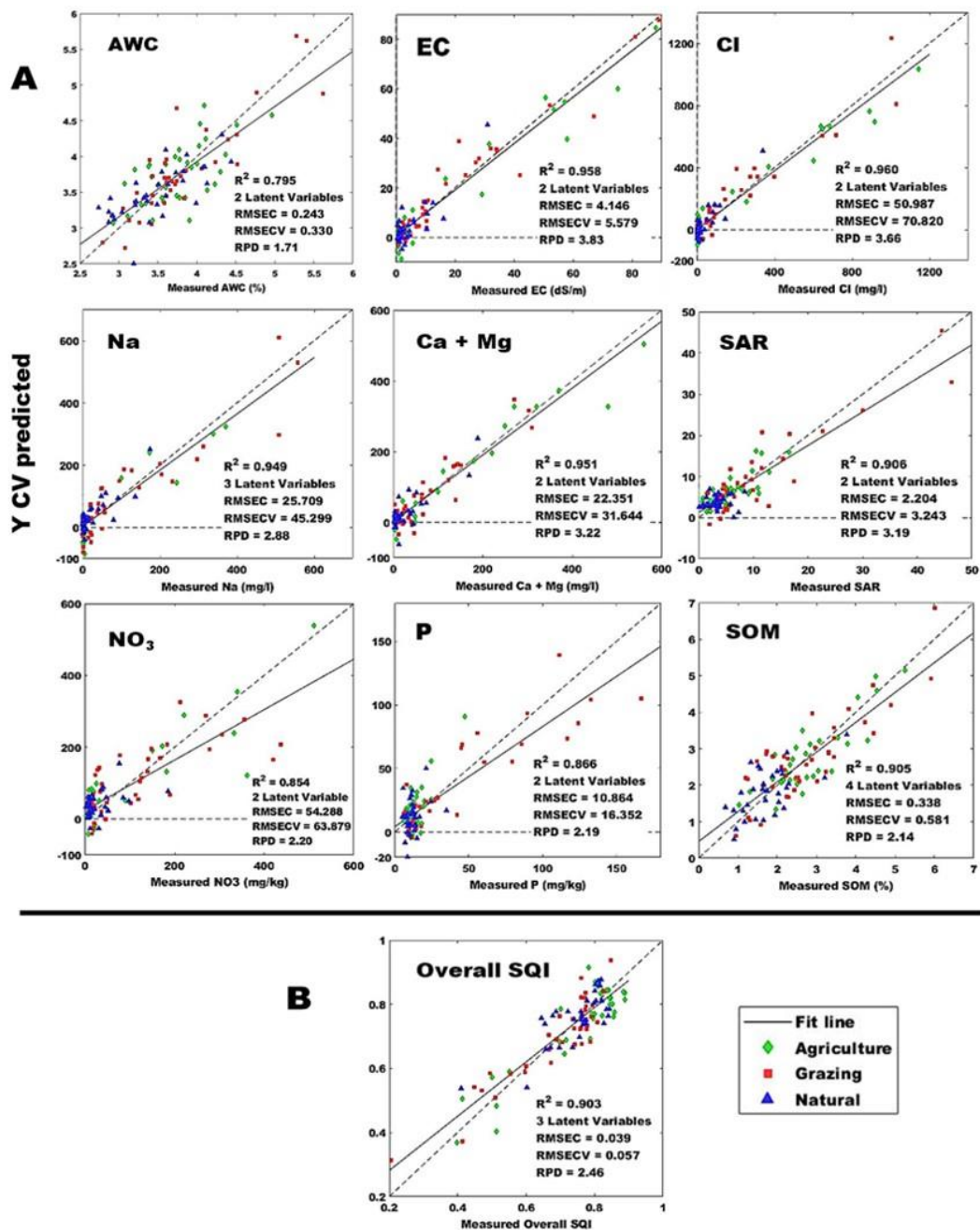


Figure 6: Partial least squares-regression (PLS-R) correlation scatterplots of predicted cross-validation (CV) values versus soil laboratory analysis values for: (A) several soil properties and (B) the soil quality index (SQI) among the three LUs in the Avdat region. RMSEC: root mean square error of calibration; RMSECV: root mean square error of cross-validation; EC: electric conductivity; Cl: chlorine; Na: sodium; Ca + Mg: calcium and magnesium; SAR: sodium adsorption ratio; NO₃: nitrate; P: phosphorus; SOM: soil organic matter. Each colored shape represents a land-use type: natural ecosystem (blue triangles), agro-pastoral grazing (red squares) and agriculture (green rhombuses).

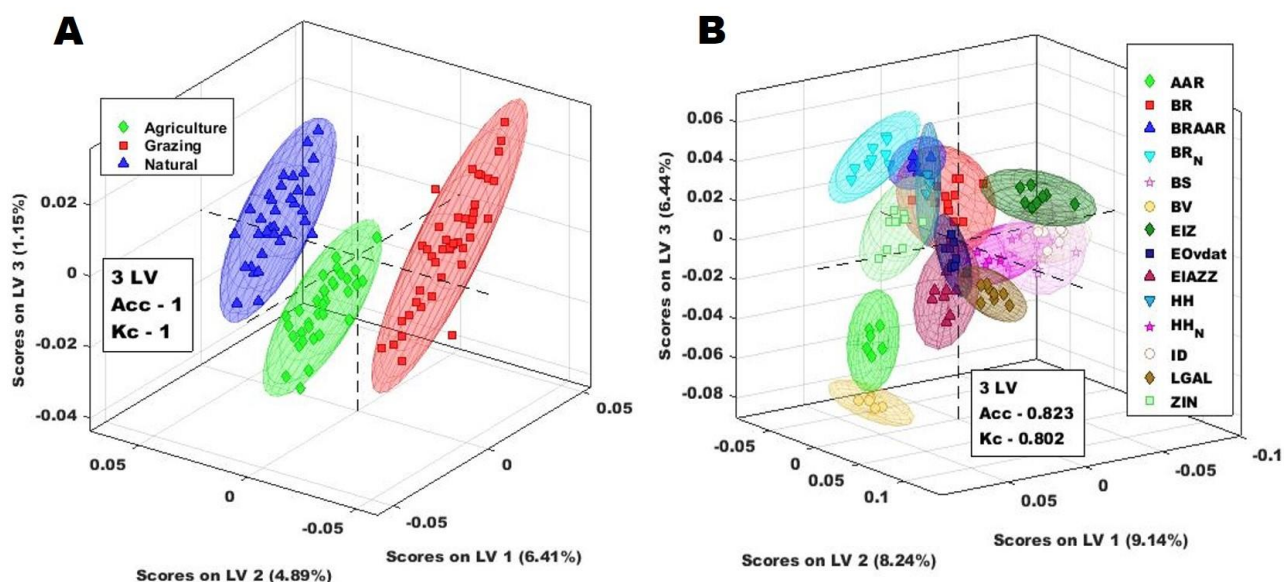


Figure 7 – Partial least squares-discriminant analysis (PLS-DA) classification of initial 2150 bands spectral resolution laboratory spectroscopy for both (A) LUs and (B) sampling sites in the Avdat region. Each figure includes the number of latent variables (LV) used, overall accuracy (Acc), and Kappa coefficient (K_c) values for each model. Colored circles indicate a 95% confidence level. Full names and the number of soil samples for all sampling sites are presented in Table 1.

4. Discussion

The effect of LU activity on soil was detected, quantified, and evaluated through a soil survey and spectral analysis of different soil indicators for comparing soil properties across different land practices. This research integrated both methods by applying the NIRS method to explain variations among LUs. The use of the NIRS approach for soil quality assessment in an arid area, such as the Avdat region in the Negev Desert, has been limited. Significant differences between LUs and sampling sites were found for almost all soil indicators and SQIs, for laboratory analyses, soil spectral measurements, and their integration with NIRS. The correlation values between measured and predicted SQI values was $R^2 = 0.903$, $RPD = 2.46$, $RMSEC = 0.034$, and $RMSECV = 0.057$. Spectral classifications resulted in high accuracy when segregating LUs, and with relatively lower values when comparing sampling sites. These results demonstrate the high effectiveness, predictability, and reliability of the NIRS model, even in such poor arid soils.

4.1 Soil Properties and the Soil Quality Index

Assessment of soil quality was done through an understanding of natural and anthropogenic processes that affect expected soil processes, land use, and management practices, which are represented by a set of multiple different soil properties. This measurement and analysis process of multiple soil properties usually results in high costs and time consumption. The SMAF protocols were used as a guideline for selecting the soil indicators with adjustments that were applied to the physical,

biological, and chemical soil properties for developing a statistically modeled integrative SQI. This research sought to evaluate how soil quality and properties are affected under varying LU and management practices. To achieve this goal, data underwent processing and statistical methods, such as logistic transformations and PCA, to define the correct indicators with which to build the appropriate soil quality model. Since this study emphasized soil quality differences in an arid area, the soil indicators were transformed using a scoring function, in which the natural LU was set as a reference when comparing the other two anthropogenic LUs.

The SQI scores showed that in most cases, significant differences were identified. When looking at the mean overall SQI scores, the central agricultural LU was the only one to show significantly higher values. This may imply better soil management of the central agro-ecosystem sampling sites, for which the chemical components (including soil salinity indicators and soil nutrients) had significantly higher values, indicating low saline and well-fertilized soils. This finding is well correlated with higher physical SQI component scores, represented by AWC, indicating well-irrigated fields in the central part, unlike the SQI scores for agriculture in the north that showed an opposite trend (Gupta and Huang, 2014). As expected in an arid area, the AWC levels showed much lower scores in the natural LU in both the central and southern parts, whereas the northern agriculture LU showed relatively similar scores to those of the natural LU; this may indicate poor irrigation in comparison to the central part. For the biological properties represented by NO_3^- and SOM, in all locations, the natural LU displayed significantly lower scores due to low vegetation abundance, fertilizers, and manure input to the soil and livestock activity (Haynes and Naidu, 1998). The high scores of this component for the grazing LU in all geographical units affirm the effects of herding, such as grazing, trampling, urination, and feces, particularly on the levels of pH (Smet and Ward, 2006), soil organic matter (Smet and Ward, 2009), and nitrogen and phosphorus (Perkins and Thomas, 1993).

The results demonstrate that soil quality under different LUs can be measured and distinguished when using an appropriate number of soil indicators. On the one hand, the ability to calculate and produce a reliable and accurate tool for soil quality assessment constitutes the SQI model's significant advantage. On the other hand, the creation of such a tool remains expensive, include extensive soil analyses, and although accurate, it is still explanatory for the point-scale only. Therefore, the correlation to spectral data was performed to reduce the dependence on costly and prolonged soil sampling and laboratory analysis procedures.

4.2 Soil properties and SQI correlations with soil spectroscopy

The results showed that the model managed to predict most soil properties accurately, as well as the SQI (Fig. 6B), when correlated against their respective spectral measurements using PLS-R analysis. In order to evaluate and compare each of the soil properties' prediction performance, the RPD was calculated. The successful prediction performance scores were placed in "excellent" (RPD > 2.5), including EC, Cl, Na, Ca + Mg and SAR, and "good" (2 < RPD < 2.5) categories, including NO₃⁻, P, and SOM. The prediction accuracy of each soil property may vary under different locations, and environmental and practical conditions, such as topography, soil composition, time of the year, land and soil management, etc., as well as by sampling point group sizes and numbers and heterogeneous representations of the study area's spatial variability. This can also be seen by the RMSEC and RMSECV values for each soil property. For example, indicators with high RPD scores, such as soil salinity properties (e.g., EC, Cl, Na, Ca + Mg and SAR), also have smaller calibration and cross-validation errors and prediction intervals than other properties, such as NO₃⁻ and P. In this study, higher R² and RPD values are well correlated with lower RMSEC and RMSECV values and present smaller prediction intervals, which confirm the success of the prediction models. RMSEC represents the error of the calibration model, and its error value is always smaller than the one of the RMSECV due to the larger number of observations, which minimizes error sizes (Wise et al., 2006). Trends can be seen in the PLS-R correlation plots in Fig. 6A. For example, as mentioned in the previous section, soil salinity properties showed significant differences in the agricultural LU between the northern and the central parts. Higher values, which correspond to the under-treated fields in the northern part, are distinct from the lower salinity levels in the well-managed fields in the center. This corresponds to the higher SQI scores shown in Fig. 6B. Similarly, SOM concentrations were significantly higher under the agricultural and grazing LUs, whereas in the natural soils, the spectral regression confirmed much lower levels. The same is true for soil nutrients such as NO₃ and P. The prediction of overall SQI (Table 5, Fig. 6B) resulted in "good" performance values (R² = 0.903, RPD = 2.46, RMSEC = 0.034, RMSECV = 0.057). This was made possible not only by each soil property's contribution to the model but also by the interaction between them all and the spectroscopy data under an integrative index approach.

The PLS-R analysis also generated the recognition of significant sensitivity bands for soil properties. The detection of differences between LUs and sampling sites based on spectral-specific bands can be attributed to chromophores. Chromophores are defined by their physical and chemical interactions with electromagnetic radiation, which affect certain spectral regions, notably in the VIS-NIR (IUPAC, 1994), although many elements in the soil show sensitivity in the SWIR region as well (Ben Dor et al., 2015). Prevalent molecular bonds, such as C-H, N-H, C-O, C-N, and O-H groups, create different chromophores (Bushong et al., 2015; Fidêncio et al., 2002). Hence, they allow the

detection of a variety of soil properties, such as SOM, AWC, EC, pH, and soil texture characteristics (Cécillon et al., 2009; Gholizadeh et al., 2013; Knadel and Katuwal, 2018). The results of the highly significant soil salinity indicators within the 1350–1450 nm, 1830–1990 nm, and 2200–2350 nm spectral ranges are attributed to the presence of hygroscopic water and carbonate, which derives from the predominant sandy-loam soil texture (Table 2) (Ben Dor et al., 2015). Sensitivity bands for the biological properties, including SOM and NO₃, were generated by the model as well, in which SOM peak wavelengths were found in several regions across the VIS-NIR-SWIR. For SOM, the presence of organic matter (i.e., plant tissues, humus, manure, etc.) is connected to the C–H bond and VIS-NIR absorption peaks at the wavelength range of 590–739 nm, and microbial activity and water retained in the soil and in the organic matter itself generated the peaks at 1350–1450 nm and 2200–2350 nm, respectively (Ben-dor, 2017). Although nitrogen is known for its lack of direct universal absorption wavelengths (Yong et al., 2015), it can be measured by indirect absorption of the soil features mentioned above. The model for NO₃ found several sensitivity bands, notably at 562, 1420, 1901, and 1974 nm, related to water absorbed in the organic compounds, and at 1773 nm, which can be related to free and/or structural iron content (Ben-Dor and Banin, 1995; Rinnan and Rinnan, 2007). The resultant bands for the SQI prediction comprise the most dominant contributors to the model's variability and sensitivity. Hence, the strongest significances are attributed to water absorption, organic matter, and carbonate abundance, with their respective wavelengths previously mentioned.

These results strengthen the use of NIRS as a reliable, non-destructive, and time-efficient tool for soil quality analysis. Soil spectroscopy stands out as an adequate and reliable approach for individual soil properties and the multivariate evaluation of SQI. Thus, PLS-R is suitable as a time- and cost-efficient method for analyzing a big dataset of soil samples under a broad set of variables testing soil quality.

4.3 LU and sampling sites' spectral classification

To test the capabilities of the spectral signatures' classification in the model, a partial least squares discriminant-analysis (PLS-DA) was calculated for both different LUs and sampling sites. For the LU-based classifications, both the overall accuracy and the Kappa coefficient had an absolute value of 1. This indicates the success of the model to predict and classify the data accurately. For the sampling site classification (Fig. 7B), the performances were less accurate. Both the overall accuracy and the Kappa coefficient results were significantly lower than those of the LU-based classification, resulting in more significant spectral mixing among groups, possibly due to the smaller sampling size. Hence, it could be concluded that the success of the classification is affected by a set of influencing factors, including the spectral separability and variance between classes, the number of

grouping classes, the sample number, the spectral resolution, the noise-induced mistakes, and the modification of raw spectral signatures using PPTs. The PPTs transform and enhance the spectral separability between classes and strengthen the grouping factor within each category, hence, improving the classification accuracy of the model. In this study, the autoscale transformation and GLSW were applied and resulted in the best separation between classes, the smallest CV errors, and the highest classification accuracy.

5. Conclusions

In this study, we aimed to demonstrate the effects of LU activity, represented by human-dominated LUs, on the natural landscape in an arid environment, by evaluating and comparing their soil quality. This goal was achieved by conducting a comparative analysis of both soil laboratory surveys and reflectance spectroscopy of the VIS-NIR-SWIR spectral regions. The ability to differentiate between physical, biological, and chemical soil properties plays a major role in the SQI model in recognizing and characterizing various soil processes in an integrative approach. The transformation scoring functions of soil attributes, as an adjustment tool for SQI, is a key principle that makes the SQI model suitable for monitoring the soil quality differences in soil properties between different LUs. The addition of the spectral dimension into the analysis has proved the effectiveness of NIRS as a comprehensive, non-destructive, and time- and cost-efficient method for monitoring and assessing soil quality and a variety of soil properties based solely on spectral differences. Results back these claims, in which the predicted SQI scores are well correlated with their calculated values ($R^2 = 0.903$, $RPD = 2.46$, $RMSEC = 0.034$, $RMSECV = 0.057$). Almost all soil properties could be predicted with at least “moderate” performance value, although only those with “good” and “excellent” scores are likely to be used as model prediction accuracy representatives. The implementation of advanced mathematical and statistical methods, such as linear parametric transformations, PCA, PLS-R, and PLS-DA, helps to solve the challenges linked to the multi-dimensional and high-collinearity of some variables in the analysis process. This advantage is reflected in the significant improvement of the results, demonstrating the soil property and SQI prediction accuracy. However, despite its excellent performance, the model is spatially limited to a site-specific point scale. To provide a complete accurate assessment of an entire region’s soil quality, upscaling of the spectral resolution would be necessary in future research. This would enable the SQI to be mapped at any given location, which would deepen the understanding of soil functions’ spatial trends and improve land management sustainability and conservation in the future.

Acknowledgments

The project leading to this research was partially funded by the European Union’s Horizon 2020 Research and Innovation Programme under grant agreements no. 641762 (Ecopotential).

Chapter 2: Soil quality index for assessing phosphate mining restoration in a hyper-arid environment

Levi N, Hillel N, Zaady E, Rtem G, Ziv, Y, Karnieli, A., and Paz-Kagan T. 2020. Soil quality index for assessing phosphate mining restoration in a hyper-arid environment. *Ecological Indicators*. 125: 107571. (IF= 4.858; Category: Environmental science; Rank= 72/274 (Q1)). <https://doi.org/10.1016/j.ecolind.2021.107571>

1. Introduction

Mining contributes significantly to economic development at both the local and global levels. However, these contributions are frequently accompanied by extensive environmental damage, such as widespread land degradation, water, and air pollution, and other environmental disturbances (Feng et al., 2019). Mining entails the removal of vegetation, soil seed-banks, and topsoil layers, which alters the landscape, changing surface and subsurface hydrology, and causing soil quality deterioration (Martins et al., 2020). Therefore, the ecological restoration of mining areas presents a significant challenge (Zou, 2019). Mining restoration can be applied in three main techniques: (1) reclamation aims to stabilize the land surface and to return the surface to its original topography, mainly as an aesthetic improvement and to ensure public safety; (2) rehabilitation intends to transform the land into a different state than the original one by repairing the impact of mining and improving land productivity (Aronson et al., 1993; Mensah, 2015); and (3) restoration that seeks to return the land to its original function and conditions, thus restoring the ecosystem that was degraded or damaged to its previous state (Maiti, 2012). Although full recovery of the ecosystem function and structure is almost impossible in the short run, the recovery processes can be examined by selecting pre-defined indicators to evaluate restoration success (Bradshaw, 1997). The massive damage caused by mining has led many countries to establish restoration and rehabilitation policies (Maiti and Ahirwal, 2019). Therefore, selecting reliable indicators to assess restoration success is necessary for determining policy and decision making.

Restoration processes include two types of practices: active and passive. The active-type procedures are based on human intervention, such as topsoil and seedling application and plantation. The passive type is established upon natural regeneration processes (Bandyopadhyay and Maiti, 2019). Many studies have proposed various indicators to evaluate mining restoration (Bandyopadhyay and Maiti, 2019; Borges et al., 2019; Toktar et al., 2016; Wang et al., 2018). These indicators are divided into six groups, including soil quality assessment, enzymatic activity, litter accumulation and decomposition, plant cover and species composition, faunal communities, microbial communities, and biomarkers (Bandyopadhyay and Maiti, 2019). One of the means for assessing mine restoration is by using the soil quality approach. Soil quality, which considers several

physical, biological, and chemical soil properties, refers to the soil's capacity to sustain and support its health and productivity within the related ecosystem (Karlen et al., 1997; Lal, 2011). Assessment of soil quality is often discussed in the context of agricultural activities (Doran and Zeiss, 2000; Lal, 2015), whereas less attention has been given to other practices, such as mining (Borůvka et al., 2012; Menta et al., 2014; Muñoz-Rojas, 2018). Therefore, defining soil quality indicators by selecting soil properties for evaluating restoration practices that include adding topsoil is an essential step in determining their success.

The soil quality index (SQI) is a diagnostic procedure to evaluate soil function and overall health. The SQI usually integrates physical, biological, and chemical properties into a single weighted number (Bastida et al., 2008). The selected soil properties need to be relevant to soil processes, consistent, reproducible, and relatively easy and affordable to sample (Bünemann et al., 2018; Moebius-Clune, 2017). The physical properties examined to assess restoration success are related to soil structure, including texture, bulk density, water holding capacity, infiltration rate, penetration resistance, available water content, and aggregate stability (Bandyopadhyay and Maiti, 2019). Biological properties refer to macro- and micro-organisms in the soil, such as microbial biomass, respiration, community composition, and enzymatic activity (Muñoz-Rojas, 2018), as well as processes related to soil organic matter and active carbon (Sheoran et al., 2010). The soil chemical properties include pH, salinity, nutrient availability (e.g., ammonium (NH_4^+), nitrite (NO_3^-), phosphorus (P), and potassium (K)), cation-exchange capacity, nutrient cycling, and heavy metals content (Dunger and Voigtländer 2005; Gómez-Sagasti et al., 2012; Melgar-Ramírez et al., 2012; Sheoran et al., 2010). The physical, biological, and chemical soil properties are interlinked, affecting biocrust and vegetation regeneration and growth. For example, low pH increases the solubility of naturally occurring micro-nutrients (e.g., Fe, Mn, Cu) to toxic levels, limiting most plants' growth in mining areas (Wong, 2003). Therefore, a holistic approach for assessing soil quality is a valuable asset in evaluating restoration success in mining areas.

Each soil property should be carefully considered to avoid time-consuming and costly efforts while enabling an adequate restoration success assessment. Thus, the first step in developing an SQI is selecting the most suitable and relevant properties and creating a minimal dataset that best represents the soil characteristics and management practices (Asensio et al., 2013; Karlen et al., 2003; Puglisi et al., 2006). Once the minimal dataset is established, each soil property is then transformed into unitless scores, allowing the grouping of the selected properties to produce a single scaled value ranging from 0 to 1 (Andrews et al., 2002; Karlen et al., 2003). The SQI is then weighted by a PCA and/or summarized to calculate the overall SQI. The uses of SQIs are varied, and they are applied to assess agricultural, natural, and polluted soils (e.g., Armenise et al., 2013; Beniston et al., 2016;

Karlen et al., 2003; Levi et al., 2020; Masto et al., 2008; Paz-Kagan et al., 2015). Less frequently, these indices have been applied to determine management effects on restoration success in open-pit mines (Asensio et al., 2013; Mukhopadhyay et al., 2014; Pietrzykowski, 2014). Moreover, although the SQI has proved to be a highly reliable approach, it has seldom been applied in arid environments (Blecker et al., 2012). Since arid soils are often alkaline and highly saline, have a low nutrient and organic matter content, and are generally more erodible (Mendez and Maier, 2008), restoration of degraded soil is a slow and complicated process (Yirdaw et al., 2017). All these characteristics highlight the challenges in the recovery of degraded mining areas in hyper-arid environments and the need to select appropriate soil properties to determine the overall SQI.

The present study strives to evaluate the effects of restoration practices (i.e., topsoil restoration) on soil quality properties compared to adjacent natural areas in an open-pit phosphate mine in a hyper-arid region of Israel. It should be noted that the topsoil mostly contains soil organic matter (SOM), nutrients, and plant seed banks (Borůvka et al., 2012), and is the habitat of soil microbiota, all supporting the overall soil restoration (Bowker et al., 2005; Visser et al., 1984). Therefore, it has been shown that using topsoil as an amendment improves the physical, biological, and chemical properties for ecological soil restoration in mines (McGinnies and Nicholas, 1980; Mensah, 2015; Sheoran et al., 2010; Visser et al., 1984). Accordingly, our first goal was to find out whether an area to which the topsoil conservation method was applied resembles the adjacent natural area in terms of soil properties and overall soil quality, despite the extreme environmental and climatic conditions in this hyper-arid region. Our second goal was to evaluate the restoration success based on the SQI approach as a function of time by comparing the different restoration stages applied in various sites. Therefore, the hypothesis is that the topsoil method in mines would enhance overall SQI and restoration efforts, where the timespan since restoration would also affect the emerging processes due to the poor, slow soil development in such a hyper-arid environment.

2. Methods

2.1 Study area and mining restoration practices

The study took place in an open-pit phosphate mine in the Negev Desert, Israel. The Zin phosphate mine includes 30.4 km² that have been mined over the last four decades (Figure 1). It is one of several mining fields located at the eastern edge of the Negev Highlands. The local climate is hyper-arid with a long-term annual average rainfall of about 50 mm and high potential evapotranspiration rates. The long-term monthly average temperature is 26°C during the summer months of July and August, and 10°C during the winter month of January (Israel Meteorological Service, IMS). The geology of the study area is characterized by a sequence of the northeast to

southwest trending synclines and anticlines formed during the Upper Cretaceous geological period, about 72–84 MYA. Flooding of the area in geological times resulted in the deposition of marine sediments, reflecting high productivity (Soudry, 1992). The phosphate deposits are layered within sequences of cherts, chalk carbonates, and limestone, located mainly at the northern edge of the synclines (Nathan et al., 1997). The rich phosphate deposit comprises approximately 2–6 layers (0.5–1.5 m thickness), mixed with other (low-level) phosphate layers that are not relevant for mining. The phosphate deposit rock is from the same geological period and is part of the Mediterranean phosphate belt that extends from Turkey through Jordan to Israel.

The Zin mining site has been active since the 1970s and is the largest of its kind in Israel. Until the 1990s, minimal efforts were made to rehabilitate the area. These efforts mainly included redistributing the overburden into the open pit and stabilizing the surface using road rollers to return it to its original topography and were prevalent until the beginning of the 1990s. However, for the past 20 years, the mining practices have changed towards a more ecological restoration approach that includes topsoil applications with the following steps. First, topsoil (upper 50 cm) is removed and kept separately. According to the original topography, the overburden is then returned to the open pit after mining and rearranged into a predetermined geo-morphological design. Finally, the topsoil that was removed from an adjacent open-pit mining area is placed over the fill material and turned over to increase the large stone cover (Cohen-Golan, 2017). This method enables a rapid placement of the topsoil rather than piling it up over time (Ghose, 2004). The restored site is returned to its original topography and is designed to slow runoff to create micro-climate conditions and diverse habitats, to enhance efforts to restore the soil micro-organisms, seed banks, and biocrusts. The applied restoration practice has a substantial impact on soil quality indicators, as seen in various sites at different timespans since restoration (Menta et al., 2014). In this study, three restoration sites of three different time periods since restoration were evaluated and compared to their adjacent natural areas, based on the SQI approach.

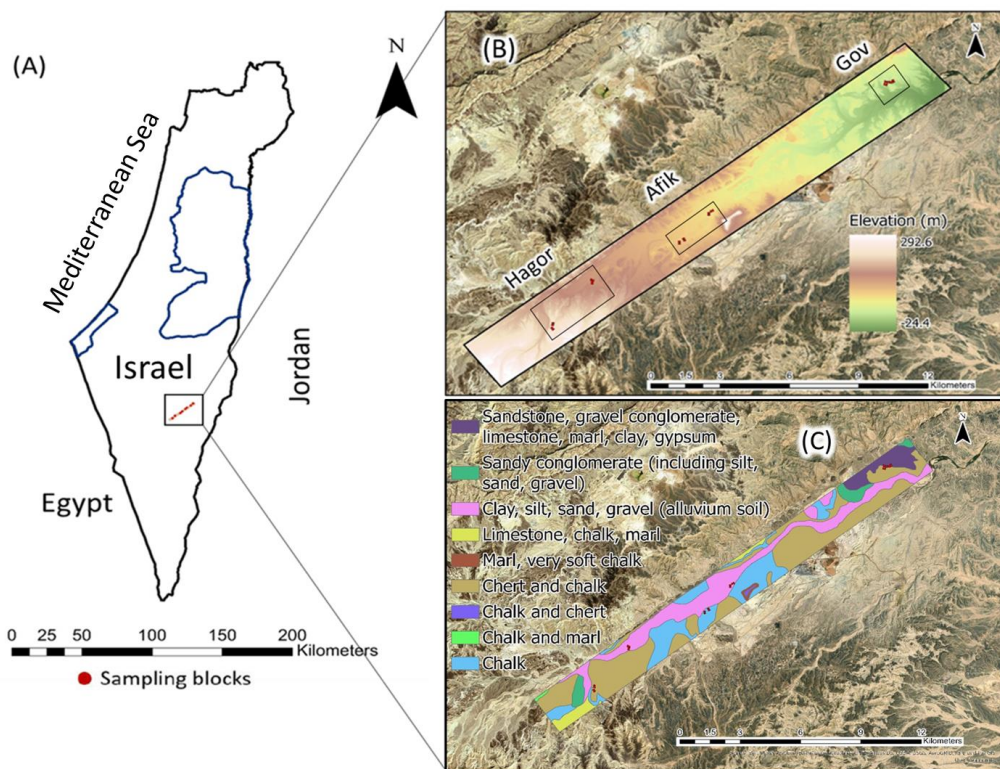


Figure 1: Schematic map with the location of the Zin phosphate mining field (A); Zin mining field topographic (B); and geological map (C) with the sampling blocks of the three study sites of Gov, Afik, and Hagor (red points).

2.2 Soil sampling design

Three restoration sites at the Zin open-pit phosphate mines were chosen for the study, representing both temporal and spatial variations. The restoration sites include the Gov, Hagor, and Afik sites. These sites were restored at different periods, in 2007, 2010, and 2014, respectively. Soil sampling in all sites took place during April 2017. The experimental design includes two pre-designated plots of 50×100 m, divided into 100-m^2 grid cells. To compare the restored sites with the adjacent natural area, we selected a nearby undisturbed natural site. Two additional pre-designated plots of 50×100 m divided into 100-m^2 grid cells were established (Figure 1). Five soil samples were collected from the four corners and the center of the grid cells in each plot for each block, resulting in a total number of 60 soil samples of 30 restored and 30 natural samples, classified by their respective restoration site. For each of the soil samples, 15 soil properties were selected to evaluate the overall SQI. Samples were collected in paper bags from a depth of up to 20 cm and transferred to the laboratory for wet chemistry analysis. Therefore, the soil samples represent only the upper layer of the topsoil to evaluate the restoration processes and biocrust development in this hyper-arid region. In addition, samples for biocrust analysis were collected in 64-cm^2 Petri-dishes. Penetration and infiltration rates were measured in the field for all soil samples.

2.3 Selecting soil properties

Overall, 15 soil properties were selected due to their relevance to mining restoration success. These were divided into physical, chemical, and biological properties. Table 1 shows the selected properties and their importance for the soil quality assessment in evaluating restoration success. The physical properties include soil texture (sand, silt, and clay fraction) for determining water storage and the infiltration rate. The available water content (AWC) was used to assess water availability in the soil, water storage capacity, and drought resistance. AWC is the difference between water stored in a field capacity and at the wilting point (Schindelbeck et al., 2008). The infiltration rate indicates hydrological processes, such as runoff, infiltration, and soil moisture. Dryland soils support rich microphytic communities that are critically important for developing and establishing biocrust cover, which regulates water delivery and retention, reduces surface ponding, inhibits runoff and sediment production, and improves moisture storage (Eldridge et al., 2020). Yet, biocrust are also clearly physical features of the soil, given that the component organisms are in direct contact with the upper soil surface layer (Bowker et al., 2018). Thus, biocrusts development regulates hydrological processes and plays an essential role as ecosystem engineers (Jones et al., 1997), enhancing ecosystem quality in a hyper-arid context. The biological properties include soil organic matter (SOM), related to nutrient storage, and water availability in the soil. Soil protein and polysaccharides are related to micro-organisms and biocrust development. The chemical soil properties include pH, electrical conductivity (EC), and its derivatives, comprising sodium (Na), calcium and magnesium (Ca + Mg), and chlorine (Cl), which are related to soil salinization and salt content. Also, phosphorus (P), potassium (K), nitrate (N-NO₃⁻), and ammonium (N-NH₄⁺) were extracted. These elements are related to nutrient content and use efficiency, which are necessary components for plant regeneration, growth, and health.

Table 1 depicts the selected soil properties and the analytical method applied for their analysis in the laboratory. Soil texture refers to a mixture of mineral particle sizes and the fraction of sand, silt, and clay in the evaluated soil, based on Schindelbeck et al. (2008). Thus, soil texture is not part of the SQI since it is a relatively constant and mostly descriptive parameter (Karlen et al., 2003). However, soil texture is essential to interpret most soil properties in the SQI. Available water content (AWC) was measured by calculating the differences between saturated soil (i.e., water content at field capacity) and the permanent wilting point based on soil physical and hydraulic properties according to soil texture (Farrick et al., 2019). The infiltration rate was measured in-situ using a mini-disk infiltrometer (Madsen and Chandler, 2007). Soil organic matter (SOM) was measured by oven-drying the soil samples for 3 h at 105°C, followed by burning the soil at 500°C for another 2 h and weighing the soil samples before and after burning (Casida et al., 1964). Potassium chloride

extractions were measured to evaluate the extractable nitrate (NO_3^-) and ammonium (NH_4^+) content (Drinkwater et al., 2015). Soil proteins were measured by the Lowry method, extracted by 0.1 N NaOH (Lowry et al., 1951), and polysaccharides were measured by sulfuric acid extraction. Soil nutrients (P, K, Na, Ca, Mg) were analyzed by inductively coupled plasma mass spectrometry (ICP-MS), using an ammonium acetate and acetic acid solution (Brady and Weil, 1999). The pH values were determined by using a pH electrode probe. Finally, EC was measured using an EC meter on well-stirred soil.

Table 1. Soil properties for soil quality assessment in open-pit phosphate mines, their functions, their laboratory chemical analysis methods, and their measurement units.

Indicator	Reason for selection	Unit	Method
<i>Physical</i>			
Soil texture (sand, silt, and clay)	Related to SOM levels, defines water storage in the soil and infiltration rate.	%	Particle size suspension
Available water content (AWC)	Explains potential soil water availability, plant available water storage capacity, and drought resistance	%	Oven drying
Infiltration rate	Explains potential runoff, soil erosion and leaching, soil porosity, and compaction	cm/sec	Mini-disc infiltrometer (Madsen and Chandler, 2007)
<i>Chemical</i>			
pH	Influences plant growth, toxicities, and metals availability, affecting the available macro and micro-nutrients		Water-soil suspension
Electrical conductivity	Defines soil salinity, affecting plant growth	dS/m	Water-soil suspension ICP-MS
Cl	Defines soil salinity, affecting plant growth	mg/L	
Na	Defines soil salinity, affecting plant growth	mg/L	
Ca + Mg	Defines soil salinity, affecting plant growth	mg/L	
N-NO₃	N containing life-building blocks, N release	mg/kg	
N-NH₄	N containing life-building blocks, N release	mg/kg	
Phosphorus (P)	Influences plant productivity, helps in mineralization of SOM, vital nutrients to plant development	mg/kg	
Potassium (K)	Influences plant productivity, helps in mineralization of SOM, vital nutrients to plant development	mg/kg	
<i>Biological</i>			
Soil organic matter	Source of nitrogen, phosphorus, and sulfur, improves aggregation and infiltration, increases water and nutrient availability	%	Organic carbon furnace method (Schulte, 1995)
Protein	Microbial abundance and activity and development of soil biological crust	mg/g	Lowry method, 0.1N NaOH (Lowry et al., 1951)
Polysaccharides	Microbial abundance and activity and development of soil biological crust	mg/g	Anthron, sulfuric acid (Dische, 1955)

2.4 Soil quality index development

SQI development involves several statistical steps. The first step is to transform all properties into unitless scores ranging from 0 to 1. This process is necessary to standardize each soil property so they will have comparable units. However, before applying the transformation functions (Figure 2), outlier detection and removal and missing data completion based on a regression imputation was applied (Dumedah and Coulibaly, 2011). The median absolute deviation (MAD) approach for removing a minimum number of outliers to exclude only the most extreme values was used. Thus, only outliers that were either higher or lower than three standard deviations around the median were removed (Levi et al., 2020; Leys et al., 2013), resulting in a less than 5% reduction for each soil property. The second step involves calculating the SQI (Andrews et al., 2002; Paz-Kagan et al., 2015; Rezaei et al., 2006; Sharma et al., 2005). This step was performed by assigning one of three scoring functions to each indicator according to its performance and based on previous literature (Figure 2; Karlen et al., 2003; Mastro et al., 2008; Mukhopadhyay et al., 2014). To exclude highly correlated indicators from the SQI analysis, Wetschoreck et al. (2020) developed the predictive power score (PPS) method that normalizes the various pairwise relationships to their local baseline (values range from 0 to 1), both linear and non-linear correlations of higher dimensions, and also presumes asymmetry, where the two halves of the prediction matrix account for the direction of the relationship (i.e., $X \sim Y \neq Y \sim X$). Pairs of predicted scores with $PPS \geq 0.5$ were excluded. The PPS calculation scheme was imported from python into R (Zavarella, 2020), using the "reticulate" package (Ushey et al., 2020).

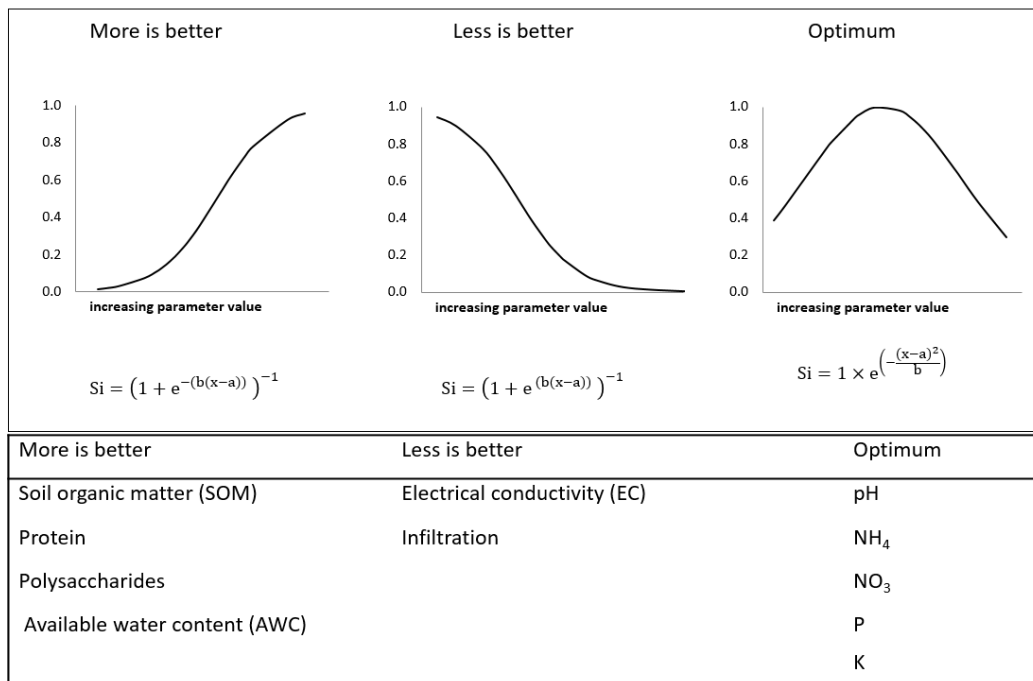


Figure 2. Scoring functions for data standardization, assigning the appropriate term and function to each soil property. S_i is the soil property score, x is the parameter value, a is the soil property average, and b is $2\sigma^2$ of the data. Graphs adapted from Karlen et al. (2003). AWC: available water content, SOM: soil organic matter, EC: electrical conductivity, K: potassium, and P: phosphorus.

The second step involves calculating the SQI (Andrews et al., 2002; Paz-Kagan et al., 2015; Rezaei et al., 2006; Sharma et al., 2005). The SQI calculation is based on a principal component analysis (PCA) on the scored data. The variance of the data is binned into statistically distinct low-covariable classes, named principal components (PCs), where each PC accounts for a portion of the model's variance, and the minimal number of the most explanatory PCs is selected to reduce the dimension and complexity of the model (Jolliffe et al., 2016). A PCA was calculated for all restoration sites combined and also for each separately. PCs with eigenvalues (i.e., weighted proportion of variance) greater than 1 and that also explain more than 5% of the model's variation were included in the model. The highest loadings, defined as having an absolute value within 10% of the highest factor loading for the soil indicators, were used to indicate the most influential PC on each soil property (Masto et al., 2008). However, the contrast among PCs for highest loadings wasn't distinct enough for some soil properties, which might create ambiguity arbitrary factor loadings than a significant relationship in the correlation matrix. Therefore, a varimax rotation PCA was applied to the results of the initial PCA (Kaiser, 1958). The rotation of the projected correlations enhances the variations, maximizes the contrasts among the selected amount of PCs, and maintains the total cumulative proportion of variance. The third step includes the final SQI calculation by dividing the proportion of each rotated principal component variance by the cumulative variance to generate the weights, which are then multiplied by the number of the highest correlated variables related to each rotated PC (Masto et al., 2008). Each indicator is then multiplied by its corresponding weight to calculate the overall SQI (Eq. 1). The scored values were multiplied with their weighted values for calculating the soil quality index (SQI):

$$SQI = \sum_{i=1}^n PW_i \times S_i' \quad (1)$$

where PW_i is the PCA weighting factor, and S_i' is the scoring function's ranks of each soil property, indexed as i , and n is the total number of properties.

2.5 Statistical analysis

Once the scores and the SQI were calculated, the differences were tested for their significance between the treatments (natural vs. restored) for each soil property in each site and between sites, as

well as for the overall SQIs and their respective physical, biological, and chemical components. The sampling pattern includes spatially various sites that subsume multiple self-dependent plots with low variances within each. Therefore, the mixed-effects nested design analysis of variance (ANOVA) model (Schielzeth and Nakagawa, 2013) was used to examine significant differences, where sites and treatments were determined as fixed factors and the nested plots were defined as random. The ANOVA was first used to explore the overall success of the ecological restorations and their adjacent natural areas. Second, to measure differences between the individual study sites for each group of indicators—physical, biological, and chemical—and overall SQI scores. The basic assumptions of the ANOVA for normal distribution of the model's residuals and homoscedasticity of the scored properties were tested. The residual distribution histogram results of the mixed-effect ANOVA tests for the individual scored soil indicators are shown in Appendix A. For properties that had their assumptions unmet ($p < 0.05$), a non-parametric rank-transformation approach was used, where the scored values were gradually rated from lowest to highest scores (Conover and Iman, 1981) and were then compared using the nested ANOVA test. Multiple comparisons among all factor levels were calculated using the Tukey HSD test. The level of significance for the soil indicators and SQI was determined at $\alpha < 0.05$. The regular and the varimax rotation PCA, and the nested design ANOVA tests were performed using JMP® Pro software version 15.0.0 (SAS Institute Inc., Cary, NC, USA).

3. Results

3.1 Soil quality indicators

The results of the predictive power score (PPS) matrix for the scored soil properties show that Cl and Na were highly correlated with EC ($PPS_{(Cl \rightarrow EC)} = 0.7$ and $PPS_{(Na \rightarrow EC)} = 0.68$, respectively) and with each other. Although Mg + Ca correlation with EC was lower than 0.5 ($PPS_{(Cl \rightarrow EC)} = 0.48$), due to its relatively close value, it was joined with Cl and Na to be excluded from further discussion to prevent collinearity and redundancy in the SQI model (Figure 3). Also, relatively strong correlations were found for NO_3 and EC ($PPS_{(NO_3 \rightarrow EC)} = 0.4$) and Cl ($PPS_{(NO_3 \rightarrow Cl)} = 0.34$), but eventually, it remained in the SQI calculation model. In total, four out of the initial 15 properties were omitted from the SQI development, including the Cl, Na, and Ca + Mg that were highly correlated to EC and represent salinity indicators. The soil texture was not part of the SQI since it is a relatively constant and mostly descriptive parameter, so soil texture and its fractions were not included in the SQI calculation. Table 2 displays the results of the significant differences found for the scored soil properties in the nested ANOVA for the individual and combined restoration sites (i.e., Gov, Hagor, and Afik) compared to their adjacent natural areas. Most scored indicators were eligible for the nested ANOVA test using their scored values, whereas five were tested based on their ranked-transformed values, including pH, $N-NH_4^+$, $N-NO_3^-$, K, and proteins, as their basic assumption for normal

distribution of the model's residuals was unmet (Appendix A). The number of significantly different soil properties was reduced in response to the time since restoration. SOM was the only parameter to be consistently significant for all sites, and infiltration was significantly different at the younger Hagar and Afik sites. When comparing all restored plots and their natural counterparts, significant differences were found for four out of 11 indicators, including infiltration, SOM, polysaccharides, and P.

Figure 4 presents the box-whisker plot of all scored soil indicators, comparing each study site with its adjacent natural area. The spatial variability has no consistent increasing or decreasing pattern between the different sites and the time since restoration. The restored and related natural plots also displayed different trends within the study sites, mainly in the Afik study site. Despite being the most recently restored, the AWC, SOM, protein, and polysaccharide indicators showed generally higher scores than those of Hagar and Gov. In most cases, two study sites—Gov and Hagar—exhibited similar trends to each other with regard to their natural sites. The Hagar site presented a unique trend of slightly, yet not significantly, higher scores in the restored plots for some of the indicators, including AWC, proteins, and polysaccharides. The SOM indicator's differences were significant in all study sites, showing a similar trend in comparing restoration sites and their adjacent natural sites, with a higher SOM value in the natural sites. A high infiltration rate was found in all restored sites, with lower scores than their natural counterparts.

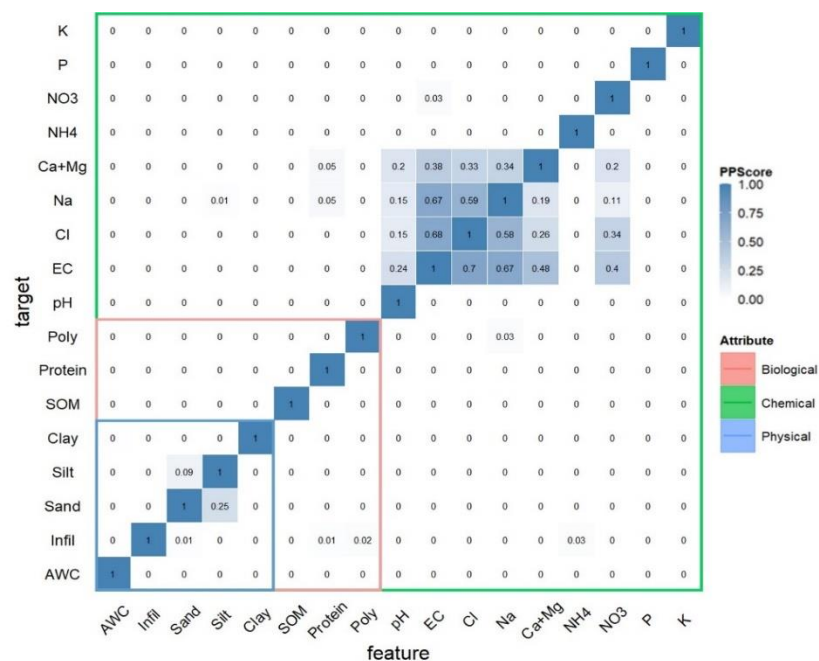


Figure 3. Predictive power score (PPS) matrix results for all the scored soil properties. Darker shades of blue represent stronger correlations between each pair of variables. The colored frames represent the associated physical, biological, and chemical components of the soil properties. SQI: soil quality index, AWC: available water content, SOM: soil organic matter, EC: electrical conductivity, K: potassium, P: phosphorus, and Poly: polysaccharides.

Table 2. Significant differences (p-values) between sites' restoration and their adjacent natural areas. Bold values are statistically significant ($\alpha < 0.05$)

Soil properties	Gov natural vs. restoration	Hagor natural vs. restoration	Afik natural vs. restoration	All-natural vs. restoration
AWC	0.988	0.766	0.424	0.963
Infiltration	0.848	0.002	0.005	0.005
pH	0.518	0.888	0.994	0.481
EC	0.837	0.868	0.986	0.748
N-NH ₄	0.487	0.999	0.017	0.125
N-NO ₃	0.029	0.985	0.984	0.548
P	0.779	0.043	0.994	0.024
K	0.245	0.763	0.275	0.442
SOM	0.037	0.000	0.000	0.000
Protein	0.252	0.691	0.818	0.314
Polysaccharides	0.694	0.611	0.008	0.033
Significant	2	3	4	4

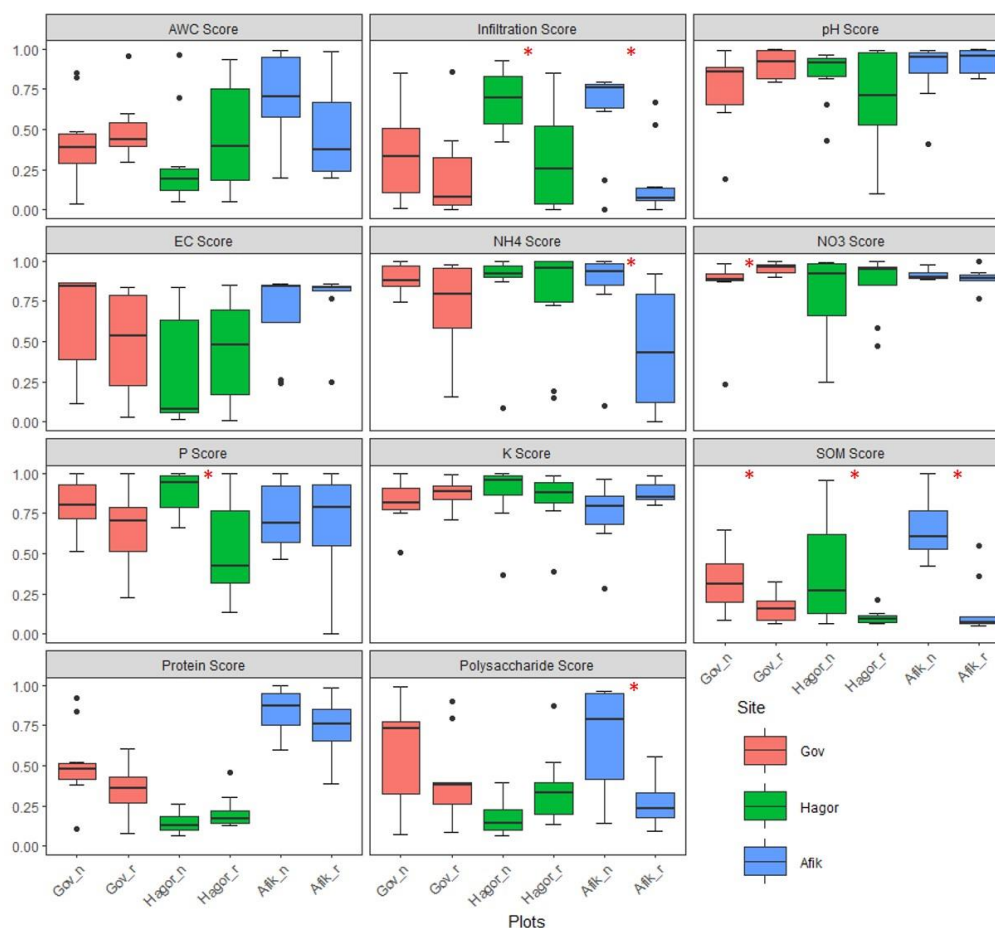


Figure 4. Box-whisker plot showing the value distributions and outliers of each of the soil properties in the natural and restored study sites. Red asterisks represent significant differences ($p < 0.05$) between treatments within sites. AWC: available water content, SOM: soil organic matter, EC: electrical conductivity, K: potassium, and P: phosphorus; n refers to the natural area, and r refers to restored.

3.2 Soil quality index

Figure 5 shows spider diagrams that demonstrate the differences between the natural and

restored plots. Values are given in unitless scores ranging from 0 to 1, based on the transformed properties' mean values. A combination of all sites shows noticeable differences in the physical, chemical, and biological soil properties. When observing the study sites separately, varying patterns emerge. In the Hagor and Afik sites, there is a clear difference between the spider patterns for each treatment, whereas, at the Gov site, the scoring values are relatively similar for most soil properties. Performing the PCA and applying the weights on the scored data translated the values into SQI scores, which allowed us to compare the topsoil restoration treatment with the natural soils relative to one another.

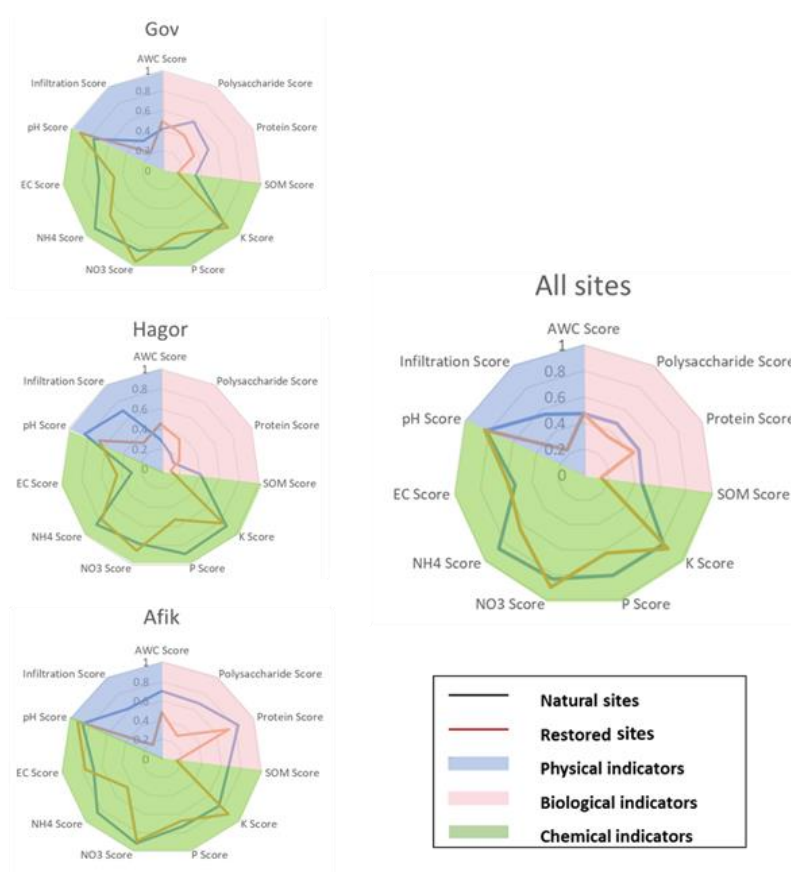


Figure 5. Spider diagrams showing the differences between the natural and restored plots in unitless scores. AWC: available water content, SOM: soil organic matter, EC: electrical conductivity, K: potassium, and P: phosphorus.

Based on the transformed physical, biological, and chemical data using the three scoring functions (Figure 2), the SQI was developed (Eq. 1). The SQI model was applied for each site separately and all sites together. The PCA for all sites combined showed that four PCs had eigenvalues greater than one and had a greater proportion of variance than 5%. However, PC5 had a very close eigenvalue of 0.993. Therefore, it was incorporated into the accounted PCs, which eventually explained 68.1% of the total cumulative variance. The respective enhanced varimax rotated factor loadings for the five PCs are presented in Table 3. The PCA models showed that Gov

had three, Hagor had five, and Afik had three PCs that met the two conditions, respectively. The models had an overall cumulative variance for the Gov, Hagor, and Afik sites of 65.9, 77.5, and 67.2%, respectively. The detailed varimax rotation PCA results for each site separately are shown in Appendix B.

Figure 6 presents the integration of the physical, biological, and chemical scores and the overall SQI for all three sites, independently and combined. The results reveal the significant differences between Gov, Afik, and all sites between natural and restored sites. The mean SQI scores for all sites combined were higher in the natural than in the restored sites ($F_{(1,48)} = 6.005$, $p < 0.05$), with 0.617 and 0.536 SQI values, respectively. Our results suggest that all the individual restored sites suffer from a reduction in their overall SQI values and reveal a trend in accordance with the time passed since restoration, where the oldest restored site of Gov scored highest (0.652 and 0.574 for natural and restored, respectively; $F_{(1,16)} = 2.642$, $p < 0.05$), followed by Hagor (0.615 and 0.552; $F_{(1,16)} = 0.712$, $p = 0.057$), and the most recently restored site, Afik, was ranked (0.608 and 0.507; $F_{(1,16)} = 10.364$, $p < 0.05$). The biological attributes presented significant differences between the natural and the restored areas, as found for the Gov, Afik, and all sites together ($F_{(1,48)} = 8.189$, $p < 0.05$). The physical properties presented significant differences between the natural and the restored areas in Afik and all sites together ($F_{(1,48)} = 4.031$, $p < 0.05$). In the chemical properties of the Hagor site, the soil indicators have significant differences between the natural and restored sites ($F_{(1,16)} = 4.039$, $p < 0.05$).

Table 3. Varimax rotation PCA results of all sites for scoring soil properties from the restored and the natural sites combined. The bolded soil properties refer to the absolute highest loading within 10% of the factor loading. The overall model had a cumulative percentage of 68.1%. AWC: available water content, SOM: soil organic matter, EC: electrical conductivity, K: potassium, and P: phosphorus. Bold numbers refer to the highest factor loading for each soil indicator by its corresponding PC.

	<i>PC1</i>	<i>PC2</i>	<i>PC3</i>	<i>PC4</i>	<i>PC5</i>
<i>Eigenvalues</i>	2.579	1.541	1.348	1.029	0.993
<i>Proportion of variance</i>	15.089	14.289	13.863	13.271	11.596
<i>Cumulative percentage</i>	15.089	29.378	43.241	56.512	68.108
<i>No. of properties</i>	2	4	2	2	1
<i>AWC Score</i>	0.128	-0.065	-0.672	0.395	-0.313
<i>Infiltration Score</i>	-0.226	-0.606	0.005	0.393	0.420
<i>pH Score</i>	0.129	0.490	-0.392	0.135	0.364
<i>EC Score</i>	0.662	0.100	-0.429	0.034	-0.041
<i>N-NH₄⁺ Score</i>	-0.058	-0.116	0.813	0.222	0.078
<i>N-NO₃⁻ Score</i>	0.325	0.608	-0.148	0.230	-0.101
<i>P Score</i>	0.055	0.029	0.214	-0.023	0.827
<i>K Score</i>	-0.199	0.747	0.037	-0.002	0.116
<i>SOM Score</i>	0.025	0.069	0.008	0.847	0.074
<i>Protein Score</i>	0.859	-0.007	0.010	0.037	0.099
<i>Polysaccharide Score</i>	0.497	0.060	0.068	0.556	-0.372

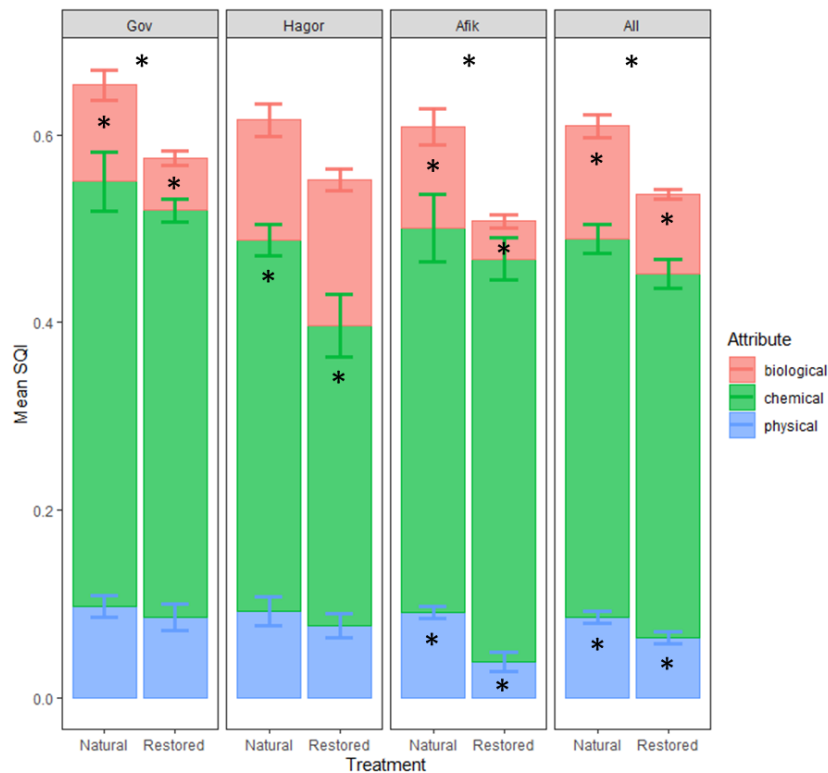


Figure 6. Stack graph of indicator groups for the restoration practice for each site and their combination. An asterisk under the site name represents an overall significant difference between the restoration practices. The asterisks within the colored bars show significant differences between the groups of indicators (i.e., biological, chemical, and physical).

4. Discussion

Mining restoration depends on the practices used and the time since the restoration was applied (Andrés and Mateos, 2006). Evaluating restoration success using the SQI approach could be used as a management tool, mainly in an arid environment where the vegetation is sparse. Most soil recovery processes are long-term (Costantini et al., 2016; Mukhopadhyay et al., 2014). Most studies on ecological mining restoration have focused on forest, grassland, and wetland ecosystems, while fewer have examined arid regions (Guan et al., 2019). Extensive literature exists on indicator selection for evaluating the ecological restoration success and recovery rate after mining (Martins et al., 2020). Several physical, biological, and chemical soil properties were suggested for developing the SQI to assess the effect of topsoil restoration practices (topsoil compared to the natural area) in phosphate mines in a hyper-arid region. The properties were selected and analyzed to determine the restoration efforts and identify spatial and temporal variations in the successional processes (Costantini et al., 2016). Significant differences in the SQI were found between several soil properties' scores and between SQI models in the different sites, indicating a general trend of higher SQI in the natural sites than in the restored ones. It was found that the biological indicators were the most affected properties with significant differences in Gov, Afik, and all sites together, followed by the physical ones with significant differences in, Afik and all sites, and the chemical components showing significant

differences only in Hagar site. Therefore, it is suggested that the selection of soil properties should focus more on soil biological and physical properties, which could help evaluate phosphate mines' restoration in an arid region.

4.1 Indicator selection: a minimum dataset for soil quality measurement

SQIs are useful tools to assess restoration efforts and evaluate the recovery rates (Muñoz-Rojas et al., 2016). Although some indicators could be more relevant than others for capturing soil differences (Bastida et al., 2008; Muñoz-Rojas et al., 2016), using one soil property constitutes a critical limitation (Muñoz-Rojas et al., 2016). Consequently, the SQI is increasingly used to estimate restoration success, determine the direction of change with time, and highlight the differences between restoration practices (Shukla et al., 2006). However, creating a minimum dataset by selecting indicators that can sufficiently and accurately assess mining restoration efforts is a complicated matter (Bünemann et al., 2018; Muñoz-Rojas et al., 2016). Our results demonstrate the need for further refinement after initially selecting a minimum dataset to reduce additional dataset complexity and adequately represent the soil quality conditions for arid regions. The soil properties with significant differences between mining areas and natural areas were infiltration rate, SOM, and polysaccharides. Previous studies have shown that SOM is a reliable soil indicator, pointing to mining restoration success and land degradation (Bodlák et al., 2012; Chaudhuri et al., 2015). SOM was one of the soil properties that showed a clear scoring reduction trend in the topsoil mining sites compared to the natural areas. Moreover, the infiltration rate showed a similar pattern in all sites with a higher infiltration rate in the restored sites, resulting in lower scores than natural sites. N-NH₄⁺, P, and K were selected as potential nutrient availability indicators since they are key nutrients, although only a small fraction may be available to plants (Andrés and Mateos, 2006). These are essential for the plant regeneration necessary for successful restoration processes in arid regions. Eventually, only P was found significant in the integrated model, whereas N-NH₄⁺ was significantly different in the Afik site only, and K had no notable differences in any of the sites.

Polysaccharides and proteins indicate biocrust development, which plays a considerable role in stabilizing the soil surface, affecting the infiltration rate that reduces erosion by water and wind in arid regions (Zaady et al., 2016). The development of biocrusts, composed of cyanobacteria, moss, and/or lichens, could be used as an indicator for mining soil recovery and restoration success (Dangi et al., 2012; Mukhopadhyay et al., 2017; Muñoz-Rojas et al., 2016). Restoration of mining areas accelerates the development of biocrust structures and functions to assess and speed up the recovery of a degraded ecosystem (Zaady et al., 2016). Soil micro-organisms' diversity and abundance provide surrogates for soil recovery. Polysaccharides are related to soil microbial biomass that is extensively used in SQI assessments (Mager and Thomas, 2011). Usually, increases in polysaccharides are

considered beneficial to soil development in arid regions (Mendoza-Aguilar et al., 2014). However, additional analyses, such as phospholipid fatty acid (PLFA), could be used to assess the difference in the microbial community over time and describe its structure and composition (Bandyopadhyay and Maiti, 2019; Ben-David et al., 2011; Dungait et al., 2011). Cyanobacteria are some of the most dominant life forms found in biocrusts in arid environments, including the Negev Desert (Chamizo et al., 2019; Ferrenberg et al., 2015; Karnieli et al., 1999; Zaady et al., 2010). Although biocrust only occupies the upper few millimeters of the soil profile (Dixon, 2009), cyanobacteria greatly influence different soil properties and the overall SQI in various ways. Cyanobacteria stabilize the soil surface, control runoff, infiltration, and percolation, increase the soil moisture content, and improve the nutrient content and soil fertility (Belnap, 2006; Chamizo et al., 2019; Kuske et al., 2012), which are all highly related to soil recovery after mining. Studies have shown that biocrust development affects hydrological processes in drylands, resulting in a decline in infiltration rate and soil moisture (Eldridge et al., 2020). These soil features are affected by the biocrust community composition and the soil properties (e.g., soil texture). Among the microbial communities, cyanobacteria are the most resilient (Belnap and Eldridge, 2001) and can survive on minimal and irregular amounts of water (Mazor et al., 1996), typical conditions in arid regions. Eventually, polysaccharides were significantly lower in the Afik site and in the combined model than restored and natural plots. These could be related to the time passed since restoration, where the Afik site is the youngest restored site—referring that the time passed since restoration wasn't enough for the biocrust to recover.

4.2 Evaluation of restoration practice with time since restoration

Soil quality estimations in restored mining areas either compare pre-and post-recovery conditions or disturbed land and nearby undisturbed land to assess the restoration process's rate and quality (Sheoran et al., 2010). By comparing the restoration practices between both the natural and restored sites, significant differences were seen across indicator groups (mainly biological and physical indicators) and overall SQI. Only a few significant differences between the natural and restored sites, as a result of topsoil restoration, were previously documented (Muñoz-Rojas et al., 2016). When observing each study site separately, significant differences between the natural and restored sites were found. The topsoil restoration practices mitigate the destructive severity of mining (Albert, 2015), thus, reducing the differences between the restored and natural plots, seen mainly at the Gov plot. In drylands, topsoil restoration is a critical practice due to the unpredictable climatic conditions with the potential for long and frequent droughts, along with the severely limited abundance of seeds, nutrients, and micro-organisms that are considered to be key elements in soil restoration, limit plant development, and growth in arid regions (Golos et al., 2016; Muñoz-Rojas et al., 2016).

We found that topsoil restoration enabled partial recovery of the Hagor and Gov sites. The period between the ecological restorations may have promoted natural restoration processes, as shown in the Gov site. However, the slightly higher levels of AWC, proteins, and polysaccharides in the restored plots shown at the Hagor site can be attributed to higher site suitability. Thus, low polysaccharide concentrations indicate a delay in biocrust development over the past 20 years. The initial process of soil recovery begins by establishing physical, followed by biological indicators, and therefore, the topsoil amendment method is crucial for promoting soil restoration efforts. Further study could test the differences in restoration practices with and without topsoil and their implications for soil quality and restoration success. Thus, integrating physical, chemical, and, more importantly, biological indicators necessary to evaluate soil recovery in arid environments.

4.3 Assessment of soil quality index

The SQI combines various soil properties to provide a single value representing the overall soil quality. The SQI approach, based on the varimax rotation PCA scores, was found to be valid for assessing mine restoration in arid regions (Asensio et al., 2013; Mukhopadhyay et al., 2014; Pietrzykowski, 2014). Defining restoration practices in mining areas required identifying specific soil indicators associated with soil quality (Menta et al., 2014). Our results show significant differences in most study sites, mainly due to biological indicators and physical soil indicators, such as SOM, infiltration rate, and polysaccharides, with a significant difference in these indicators between the natural and restored plots, as shown in the SQI (Figure 6). In contrast, the group of chemical indicators showed no significant differences between most sites for the overall soil quality (except for Hagor). The soil indicators used for this task may differ depending on local conditions and the disturbance's extent. Therefore, we concluded that restoring the physical biological soil indicators are complex process in mine restoration. These required rehabilitating the biological indicators of the biocrust community, which is crucial in hyper-arid areas. Biocrust has a multifunctional effect on soil function and structure. They regulate soil nutritional stocks through N fixation (Elbert et al., 2012), influencing hydrological processes (Chamizo et al., 2016) stabilizing soil, among other aspects. In general, our results reflect a slow recovery of the SQI in the restored sites, demonstrating that achieving the quality of the natural areas requires a long-term recovery process. Moreover, the physio-biological indicators were found to be more suitable for reliably assessing mining restoration practices.

5. Conclusions

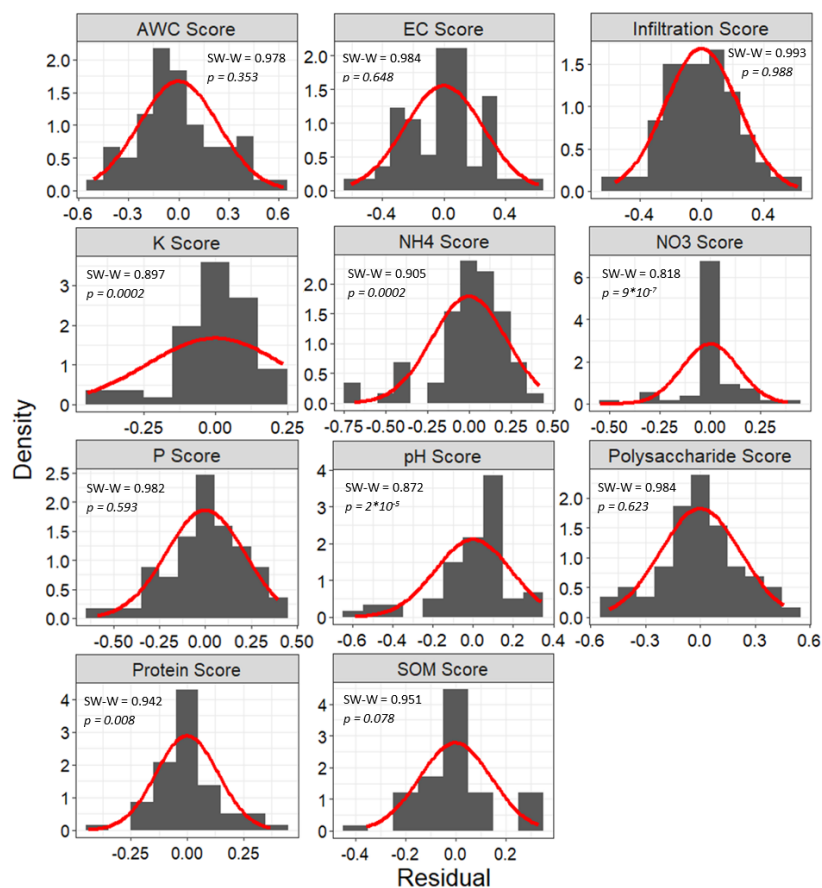
This study took place in an open-pit phosphate mining area, which is located in a hyper-arid environment. Developing an SQI and incorporating physical, biological, and chemical properties of soil restoration practice was accomplished. In conclusion, using the SQI method on the different

restored sites shows reduced soil quality compared to the natural sites. The biological and physical indicators demonstrate the importance of the topsoil restoration method for recovering the biocrust community. For the overall SQI, chemical indicators alone cannot significantly distinguish between restoration practices, either because of natural processes or the change in soil chemical characteristics during mining practices in such an arid environment. Given these results, further SQI assessments and restoration follow-ups should focus on the vitality and evolution of the soil microbial community and biocrust development after using the topsoil method in restored phosphate mines. Moreover, the groups of biological and physical indicators should be considered as the primary tools in any SQI assessment to estimate the recovery success of mining sites in arid areas, where vegetation is scarce and soil recovery is a long-term process.

Acknowledgments

We thank Abu-Glion H. and Shuker S. for their help in the field and laboratory work. We are profoundly grateful to the Israel Chemicals Ltd. company for their support and assistance throughout the research.

Appendix A. Residuals distribution histograms of the mixed-effect ANOVA tests for the individual scored soil indicators. The red curves represent the normal distribution for each of the indicators. Properties that had their residual normal distribution unmet ($p < 0.05$) were then transformed using the non-parametric rank-transformation method (Conover and Iman, 1981). ANOVA: analysis of variance, SW-W: Shapiro-Wilks W-test, AWC: available water content, EC: electrical conductivity, K: potassium, NH₄: ammonium, NO₃: nitrate, P: phosphorus, and SOM: soil organic matter.



Appendix B. PCA results for all soil properties from the: (1) Gov, (2) Hagor, and (3) Afik sites compared to their natural sites. Abbreviation: AWC: available water content, EC: electrical conductivity, P: phosphorus, K: potassium, SOM: soil organic matter and bold numbers refer to high factor loading for each PC.

(1) Gov model	PC1	PC2	PC3
Eigenvalues	3.113	2.178	1.958
Proportion of variance	28.308	19.806	17.802
Cumulative percentage	28.308	48.114	65.916
No. of properties	5	3	3
AWC Score	0.155	0.720	-0.268
Infiltration Score	-0.711	0.170	-0.188
pH Score	0.832	0.274	-0.289
EC Score	0.032	0.821	0.047
N-NH ₄ ⁺ Score	-0.511	-0.153	0.288
N-NO ₃ ⁻ Score	0.823	0.269	-0.142
P Score	0.255	0.384	0.460
K Score	0.916	-0.007	0.242
SOM Score	-0.214	0.237	0.820
Protein Score	0.017	-0.192	0.820
Polysaccharide Score	0.051	0.739	0.215

(2) Hagor model	PC1	PC2	PC3	PC4	PC5
Eigenvalues	2.018	1.967	1.783	1.578	1.181
Proportion of variance	18.352	17.889	16.21	14.353	10.739
Cumulative percentage	18.352	36.241	52.451	66.804	77.543
No. of properties	3	3	2	2	1
AWC Score	0.811	0.018	-0.362	-0.209	0.114
Infiltration Score	-0.189	0.699	0.084	-0.441	0.020
pH Score	0.050	0.085	0.039	0.015	0.892
EC Score	0.757	0.143	-0.045	0.010	-0.376
N-NH ₄ ⁺ Score	-0.839	0.134	-0.140	-0.063	-0.208
N-NO ₃ ⁻ Score	-0.045	-0.153	-0.145	0.932	-0.059
P Score	0.011	0.774	0.319	0.229	-0.023
K Score	-0.050	-0.119	0.874	-0.005	-0.090
SOM Score	-0.157	0.141	0.536	0.587	0.303
Protein Score	-0.124	-0.812	0.260	0.136	-0.131
Polysaccharide Score	0.038	-0.342	-0.617	0.227	-0.258

(3) Afik model	PC1	PC2	PC3
Eigenvalues	2.703	2.372	2.318
Proportion of variance	24.575	21.563	21.078
Cumulative percentage	24.575	46.138	67.216
No. of properties	4	3	4
AWC Score	0.007	0.595	-0.589
Infiltration Score	-0.052	0.403	0.588
pH Score	-0.437	-0.395	-0.286
EC Score	0.967	-0.130	-0.018
N-NH ₄ ⁺ Score	-0.021	0.123	0.622
N-NO ₃ ⁻ Score	0.913	0.128	-0.016
P Score	-0.115	-0.177	0.761
K Score	0.643	-0.157	-0.394
SOM Score	-0.120	0.897	-0.039
Protein Score	0.536	0.172	0.610
Polysaccharide Score	0.107	0.873	0.222

Chapter 3- Airborne imaging spectroscopy for assessing land-use effect on soil quality in drylands

Levi, N, Karnieli A, and Paz-Kagan, T. (2022). Airborne imaging spectroscopy for assessing the land-use effect on soil quality in drylands. *ISPRS journal of photogrammetry and remote sensing*. 186: 34-54. (IF=8.979; Category: geosciences multidisciplinary; Rank: 5/200 (Q1)). <https://doi.org/10.1016/j.isprsjprs.2022.01.018>

Table 1 – abbreviations list and acronyms used in the chapter.

Abbreviation	Definition	Abbreviation	Definition
ANOVA	Analysis Of Variance	NIRS	Near-Infrared Spectroscopy
ASD	Analytical Spectral Device	NO ₃ ⁻	Nitrate
AWC	Available Water Content	OA	Overall Accuracy
BRDF	Bidirectional Reflectance Distribution Function	P	Phosphorus
BREFCOR	BRDF Effect Correction	PC	Principal Component
Ca + Mg	Calcium and Magnesium	PCA	Principal Component Analysis
Cal	Calibration	PLS-DA	Partial Least Squares-Discriminant Analysis
Cl	Chlorine	PLS-R	Partial Least Squares-Regression
EC	Electrical Conductivity	PPS	Predictive Power Score
EMR	Electromagnetic Radiation	Pred	Prediction
EPSG	European Petroleum Survey Group	R ² _{adj}	Adjusted Coefficient of Determination
F(df)	F-statistic and Degrees of Freedom	RBF	Radial Basis Function
FWHM	Full Width at Half Maximum	RHS	Runoff-Harvesting System
GPS	Global Positioning System	RMSE	Root Mean Square Error
ICP-MS	Inductively Coupled Plasma-Mass Spectrometer	RPD	Ratio of Performance to Deviation
IMU	Inertial Measurement Unit	RPIQ	Ratio of Performance to Interquartile Range
IQR	Interquartile Range	SAR	Sodium Adsorption Ratio
IS	Imaging Spectroscopy	SD	Standard Deviation
K	Potassium	SMAF	Soil Management Assessment Framework
Kc	Kappa Coefficient	SNR	Signal to Noise ratio
LTER	Long-Term Ecological Research	SOM	Soil Organic Matter
LU	Land-Use	SQI	Soil Quality Index
LULC	Land-Use Land-Cover	SSQI	Spectral Soil Quality Index
LV	Latent Variable	SVM-R	Support Vector Machine-Regression
MAD	Median Absolute Deviation	SWIR	Shortwave Infrared
MDS	Minimum Data Set	Val	Validation
Na	Sodium	VIP	Variable Importance in Projection
NDVI	Normalized Difference Vegetation Index	VIS	Visible
NIR	Near-Infrared		

1. Introduction

Based on some scenarios, the global population might reach up to 12 billion people by the end of the century (UN-WPP, 2020). Consequently, providing food security and essential ecosystem services is necessary to maintain basic livelihood requirements, including habitat sustainability, shelter, and other necessities (FAO, 2019). Their provision often coerces the transformation of natural ecosystems into human-dominated lands on a global scale (Foley, 2005). Intensive land-use (LU) changes threaten environmental conditions and their ability to support ecosystem services sustainably. Such conditions include regulating natural aspects of climate, water, soil, and air quality (Metzger et al., 2006; Tschardt et al., 2005). LU changes often engender soil degradation processes and soil quality deterioration (Chesworth, 2008), and soil erosion (Alewell et al., 2019). These degradation processes undermine effective and sustainable land management and its related LU practices (Crist et al., 2017). Soil quality is determined by the ongoing soil physical, biological, and chemical processes occurring above and below the ground, affecting soil conditions (Idowu et al., 2008). In arid regions, the soil system under LU alteration is greatly susceptible to land degradation, such as soil salinization, erosion, structural modification, and organic matter and nutrient imbalance, mainly due to low organic resource and water availability (Lal, 1997).

Thus, appropriate soil quality evaluation approaches are necessary to monitor and mend the overall soil capacity to support ecosystem services (Doran and Parkin, 1994), especially for soils in dryland regions. Some soil quality assessment protocols, such as the comprehensive assessment of soil health (CASH; Idowu et al., 2008; Moebius-Clune et al., 2016), focus more on agriculture applications. Alternatively, the Soil Management Assessment Framework (SMAF; Andrews et al., 2002; Viscarra Rossel et al., 2006; Wienhold et al., 2009) is a method that allows flexibility in terms of selecting ad-hoc soil indicators under varying environmental conditions. The adoption of SMAF enables the soil quality model to be adjusted to different environments and management applications, as demonstrated in previous studies (Levi et al., 2021; Lima et al., 2016; Paz-kagan et al., 2016). It is based on selecting a minimum data set (MDS), comprising a minimum number of soil indicators (i.e., soil properties) for defining and quantifying soil conditions and function while avoiding model over-complexity. By doing so, the soil quality models are reproducible, easy to sample, and maintained at a relatively low cost (Andrews et al., 2004; Karlen et al., 1997). Once the MDS is selected, the indicators are transformed into a normalized score using different transformation functions, ranging from 0–1, then integrated into an index representing the overall soil quality index (SQI) value. In the context of ecological monitoring, resulting overall scores imply the degree of changes in their uninterrupted natural vicinity rather than

providing an absolute independent score.

Despite their accuracy, laboratory soil analyses and field surveys are still costly, time-consuming, and labor-intensive (Paz-Kagan et al., 2014). In the past few decades, the development and improvement of the near-infrared reflectance spectroscopy (NIRS) method have proven its efficiency as a rapid, reproducible, and relatively inexpensive method in remote sensing, in general, and soil spectroscopy, in particular, at the point scale. Spectroscopy measures the interactions between the studied surface (e.g., soil sample) and the incident electromagnetic radiation (EMR) by examining highly accurate point spectroscopy reflected signal that includes the visible (VIS, 400–700 nm), near-infrared (NIR, 700–1100 nm), and shortwave infrared (SWIR, 1100–2500 nm) spectral regions (Ben-Dor and Banin, 1995). Soil spectroscopy enables the detection of unique spectral absorption and reflection features (i.e., chromophores) in the spectral signature of a soil sample caused by the vibrations, stretching, and bending responses of soil minerals' elemental and molecular structures to EMR excitation (Ben Dor et al., 2015; Demattê et al., 2007). The use of spectroscopy in soil studies has been on the rise, proving its efficiency and expedience for various soil properties (Bogrekci and Lee, 2005; Freschet et al., 2011; Gholizadeh et al., 2013; Romsonti et al., 2018; Stafford et al., 2018). In recent years, efforts were made to collect, analyze, and establish worldwide open-access soil spectral libraries that store soil samples, including several fundamental soil properties analyses and their spectral attributes from 92 countries, to facilitate decision-support systems for farmers and land managers on global, continental, and national levels (Chabrillat et al., 2019; Demattê et al., 2019; Orgiazzi et al., 2018; Shi et al., 2014; Viscarra Rossel et al., 2016). These could be used to train and validate different soil models based on airborne and satellite imaging spectroscopy.

Soil spectroscopy was also most valuable for predicting SQI and other integrative assessment indices (Askari et al., 2015; Cécillon et al., 2009; Cohen et al., 2006; Kinoshita et al., 2012; Levi et al., 2020; Paz-Kagan et al., 2015, 2014; Vågen et al., 2006; Veum et al., 2017, 2015). For example, Kinoshita et al. (2012) estimated a three-category SQI in Western Kenya. Veum et al. (2015) estimated SMAF indicators and scores using VIS-NIR spectra and auxiliary laboratory data. Paz-Kagan et al. (2014) developed the spectral soil quality index (SSQI) to evaluate the overall SQI based solely on spectroscopy. Levi et al. (2020) predicted scores of soil attributes and SQI levels with reasonable accuracy. Currently, the use of hyperspectral data for SQI prediction usually corresponds to a more locale extent since it requires training the model with ground-truthing data according to the local soil characteristics. These applications were mainly demonstrated in temperate climates where the land-use had been changed into a few limited LU practices, mostly agricultural systems. The broad regional implementation is still a challenge due to the high soil spatial/geographical heterogeneity, on the one hand, and a large number of

soil samples needed for developing such models. Moreover, studies on soil spectroscopy applications for integrative soil monitoring in hyper-arid, arid, and semi-arid environments are rare (Levi et al., 2020; Paz-Kagan et al., 2015; Paz-Kagan et al., 2014). In the current research preceding this study, the integration of soil spectroscopy to assess the SQI method was performed in an arid region characterized by a water-scarce, nutrient-poor, and sparsely populated environment, with limited human activity (Levi et al., 2020).

Several statistical approaches incorporate spectroscopy for the regression-based spectral prediction of soil properties. Some algorithms are quite standard, such as partial least squares-regression (PLS-R; Rosero-Vlasova et al., 2016), support vector machine-regression (SVM-R; Shi et al., 2015), geographically weighted regression (GWR; Chen et al., 2019), and multiple linear regression (MLR; Rossel and Behrens, 2010). In recent years, additional models have been used in soil spectroscopy, such as random forest (RF; Wang et al., 2021), artificial neural network (ANN; Ayoubi et al., 2011), and other types of statistical estimation methods. Also, deep-learning NN-based feature training frameworks have been increasingly used to predict various soil properties spectrally in recent years (Padarian et al., 2019; Singh and Kasana, 2019; Tsakiridis et al., 2020; Yuan et al., 2020). Such deep-learning architectures usually require large sets of previously pre-processed data to reduce the risk of over-fitting (Srivastava et al., 2014). Therefore, conventional machine-learning regression models, such as PLS-R and SVM-R, are adequate for the task of a small-size sampling dataset (Deiss et al., 2020; Thissen et al., 2004). The SVM-R is a well-known method applied in soil spectroscopy that showed previous promising results (de Santana et al., 2021; Thissen et al., 2004; Xuemei and Jianshe, 2013). The statistical approaches affirm the accuracy, time-efficiency, and reliability of spectroscopy for soil quality assessment to determine a spectral sensitivity analysis. These could be applied for individual soil indicators or as integrated indices as SQI. However, the constraints of the soil spectroscopy approach for large-scale monitoring are specified in local point-scale and site-specific studies. Despite its solid quantitative capabilities, these are limited by the relatively small number of sampling points from a particular study area (Ong et al., 2019).

A limited number of studies have developed soil spectroscopy applications for assessing soil quality in dryland regions. For example, Levi et al. (2020) have successfully applied a spectroscopy-based model of 14 physical, biological, and chemical soil properties, with different accuracy levels, to calculate the statistically integrated SQI based on the SMAF protocol. Yet, one of the limitations of point spectroscopy is that it is related to the point scale and does not account for the spatial variability of the soil. Imaging spectroscopy (IS) compiles a large number of contiguous spectral image bands (>50) as an indirect method to assess soil biochemistry (Ben-Dor et al., 2009). IS method can be applied to soil properties and quality assessments at improved spatial and spectral resolutions, moving from the point-

scale to a larger geographical area. The regression models can be used to IS for soil property predictions at a broader scale, based on the integration of soil laboratory analyses and hyperspectral image measurements. In addition, due to many narrow wavebands, IS can be used to highlight unique spectral features, such as the absorption and reflectance of diagnostic wavelengths from the image itself, similar to laboratory spectroscopy analysis (Goetz et al., 1985). For multivariate analysis, sensitivity spectral band selection is derived from the calculated regressions via a variable importance analysis that detects the most effective wavelengths in the correlation process (Cécillon et al., 2008).

Some large-scale mapping methods for different sets of soil properties have been developed. For example, the Land-use/Cover Area frame statistical Survey (LUCAS) topsoil dataset from the European soil data center (ESDAC) provides a mapping of a great variety of soil properties across Europe and over 25 of its countries based on collected and stored soil libraries, partially including spectral measurements (Ballabio et al., 2019). The Australian Commonwealth Scientific and Industrial Research Organization (CSIRO) developed the GlobalSoilMap project, and the data are managed as part of the Australian Soil Resource Information System (ASRIS). This gives access to the "soil and landscape grid" that provides a range of soil and landscape attributes and map products across the country (Johnston et al., 2003). Geo-statistical approaches were also being used to assess soil quality at the regional scale (Rinot et al., 2019). For example, Svoray et al. (2015) suggested a method based on vicarious statistical evaluation and interpolation to quantify soil health in a spatially explicit manner over a large area. However, the incorporation of imaging spectroscopy for soil quality mapping encapsulates significant advantages, such as integrating a large set of soil properties, ground-truthing data, rigorous analytical and statistical evaluation, and the continuous precise mapping over large extents.

Moving from point spectroscopy to image spectral analysis reflects on many challenges that need to be considered. On the practical level, the transition of the SQI model from the local to the regional scale requires a shift from point spectroscopy to an IS approach. Such problems and limitations include a low signal-to-noise ratio (SNR), large and complex datasets, signal interferences from the atmosphere and mixed pixels of the non-soil area due to pixel size (e.g., vegetation and soil crust), the effects of the bidirectional reflectance distribution function (BRDF), and the necessity of highly skilled personnel for processing and analyzing the large datasets. Moreover, airborne IS is still expensive and requires a complex infrastructure to operate (Ben-Dor et al., 2009; Chabrillat et al., 2019). Despite these drawbacks, the use of airborne IS to study properties and processes related to soil has emerged and grown substantially in the last couple of decades (Chabrillat et al., 2019), through its mapping and monitoring of multiple aspects such as soil salinity (Ben-Dor et al., 2002; Zhang et al., 2019), soil composition (Li, 2020; Žižala et al., 2017), soil organic carbon (Stevens et al., 2006; Tziolas et al., 2020), soil moisture

(Haubrock et al., 2005; Diek et al., 2016), soil erosion and stability (Schmid et al., 2005, 2016), soil contamination (Davies and Calvin, 2017; Pelta et al., 2019), and many other soil aspects.

Paz-Kagan et al. (2014) demonstrated the use of 14 soil indicators in determining the variability of soil attributes among three different LU types that changed from managed to unmanaged and vice versa. They developed the spectral soil quality index (SSQI) based on the point spectroscopy of standard laboratory soil analyses. The SSQI integrates all relevant scored SQI indicators and then classifies them according to their spectral differences. In their following work, Paz-Kagan et al. (2015) have successfully applied and upscaled the SSQI method using the IS approach. They managed to map the overall SQI over several agricultural fields in two different study sites under various LUs and treatments, based solely on the spectral differences between each LU, achieving strong classification values (overall accuracy of 0.92 and 0.82 at the Israeli and German sites, respectively). The current study attempts to develop the SQI based on IS using machine-learning applications applied to an arid environment.

The current study attempts to develop the SQI based on IS using machine-learning applications in an arid environment characterized by a water-scarce, nutrient-poor, and sparsely populated environment. The novelty of the research lies in the combination of traditional chemical soil laboratory analyses and the spectral dimension based on imaging spectroscopy (IS) methods to comprehensively evaluate soil quality. It incorporates AisaFENIX airborne IS with advanced statistical analyses to study the ability to determine the soil state on a large scale by measuring the effects on the overall quality of different LUs in dryland regions. Such applicability in extreme conditions like the Avdat region, with various LUs, will exemplify its relevance in temperate climate areas. To accomplish our goals, we considered only the upper layer of the soil due to the ability of the sensor to detect only the soil surface layer. Soil properties change with the soil profile over time under field conditions with responses to soil moisture range. However, the hyperspectral airborne system's limitation could capture only the upper soil surface area.

Thus, based on the significant impact LUs have on their natural arid soil surroundings, the main goal of this research is to evaluate their effects over the study area using IS applications. Specifically, the objectives include (1) demonstrating the capability of IS for continuous mapping of multiple soil properties and the integrated SQI over the whole study area; (2) examining the combination of both conventional soil chemical laboratory survey and the contribution of the spectral dimension to the regression-based prediction capabilities of IS; and (3) evaluating the effect of LU change on the soil health patterns in arid regions that include grazing, agriculture, and runoff-harvesting systems (RHSs) for agricultural and forestry purposes.

2. Material and methods

2.1. Study area

The current study follows the work conducted by Levi et al. (2020) in the same study area of the Avdat region (Fig. 1). The site is a sparsely populated arid region in Israel's central Negev Desert, and also serves as a long-term ecological research (LTER) station (Fig. 1A; Olsvig-Whittaker et al., 2012). The study area extends over about 24 km². The landscape is characterized by barren, steep, and rocky terrain in the western and southern parts, which moderates further northward along the basin of the ephemeral Zin stream, and it consists of sparse vegetation cover (Ohana-levi et al., 2018). As a region characterized by hot, dry summers and cold, low-precipitation winters, soil water retention, available organic material, and soil nutrients are mainly concentrated along the Zin Stream and its basin and are greatly dependent on seasonal rains and runoffs (Ziv et al., 2014). The more developed soil columns are located northwards in the upper parts of the watershed and the lower and flatter parts. These regions consist of generally finer grain-sized colluvium, mostly of loess soil type that can be found as far as several meters deep in the depressed segments, situating it within the aridisol soil order (Yair and Danin, 1980).

The region comprises four LU types, of which three are human-dominated formations: single-family agricultural farms (primarily consisting of grapevine and olive cultivation), RHSs for agricultural and afforestation purposes, and agro-pastoral grazing, mainly of sheep and goats, that takes place in the vicinity of Bedouin villages. The RHSs include two types of human-made landscape structures scattered within or adjacent to the Zin stream. The first is a larger runoff-ponding catchment hedged by soil levees named *limans*, primarily used for afforestation into small-scaled cultivation and as a means of flooding mitigation while improving the soil's productivity by capturing essential environmental resources, notably organic matter, nutrients, sediments, and seeds (Paz-Kagan et al., 2019). The *limans* were mainly developed at the beginning of the 60s by the Jewish National Fund (JNF) as an afforested grove. The second is streambed stone-wall terraces that retain and regulate runoff flow, infiltration rates, and soil erosion, where some terraces include ancient systems that are still active to this day, while others are abandoned and breached (Yizhaq et al., 2020). The fourth is uninterrupted natural land (Ohana-levi et al., 2018; Paz-Kagan et al., 2017). These ancient terraces cover large dry riverbeds in the Zin Stream's basin, a systematic human intervention in arid landscapes. Terracing was introduced in the Roman (63 BCE–324 CE) and Byzantine (324–640 CE) eras to develop a fertile agro-ecosystem in arid regions. They aimed to improve water retention and soil stabilization and reduce hydrological connectivity and erosion, all of which assists in increasing the primary and secondary productivity of agroecological

systems (Beckers et al., 2013).

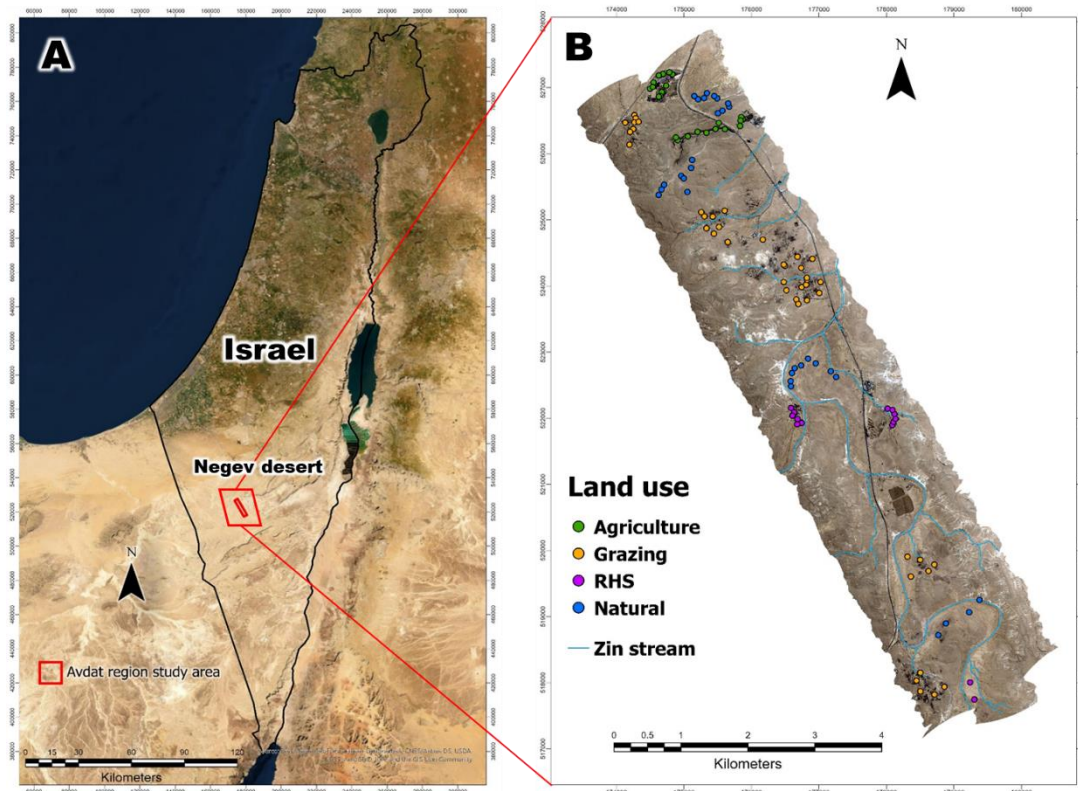


Figure 2: (A) Location of Avdat region within the Negev Desert, Israel. (B) Soil sampling sites, their respective land-use class, and the Zin Stream channel positioned over the hyperspectral image. Fully detailed information for all sampling sites is presented in Levi et al. (2020). RHS: runoff harvesting system.

2.2 Research approach and structure

Figure 2 presents the general approach of the research framework and assimilates multiple field survey procedures, laboratory analyses, and data processing and interpretation. The research structure includes three steps: (1) in-field soil sampling, chemical soil laboratory analyses, and the SQI development; (2) airborne hyperspectral image acquisition, pre-processing, and spectral data extraction; and (3) IS approach integration of the chemical soil laboratory analysis and spectral data extracted from the IS using SVM-R modeling and large-scale mapping prediction. The following sections describe the methodology performed in each step.

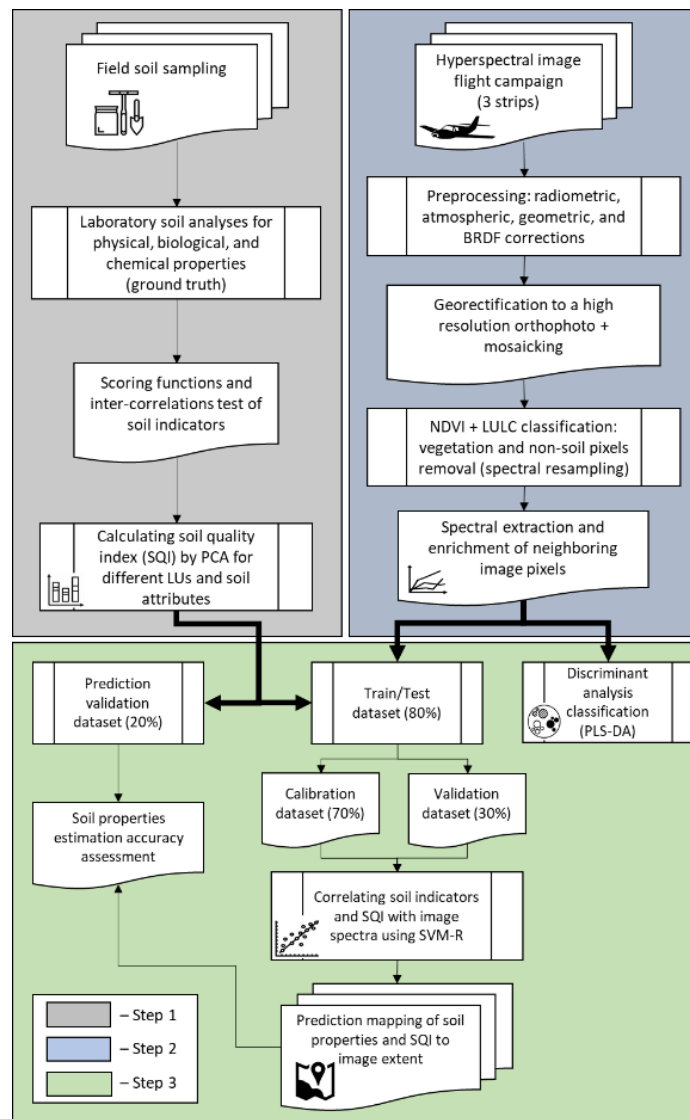


Figure 2: Study flowchart of the three steps for developing the soil quality assessment model for regional-scale imaging spectroscopy (IS) prediction mapping for individual soil properties and the overall soil quality index (SQI) in Avdat region study area.

2.3 Step 1: Soil sampling, analysis, and SQI development

2.3.1 Soil sampling and laboratory analysis

The soil collection for further physical, biological, and chemical soil surveys took place in April 2017, initially including 114 soil samples from the upper soil layer (15 cm) of the four LUs taken from 14 sampling sites scattered across the study area covered by the hyperspectral image (Fig. 1B). Sampling locations were defined based on an initial stratified random sampling design (Kothari, 2004), integrating variables such as elevation, lithology, and land-use land-cover (LULC) classification (Ohana-levi et al., 2018). Soil samples were collected from the uppermost 0–15 cm from the ground surface, and each was assigned a location using a handheld GPS device. Further elaboration on the sampling sites and methodology can be found in Levi et al. (2020).

The laboratory soil survey incorporated the analyses of 12 soil properties, following the SMAF protocol (Wienhold et al., 2009), and their respective procedures and methods are specified in Table 1. The selected properties include physical indicators of soil texture (fractional sand, silt, and clay), indicating the morphology and fragmentation of the soil. The available water content (AWC) was calculated by the difference between water holding at field capacity and the soil's permanent wilting point (Scrimgeour, 2008). This is a critical factor for water availability to plants and soil organisms, greatly affected by the changing soil texture types (Groenendyk et al., 2015). The biological indicators included soil organic matter (SOM), which initiates soil processes such as nutrient storage, enzyme activity, carbon stocking, and salinity level moderation (von Lützwow et al., 2007). The extractable nitrate (NO_3^-) represents the nitrogen available to the plant in the soil, a fundamental resource for organic life-building blocks (Pansu and Gautheyrou, 2006). The chemical indicators include pH, electrical conductivity (EC), extractable chlorine (Cl), extractable sodium (Na), extractable calcium and magnesium (Ca + Mg), and the sodium adsorption ratio (SAR). These properties serve as reliable indicators for soil alkalinity and as precursors of ongoing soil salinization and sodicity processes, on the one hand, and soil micro-aggregation, on the other (Rahimi et al., 2000). The extractable phosphorus (P) and extractable potassium (K) are valuable soil nutrient constituents of proteins and nucleic acids, which are essential components in plant tissue and are crucial in regulating different processes in plants.

Table 2: Soil quality properties and their respective affiliation, units of measurement, and analysis methods. A comprehensive review of the applied laboratory survey methods can be found in Levi et al. (2020).

Indicator	Unit	Method
Physical properties		
Soil texture (fractional sand, silt, and clay)	-	Particle size suspension (Kettler et al., 2001)
Available water content (AWC)	%	Oven drying and weight difference (Scrimgeour, 2008)
Biological properties		
Extractable nitrate (NO_3^-)	mg/kg	Potassium chloride extractions (Norman and Stucki, 1981)
Soil organic matter (SOM)	%	Organic carbon furnace method (Casida et al., 1964)
Chemical properties		
Acidity level (pH)	-	1:1 water-soil suspension extraction (Roades, 1982)
Electrical conductivity (EC)	dS/m	
Extractable chloride (Cl)	mg/l	ICP-MS (Brady and Weil, 1999)
Extractable sodium (Na)	mg/l	
Extractable calcium and magnesium (Ca + Mg)	mg/l	
Sodium adsorption ration (SAR)	-	
Extractable phosphorus (P)	mg/kg	
Extractable potassium (K)	mg/kg	

ICP-MS: inductively coupled plasma-mass spectrometer.

2.3.2 Developing the SQI model

The development of the SQI includes several statistical and mathematical procedures. One of the main goals of this study is to map SQI and soil properties over the whole study area. Therefore, the calculated SQI was developed for the four LUs and their physical, biological, and chemical attributes. First, a minimal amount of outliers were removed, using the median absolute deviation (MAD) method (Leys et al., 2013). The MAD excludes values greater or lower than three standard deviations (SDs) from each of the soil indicators' central median values, resulting in the removal of very few outliers, not exceeding 5% for any soil property. Following that, the soil properties were transformed into unitless scores ranging from 0 (poor performance) to 1 (excellent performance). For each of the selected MDS indicators for the study scheme, one of three non-linear polynomial scoring functions were selected (Eq. 1–3), for value standardization and comparability (Masto et al., 2007):

$$Si_{more} = \frac{1}{1 + e^{-b(x-a)}} \quad (1)$$

$$Si_{less} = \frac{1}{1 + e^{b(x-a)}} \quad (2)$$

$$Si_{optimum} = 1 \times e^{\frac{-(x-a)^2}{b}} \quad (3)$$

where x is the initial soil indicator value, a is the least square deviation from the mean, and b is the SD's slope of the mean ($2\sigma^2$). “More is better” assigns higher scores to properties with high raw values, notably AWC, SOM, and NO_3^- , for their severe shortage and soil biotic activity propagation. The “Less is better” transformation designates lower concentrations of potentially soil-degrading materials, including EC, Cl, Na, and Ca + Mg, linked to soil salinization processes. The designation of “Optimum” grants higher ranks to observations surrounding the indicator's mean value, incorporating pH, SAR, P, and K, which promote moderate soil acidity and the distribution of soil nutrients (Idowu et al., 2009; Moebius-Clune, 2017). The indicators' adjustment is essential in giving greater significance to prevailing soil processes that strongly affect soil quality than their natural references (Andrews et al., 2004). For this reason, the scoring calculation of soil samples from the agricultural, RHS, and grazing LUs was derived from their nearby natural LU samples by sharing their mean and SD values in the process of the SQI calculation (Masto et al., 2008).

The scored soil indicators were integrated to calculate the ultimate SQI. First, to prevent high collinearity and redundancy in the SQI model, the power predictive score (PPS) was applied for the multiple pairwise correlations amongst all 12 scored soil properties (Wetschoreck et al., 2020). The

measured relationships were locally normalized and assigned with a predictive score ranging from 0–1. The normalized PPS value expresses the power of their correlation, not only for linear and non-linear patterns in the data but also for the correlation's asymmetry and directionality (i.e., $X \sim Y \neq Y \sim X$). Strongly correlated indicators ($PPS \geq 0.5$) were excluded from further SQI development. Afterward, a principal component analysis (PCA) for statistical calculation of significantly different uncorrelated dimensions (variables) was performed (Jolliffe et al., 2016). The whole variance of the model was divided into several low-covariable principal components (PCs; Hotelling, 1933), where the number of PCs with eigenvalues (i.e., weighted proportion of variance) is greater than one and accounting for at least 5% of the cumulative variance was examined. The scored soil indicators and their respective allocated statistically distinct weighted PCs were multiplied and summed into the eventual feature-scaled (0-1) SQI score for each soil sample (Eq. 4):

$$SQI = \sum_{i=1}^n PW_i \times S_i' \quad (4)$$

where PW_i is the assigned PC weight, and S_i' is the scored soil indicator. The resultant SQIs create a simplified method for comparing and assessing the intensity of the disturbance to the soil samples relative to their natural references. The workflow of the PPS method was imported into R from Python (Zavarella, 2020), using the "reticulate" package (Ushey et al., 2020), and the PCA was performed using JMP® Pro software version 15.0.0 (SAS Institute Inc., Cary, NC, USA).

2.4 Step 2: Airborne hyperspectral image acquisition and processing

2.4.1 Hyperspectral image acquiring

The following step included applying soil indicators and SQI predictions to a more considerable regional extent. The confirmed results of the previous study were based on point-scale spectroscopy under a controlled laboratory protocol that served as reference ground-truth measurements. In this study, we applied IS as a suitable approach to predict the soil attributes and quality assessment on the regional scale. Accordingly, a flight campaign using an airborne hyperspectral imager obtained a three-stripped image, taken under good weather and clear sky conditions over the Avdat study area on April 7, 2017. The AisaFENIX 1K sensor (Specim, Spectral Imaging Ltd.) was used in the flight campaign to capture the hyperspectral image of the study area. The soil sampling collection was conducted in parallel to the flight campaign. The AisaFENIX scanner holds a single optic aperture mounted onto a light aircraft. The sensor contains 420 contiguous spectral bands across the VIS-NIR-SWIR spectral region, which provides a spectral resolution of 3.5 nm in the VIS-NIR bands (380–970 nm) and 12 nm for the SWIR bands (970–2500 nm) and a full width at half maximum (FWHM) of 3.5–6.5 nm. The sensor was carried at an altitude

of 660 m aboveground, which provided an eventual spatial resolution of 1 m per pixel. The ongoing geographical positioning of the aircraft was recorded using an inertial measurement unit (IMU) for further geometric rectification (Brook and Ben-Dor, 2015).

Yet, image-based field measurements are susceptible to signal mixing and interferences caused by various factors, such as angular illumination, surface roughness, atmospheric light scattering, water vapor absorption, topographic orientation, vegetation and stone cover, and sensor radiometric and spectral instability performance (Brook and Ben-Dor, 2015). Hence, the acquired images had to undergo a series of pre-processing and calibration procedures for further analysis to achieve near-laboratory quality reflectance information (Ben-Dor et al., 2009). Using the airborne imagery-induced ATCOR-4 software (ReSe Applications LLC), the radiometric, atmospheric, and topographic corrections were performed based on the MODTRAN radiative transfer model®. The atmospheric correction was calibrated with ground targets measured by a portable analytical spectral device (ASD), the FieldSpec Pro® spectrometer, as described by Brook and Ben-Dor (2015). Additionally, the BRDF effect correction (BREFCOR) was implemented to minimize the BRDF effects caused by various surface covers (Schläpfer et al., 2015), resulting in a color-balanced calculated surface reflectance value for the three stripes. In addition, a transformation to the Israeli Grid 05/12 (EPSG:6991) projection was applied, the same correspondent projection for all spatial datasets throughout the research. This was followed by manual georectification to a high-resolution reference orthophoto of the study area (taken in November 2015) for improved positional accuracy. Lastly, the three stripes were unified into one combined image using ENVI software's seamless mosaic workflow, where the geo-rectified hyperspectral image was precisely co-registered with the locations of the soil samples with a total error of less than 1 m (RMSE = 0.648).

2.4.2 Non-soil pixel exclusion and spectral enrichment

To easily mask out non-soil pixels, the image was first spectrally resampled to Landsat 8 resolution to simplify the image classification in terms of better contrast and spectral separability coherence among the various land-cover features. The spectral resampling was performed by calculating the normalized difference vegetation index (NDVI; Tucker, 1979). The index was calculated using the sensor's NIR and red center wavelengths (864.67 nm and 654.59 nm, respectively; Barsi et al., 2014) for removing pixels of vegetation, built-up areas, and rocks exceeding a $0.05 < \text{NDVI} < 0.25$ range value. Although vegetation indices values are universal, the exact limit of certain classes is subjected to vegetation types, local reflectance intensity, vegetation cover, and density, etc. Therefore, this study's threshold was found best to distinguish vegetation pixels from other land-cover types and was decided following a trial and error

process. Following this, a land-use land-cover (LULC) classification was performed to define the main land-cover features identified in the area. A supervised minimum distance classification (Wacker and Landgrebe, 1972) was conducted to remove very bright soils related to undeveloped and unconsolidated chalk and marl soils and additional non-soil land-cover categories. The subsequent masked image outline was used to clip the final shape of the original full spectral resolution image.

Furthermore, bands within the spectral range of susceptibility to atmospheric vapor absorption (1350–1490 and 1830–2100 nm) and noisy bands on the spectra fringes (380–439 nm) were excluded from the dataset, resulting in 336 spectral bands in total. Spectral signatures from the adjacent pixels surrounding the initial soil sample locations were extracted (3×3 neighborhoods), enlarging the model's entry to a total of 1,026 points for a development of a pixel-based model. The pixel selection process enabled us to enrich the dataset, reduce spectral heterogeneity, and improve the model's confidence due to varied land surface features and LUs. Each newly added spectral signature was assigned to the corresponding soil laboratory measurement values within its neighboring pixels by incorporating the laboratory and spectral data. The SVM-regression prediction maps were generated for the individual soil indicators and the integrated SQI.

2.5 Step 3: IS approach integration of the laboratory data

2.5.1 Discriminant analysis classification of spectra by land-use

Before integrating the spectral and the chemical laboratory soil survey datasets through a regression process, a classification analysis for the enriched image-extracted hyperspectral data of the four studied land-uses was performed. The spectral differentiation between the land-uses is a primary indication of the applicability of spectroscopy as a suitable assessment tool for further SQI and other individual soil properties regression and prediction. The spectral classification was performed using a partial least squares-discriminant analysis (PLS-DA) method. The PLS-DA is a multivariate linear method that quantifies and categorizes the continuous predictor variable (spectra – X) into different classes of the discrete variable (land-uses – Y). The model creates a hyperspace dimension that splits into statistically distinct components called latent variables (LV). Each LV represents a portion of the total cumulative variance of the observations relating to their respective class membership, which results in a well-defined classification of the multivariate feature hyperspace (Singh et al., 2005). The output of the PLS-DA provides a scatterplot that conveniently graphically illustrates the separability of the observed data according to its predetermined classes, in addition to a statistical evaluation of significant differences between classes. Similar to other classification methods, the performance of the PLS-DA model is also evaluated using overall accuracy (OA) and Kappa coefficient (Kc) metrics. In addition, the

PLS-DA also produces comparative variable importance in projection (VIP; Cécillon et al., 2008) analysis to rate the relative significance of each wavelength for the four LUs to detect the most prevalent spectral features in the model. The PLS-DA classification and graphical illustration was performed with MATLAB® PLS_Toolbox (Eigenvector, Wenatchee, Washington, USA; Wise et al., 2006).

2.5.2 Soil chemical properties and SQI regression to hyperspectral image

Once the spectral classification of the model is defined, the model regression can be applied. In this study, the regression models between the collected spectral signatures from the image itself (i.e., pixels) and the measured soil indicators at its location were used to generate the prediction maps using IS. The spectral data extracted from the image consisted of 336 spectral bands with high spectral contiguity that interacted differently with each soil indicator. Some of the soil properties, notably NO₃, EC, SAR, P, and K, had highly skewed distributions of their raw values. Hence, these properties were transformed using a log₁₀ for skewness reduction, achieving an acceptable normalized skewness value ($\gamma < \pm 1$) for the different indicators.

Various regression models have been proven satisfactory for spectral prediction of soil properties, with many attempts to minimize the squared error of the predicted values. In addition, soft-margins support vector machine-regression (SVM-R) also tries to reduce the error and conceal the values within a certain threshold around the model's hyperplane (i.e., the model's trend line; Drucker et al., 1997). The controlled amount of slack given to specific regression errors allows better flexibility to optimize the different model parameters for such relatively noisy data (Thissen et al., 2004). The resulting restrained hyperplane and boundary lines can produce an optimal trendline to fit the predicted values with minimized absolute error within the model's margins and constraints (Eq. 5-6). Optimizing the model's fit included two adjustment hyperparameters that were embedded in its calculation, including epsilon (ϵ), which demarcates the margins' width, and cost (C), which regularizes the accepted tolerance for predicted observations outside of ϵ :

$$MIN \frac{1}{2} ||w||^2 + C \sum_{i=1}^n |\xi_i, \xi_i^*| \quad (5)$$

$$|y_i - w_i x_i| \leq \epsilon + |\xi_i, \xi_i^*| \quad (6)$$

where $||w||^2$ is the minimized total squared error, $|\xi_i, \xi_i^*|$ is the original and reprojected absolute deviation from the margin ϵ while subjected to $\xi_i, \xi_i^* \geq 0$, y_i is the target, w_i is the error coefficient, and x_i is the predictor value (Drucker et al., 1997). The SVM-R can be applied in a linear form or in higher-

dimensional features that use different kernel functions to transform the non-linear dimension of the input space data into linearly separable feature space predicted observations using the "kernel trick" (Vanschoenwinkel and Manderick, 2005). In the current study, the non-linear Gaussian radial basis function (RBF) kernel method was applied (Eq. 7), with an additional hyperparameter gamma (γ) that defines the influence rate of the training dataset in terms of distance:

$$K(x, x') = \exp(-\gamma \|x - x'\|^2) \quad (7)$$

where K is the reprojected kernel location for points x and x' , while $\|x-x'\|^2$ represents the squared Euclidean distance between the two observations (Thissen et al., 2004).

For the model design, the enriched dataset was randomly split into calibration (Cal) and validation (Val) subsets using cross-validation sampling at a 70 to 30 split ratio, respectively (Mourad et al., 2005). However, to better evaluate the robustness of the predicted models and measure their accuracy, an independent validation dataset is needed for subsequent comparison against the final soil properties and SQI prediction maps (Shi et al., 2020). For this purpose, 20% of the 114 raw data points of the individual soil indicators and the calculated SQI (i.e., prior to the dataset spectral enrichment) were set apart, including 23 prediction verification points (Pred). The remaining 80%, including 91 raw observations for each measured soil indicator, was used for cross-validation sampling of Cal/Val models at a 70 to 30 split ratio. The number of initial observations slightly changed for the soil properties that had outliers removed from their raw data, referring to the abovementioned MAD outlier removal. These were then enriched to 819 points for further prediction by selecting the nine neighboring pixels from the geo-location of the soil samplings. In achieving the optimized SVM-R model parameters, a minimal amount of outliers were excluded from the enriched dataset during the regression process based on the interquartile rule ($\pm 1.5 \cdot \text{IQR}$; Iglewicz, 2011). The outlier removal did not exceed a 10% threshold for any of the enriched Cal/Val subsets, where for most indicators, only a few extreme points were excluded.

Each soil attribute was statistically evaluated using the adjusted coefficient of determination for both the calibration and validation datasets (R^2_{adjCal} and R^2_{adjVal}), as well as for the regression's F-statistic value and degrees of freedom ($F_{(\text{df})\text{Cal}}$ and $F_{(\text{df})\text{Val}}$). The selection of the R^2 assumes that every single variable explains the variation in the dependent variable. The adjusted R^2 tells the percentage of variation explained by only the independent variables that affect the dependent variable, hence, even more, accurate in model performance (Miles, 2005). The root means square errors (RMSE_{Cal} and RMSE_{Val}) were calculated as well. The ratio of performance to deviation (RPD), which equates the total variations of the measured indicators with those of the validation data in a standardized scale, was calculated as $\text{RPD} = \text{SD}/\text{RMSE}_{\text{Val}}$ for each soil attribute and the SQI (Chang et al., 2001). Despite being widely used

as a model performance evaluation metric in soil spectroscopy, the RPD assumes a normal distribution of the examined indicators. In contrast, in many cases, they are prone to a significant degree of skewness. Therefore, a suitable evaluation means was using the IQR of the measured indicators' ratio performance ($RPIQ_{Val} = IQR / RMSE_{Val}$) alongside the RPD values for a more comprehensive review of the model's accuracy (Bellon-Maurel et al., 2010).

The significance of the validation models was ranked as: “excellent” at $RPIQ \geq 3.5$, $RPD \geq 2.5$, and $R^2 \geq 0.80$; “good” at $3 \leq RPIQ < 3.5$, $2 \leq RPD < 2.5$, and $R^2 \geq 0.70$; “moderate” at $2 \leq RPIQ < 3$, $1.5 \leq RPD < 2$, and $R^2 \geq 0.60$; and “poor” at $RPIQ < 2$, $RPD \leq 1.5$, and $R^2 < 0.60$ (Chang et al., 2001; Veum et al., 2015). However, the RPIQ, RPD, and R^2 values are correlated with one another. Hence, using them as reliable indicators must be accompanied by minimizing the disparity between the error values of both calibration and validation datasets, represented by their respective RMSE, to compare the prediction intervals of the models (Mcbratney and Minasny, 2016). Furthermore, the enrichment of the dataset allocates repeated measurements of the soil indicators to newly extracted spectra from the image. Thus, this might cause potential pseudo-replications in the dataset that artificially increase the total agreement (i.e., R^2 values; Wang et al., 2000) and, subsequently, the performance metrics (i.e., $RPIQ_{Val}$ and RPD_{Val}), to a greater degree than would have resulted from a single-pixel extraction estimation. Therefore, the calibration and validation datasets' error sizes ($RMSE_{Cal}$ and $RMSE_{Val}$) were considered more reliable metrics for the success of the prediction model (Mcbratney and Minasny, 2016), where the appropriate difference was set to 25% between the two. Lastly, a VIP analysis was performed to detect and accentuate spectral features in the SVM-R model. The VIP bands of the SVM-R are compared to those of the PLS-DA to examine their relative correspondence as an additional means of model success evaluation.

2.5.3 Predicting models to the hyperspectral image

The regression models were further used to produce the image-based prediction maps. As the non-linear RBF kernel transformed the SVM-R model into a simple two-dimensional linear system, the upscaling of the retransformed regression models was employed in a linear method over the hyper-layered image (Eq. 8):

$$y = B + A_1X_1 + A_2X_2 + A_3X_3 + \dots + A_nX_n \quad (8)$$

where y is the additive predicted soil property (pixel) value, A is the calculated model weighting coefficient for each AisaFENIX waveband X , and B is the model's slope (Lugassi et al., 2017). The output of the transformation assigns each pixel in the image to its respective predicted value, generating regression-based continuous prediction maps of the study area. The adjusted R^2 and RMSE values

(R^2_{adjPred} and $\text{RMSE}_{\text{Pred}}$, respectively) were calculated to examine the relationship between the excluded independent dataset of the measured soil properties and the SQI and their corresponding pixels' locations on the map within their respective neighborhoods. Indicators with an agreement of $R^2_{\text{adjPred}} \geq 0.7$ were considered successfully predicted. The SVM-regression and prediction, including parameter grid-search tuning optimization and upscaling, were performed in RStudio with the "e1071" (Meyer et al., 2019) and "caret" (Kuhn, 2020) packages.

2.6 Statistical analysis

Significant differences between LUs for the calculated overall SQI scores were tested using a one-way analysis of variance (ANOVA) test. For the SQI's physical, biological, and chemical attributes, the non-parametric Kruskal-Wallis test was used, as some of the ANOVA's assumptions for normal distribution of the model's residuals and homoscedasticity of the data were unmet. The significance level for the different LU classes of the overall SQI F-statistic and the subgroups' chi-squared (χ^2) test was determined at $\alpha < 0.05$.

3 Results

3.1 Soil quality index (SQI) development

The descriptive statistics for the individual soil indicators' laboratory analyses and their scoring transformation were performed in the previous study and can be found in Levi et al. (2020). The predictive power score (PPS) correlation matrix for the soil properties (Fig. 3) revealed strong correlations between the various salinity indicators and EC, notably Cl ($\text{PPS}_{(\text{Cl} \rightarrow \text{EC})} = 0.82$), Na ($\text{PPS}_{(\text{Na} \rightarrow \text{EC})} = 0.73$), and Ca + Mg ($\text{PPS}_{(\text{Ca} + \text{Mg} \rightarrow \text{EC})} = 0.71$), and between themselves. The EC was left as the only representative salinity indicator to rule out possible collinearity and redundancy in the SQI model. The soil texture properties (i.e., fractional sand, silt, and clay) were based on mineral particle size fragmentation (Schindelbeck et al., 2008). These properties were mostly descriptive parameters and constant in values. Hence, soil texture was excluded (Karlen et al., 2003), leaving the SQI model with 8 out of 12 indicators. A significant correlation was also found between NO_3 and EC ($\text{PPS}_{(\text{NO}_3 \rightarrow \text{EC})} = 0.46$) and the salinity indicators, but eventually, the NO_3 remained in the SQI analysis.

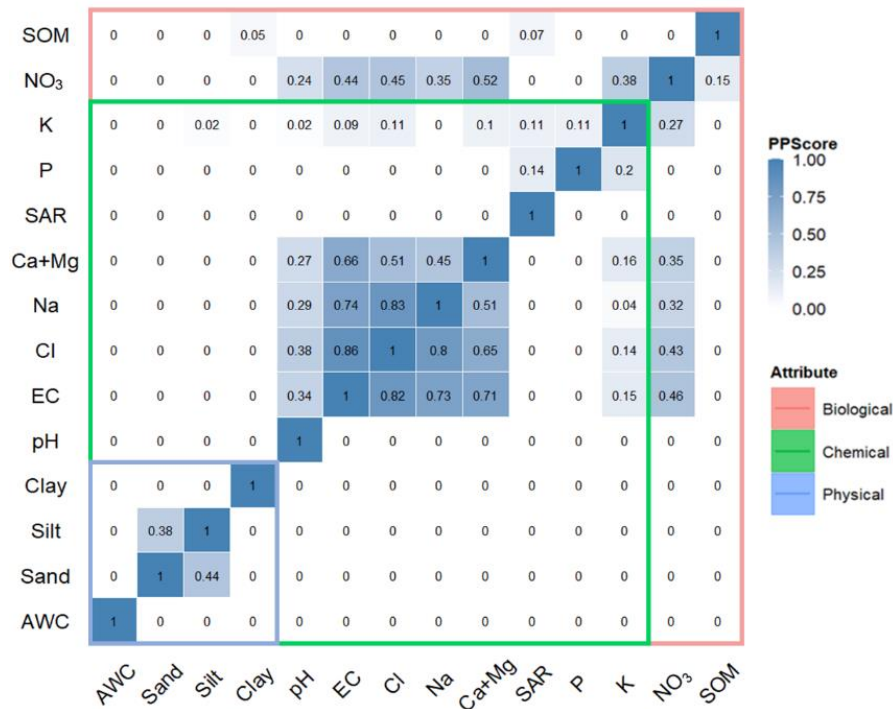


Figure 3: Predictive power score (PPS) correlation matrix for all the measured soil properties. The colored frames represent the associated physical, biological, and chemical components of the soil indicators. Pairs of soil indicators with high correlations (PPS ≥ 0.5) were excluded from further SQI calculation. SQI: soil quality index, AWC: available water content, EC: electrical conductivity, Cl: chlorine, Na: sodium, Ca + Mg: calcium and magnesium, SAR: sodium adsorption ratio, P: phosphorus, K: potassium, NO₃: nitrate, and SOM: soil organic matter.

The integrated SQI for all soil samples was generated among the LU practices using the physical, biological, and chemical scored soil properties. The results of the PCA suggest that three PCs, with an eigenvalue greater than one and accounting for more than 10% of the proportion of variance, explained 72.55% of the model's variance (Table 2). PC1 held the most explanatory variance with 40.39% and included the SAR, NO₃⁻, P, K, and SOM scored indicators, followed by PC2 with 19.58% of the variation for AWC and EC scores, and PC3 with a loading value of 12.57% for the remaining pH scoring. A PCA bi-plot of the scored soil properties on PC1 versus PC2 is shown in Appendix A. Figure 4 displays the mean overall SQI scores and their corresponding physical, biological, and chemical attributes among the four LUs. The mean overall score of all soils combined was SQI = 0.613, whereas the scores for the agriculture, grazing, RHS, and natural LUs were SQI = 0.661, 0.598, 0.566, and 0.605, respectively. Significant differences were found between some of the LUs ($F_{(3)} = 3.59$, $p < 0.05$), where agriculture was significantly higher than grazing ($p = 0.049$) and RHS ($p = 0.02$). Additionally, some significant differences emerged when observing the particular components. The biological soil properties showed the most notable significant differences ($\chi^2_{(3)} = 23.96$, $p < 0.05$), where the natural areas presented significantly lower mean rates (SQI = 0.144) than those of the other three LUs (SQI = 0.230, 0.231, and

0.165 for agriculture, grazing, and RHS, respectively). On the other hand, the scores' proportion of the chemical attributes ($\chi^2_{(3)} = 12.15, p < 0.05$) was significantly higher in the natural LU (SQI = 0.421) than in the grazing and RHS (SQI = 0.327 and 0.368, respectively). The physical subpart showed no significant differences among all four LUs ($\chi^2_{(3)} = 4.58, p = 0.21$).

Table 3: Principal component analysis (PCA) results for the scored soil indicators. The highest loading factor within each principal component (PC) for every indicator is marked bold.

	PC1	PC2	PC3
Eigenvalue	3.23	1.57	1.01
Proportion of variance (%)	40.39	19.58	12.58
Cumulative proportion (%)	40.39	59.98	72.55
No. of properties	5	2	1
AWC Score	0.16	0.64	0.06
NO ₃ ⁻ Score	0.85	-0.39	0.20
SOM Score	-0.72	-0.47	0.08
pH Score	-0.19	0.21	0.86
EC Score	-0.61	0.66	-0.21
SAR Score	-0.67	-0.55	-0.06
P Score	-0.72	-0.47	0.08
K Score	0.92	-0.04	0.08

AWC: available water content, NO₃⁻: nitrate, SOM: soil organic matter, EC: electrical conductivity, SAR: sodium adsorption ratio, P: phosphorus, and K: potassium.

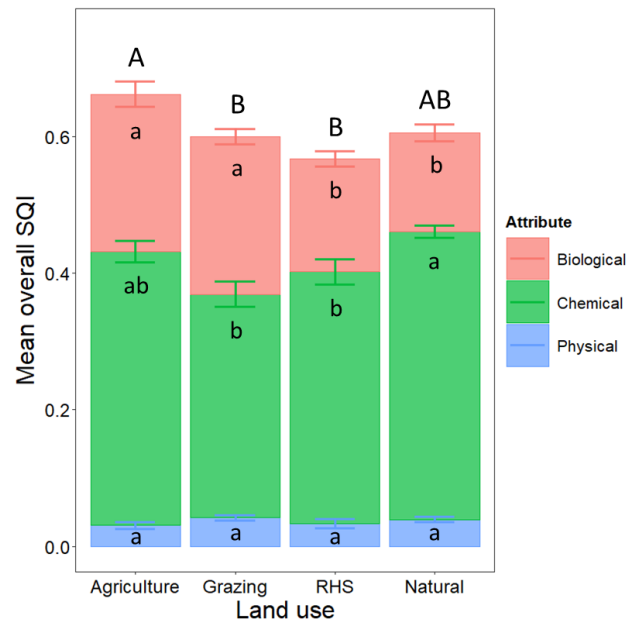


Figure 4: Mean overall soil quality index (SQI) scores and their respective physical, biological, and chemical indicators' subgroups for the four land-uses (agriculture, grazing, RHS, and natural) in the Avdat study area. Uppercase letters above the error bars indicate significant differences between the land-uses of the overall scores. In contrast, lowercase letters within the bars denote the differences between the particular attributes ($p < 0.05$). RHS: runoff-harvesting system.

3.2 Hyperspectral image pre-processing

The pre-processing of the hyperspectral image included multiple steps, readying it for further analysis and prediction. Figure 5 shows the results for the NDVI (Fig. 5A) and the LULC classification map (Fig. 5B) for non-soil pixel exclusion. High NDVI values (≥ 0.25) indicate vegetation presence, while low and negative values (≤ 0.05) imply the existence of other non-soil materials, such as rocks, paved roads, and buildings. The land-cover classification for removing additional pixels, including classes of very bright undeveloped chalky soils and built-up areas, resulted in high overall accuracy (OA = 95.11%) and Kappa coefficient (Kc = 0.93) values. The confusion matrix of the minimum distance classification is shown in Appendix 2. The largest 'soil' class that represents the most predominant loess soil in the region accounted for 68.13% of the entire area (16.03 km²), with 'dark soil' and 'bright soil' classes falling behind (17.11% and 12.63%, respectively). The 'very bright soil' and 'road/built-up' categories cover about 1% of the image each (0.25 km²). The classification output raised the issue of the BRDF effect's remnants on the image fringes, as the dark soil class suffered from a significantly lower producer's accuracy rate (78.57%; Appendix B) compared to the rest of the land-cover classes. The western edge of the image was exceedingly attributed to dark soils and very bright soil on the eastern part, while the rest of the image was highly accurate (Fig. 5B), which indicates the effects caused by sun angle directional illumination. Thus, the most extreme interrupted margins of the image were clipped and removed to reduce possible error and prevent further misinterpretation of the results (Fig. 5C). By excluding the NDVI, the LULC classification, and the image fringes, a total of 11.36% of the pixels were removed from the image. Once the pre-processing treatments were completed, the corrected and calibrated spectra were extracted from the hyperspectral image. The mean image-extracted spectral signatures of the soil samples for the different LUs are shown in Figure 6.

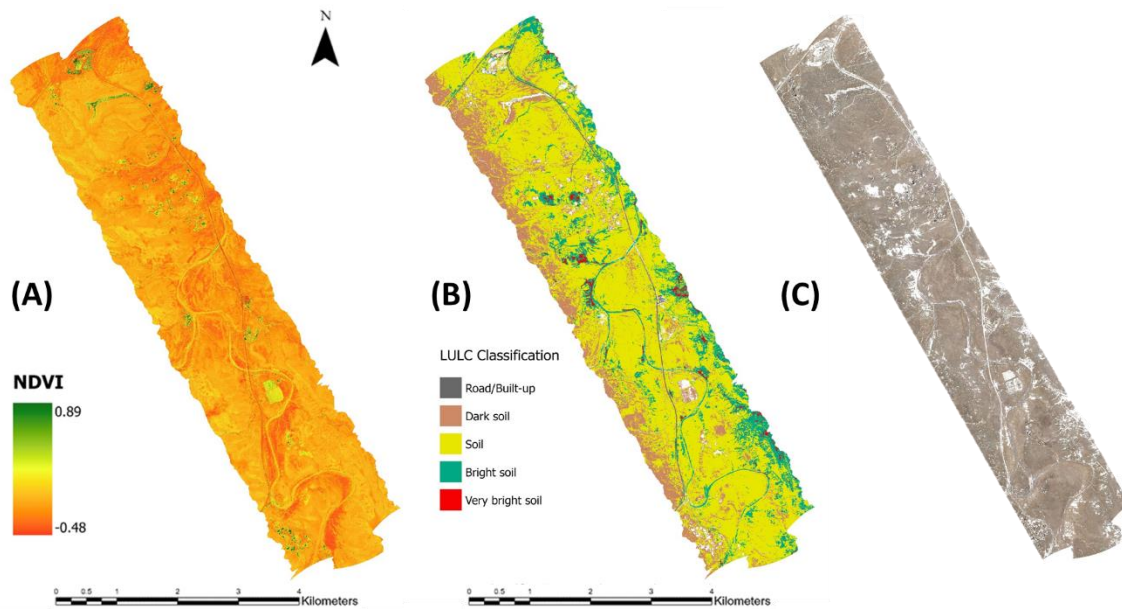


Figure 5: (A) Normalized difference vegetation index (NDVI); (B) land-use land-cover (LULC) classification map; and (C) final clipped AisaFENIX bare soil image for the Avdat region.

3.3 Spectral classification and correlation of SQI and soil indicators

The scatterplot and results of the PLS-DA classification of the image-extracted spectra according to their respective LUs are given in Figures 6-8. The performed discriminant analysis (Fig. 7) model consists of 3 LVs accounting for 68.25% of the cumulative variance, also exhibiting strong separability among the four LUs (OA = 95.31%, Kc = 0.90). The results indicate a successful classification model that is compatible with further regression and prediction. The variable importance in projection (VIP) analysis was derived from the PLS-DA classification, highlighting unique spectral features (i.e., wavelengths) for each of the examined LUs (Fig 7). Some significant spectral features were noticed across all LU practices, including 520.69, 792.21, 1537.43, and 2278.13 nm. Others were shared among several LUs, such as 2204.65 nm for agriculture, RHS, and natural, 609.69 and 2441.33 nm for agriculture and grazing, 681.91

and 2405.36 nm for agriculture and RHS, and 2357.12 nm for grazing and natural.

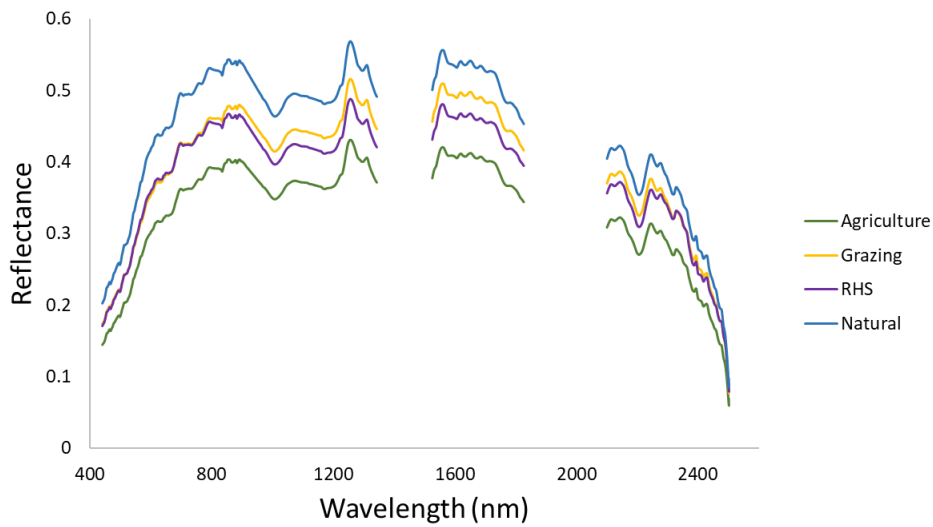


Figure 6: Mean soil spectral signatures of the four land-use practices (agriculture, grazing, RHS, and natural) extracted from the AisaFENIX hyperspectral image for the Avdat study area. RHS: runoff harvesting system.

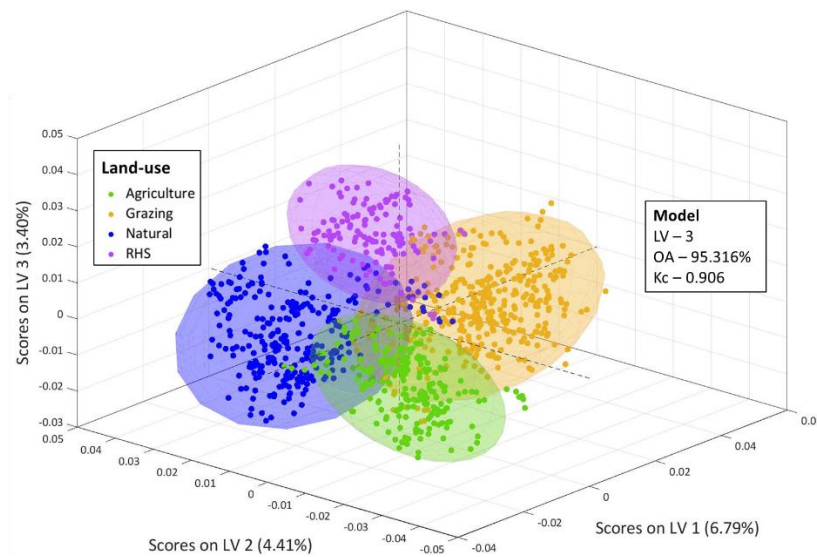


Figure 7: Partial least squares-discriminant analysis (PLS-DA) classification for the four land-use practices (agriculture, grazing, RHS, and natural) extracted spectra from the AisaFENIX hyperspectral image of the Avdat study area. The figure includes the model's number of latent variables (LV) and the overall accuracy (OA) and Kappa coefficient (Kc) statistics. Colored circles indicate a 95% confidence level. RHS: runoff harvesting system.

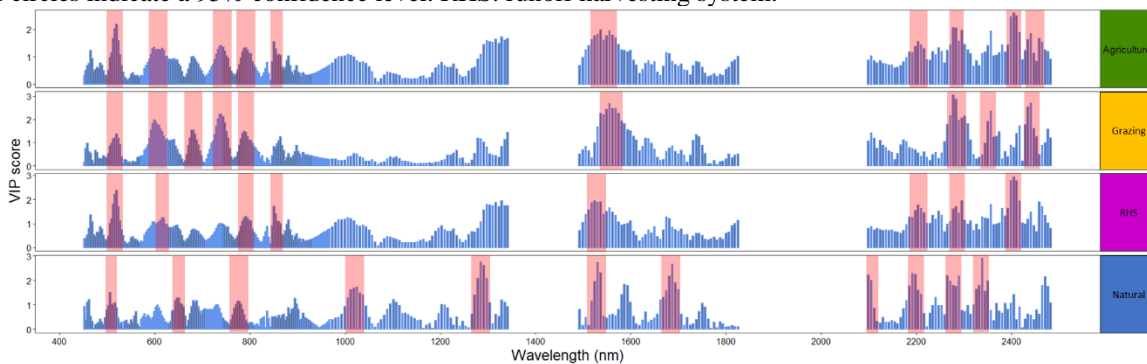


Figure 8: Variable importance in projection (VIP) plot of the agriculture (green), grazing (orange), runoff-harvesting system (RHS; purple), and natural (blue) land-uses in the Avdat region. Each bar represents the importance score of a particular hyperspectral image waveband in the partial least squares-discriminant analysis (PLS-DA) spectral classification analysis. The red sections highlight regions with spectral features with significant VIP peaks.

The full results of the SVM-R analysis are presented in Table 3, including the adjusted R^2 , RMSE, RPIQ, RPD, F-statistic values, and their significant VIP wavebands for the calibration and validation split datasets. Also, the regression scatterplots for all soil properties are shown in Figure 9. All the predicted soil indicators and the overall SQI were found significant for image-scale prediction ($RPIQ_{Val} \geq 3$, $RPD_{Val} \geq 2$, and $R^2_{adjVal} \geq 0.70$), except AWC, which presented borderline results ($R^2_{adjVal} = 0.776$, $RPIQ_{Val} = 2.67$, $RPD_{Val} = 2.00$). The overall SQI regression model resulted in an “excellent” degree of validation ($R^2_{adjVal} = 0.867$, $RPIQ_{Val} = 4.09$, $RPD_{Val} = 2.60$, $RMSE_{Cal} = 0.03$, and $RMSE_{Val} = 0.03$). The log-transformed EC ($R^2_{adjVal} = 0.837$, $RPIQ_{Val} = 4.21$, $RPD_{Val} = 2.47$, $RMSE_{Cal} = 0.21$, and $RMSE_{Val} = 0.25$) and P ($R^2_{adjVal} = 0.861$, $RPIQ_{Val} = 4.12$, $RPD_{Val} = 3.19$, $RMSE_{Cal} = 0.10$, and $RMSE_{Val} = 0.12$) exhibited the strongest evaluation metrics of the successfully correlated indicators. The regression models of the fractional sand, NO_3^- , SOM, pH, SAR, and K properties had an “excellent” performance as well. The 25% error ratio (i.e., $RMSE_{Val}/RMSE_{Cal}$) was compromised only by K at 28.12%.

Figure 10 presents the inclusive variable importance for distinguishing subtle spectral response differences among all soil indicators. A higher VIP score for a particular wavelength implies the existence of a significant spectral feature, where accentuated peaks were noticed across different spectral ranges for the soil indicators. Despite the extracted spectra being subjected to noticeable signal disturbances (Fig. 6), recognizable differences between the mean LUs’ spectra indicate the soil materials’ content variations. The general reflectance is relatively high, referring to the predominant quartz-rich sandy-loam soil texture class, including disparities of specific spectral features. The VIS-NIR range (400–1100 nm) presented some notable VIP attributes: the 680–740 nm range, known for organic matter content, has shared importance for SOM, pH, EC, SAR, and P, and the 870–905 nm is significant for AWC, silt, clay, NO_3^- , and P. However, the SWIR region (1100–2500 nm) showed the most prominent spectral features. The soil moisture absorptions at the 1493.44 nm waveband strongly peaked for AWC, sand, NO_3^- , SOM, EC, P, and K, and at 1593.95 nm for AWC, silt, NO_3^- , pH, and EC, as well as at 2100–2180 nm for AWC, silt, clay, SOM, pH, EC, and K. This was even more so the case for the organic compounds, clay minerals, and carbonates’ various absorption attributes across the 2200–2450 nm for almost all soil properties. The spectral regions identified for the SQI model coincide with those of its indicator counterparts, including the 520.69, 678.46, 1593.95, 1763.26, 2223.06, and 2399.35–2435.35 nm wavebands. Most of the regression VIP bands were relatively similar to the spectral regions found by the VIP bands derived from the PLS-DA classification.

3.4 Soil indicators and SQI prediction maps

The final prediction maps for the overall SQI and the individual soil indicators are presented in Figures 11 and 12, respectively, and their statistical evaluation is given in Table 3 and Fig. 9. For the predicted properties, 8 out of 12 soil indicators were successfully mapped ($R^2_{\text{Pred}} \geq 0.7$), including the SQI, fractional sand and clay, SOM, pH, EC, SAR, and P. The map of the overall SQI (Fig. 11A) provided a significant prediction agreement with the excluded verification dataset ($R^2_{\text{adjPred}} = 0.779$, $\text{RMSE}_{\text{Pred}} = 0.03$), distinguishing well the continuous SQI score patterns in accordance with the different LU practices (Fig. 11B), land-cover features (Fig. 11C), and topography (Fig. 11D).

The successfully upscaled prediction maps of the individual soil indicators (Fig. 12) show that fractional sand and EC had the strongest agreement values ($R^2_{\text{Pred}} = 0.853$, $\text{RMSE}_{\text{Pred}} = 0.05$ and $R^2_{\text{Pred}} = 0.84$, $\text{RMSE}_{\text{Pred}} = 0.32$, respectively), whereas fractional clay and SOM had the most marginal ones ($R^2_{\text{Pred}} = 0.706$, $\text{RMSE}_{\text{Pred}} = 0.02$ and $R^2_{\text{Pred}} = 0.722$, $\text{RMSE}_{\text{Pred}} = 0.43$, respectively). When observing the different properties' maps separately, varying patterns emerge. For example, contradictory trends are observed between the sand and clay maps (Fig. 12A and 10B, respectively), where higher sand concentrations correspond with lower clay fractions. Greater predicted SOM (Fig. 12C) and P (Fig. 12F) contents were observed within and around the interrupted human LU soils and the Zin streambed. A similar trend occurred for pH (Fig. 12D) and EC (Fig. 12E), where both were also affected by the landscape's topographical features. The unsuccessfully predicted properties, including AWC, fractional silt, NO_3^- , and K, all presented poor correlations and large error sizes, and are thus unreliable for soil mapping in this case.

Table 4: Support vector machine-regression (SVM-R) analysis and image upscaling of prediction results of Avdat region. For each of the soil properties in the model, the number of support vectors (SVs), the adjusted coefficient of determination for the calibration and validation datasets (R^2_{adjCal} and R^2_{adjVal}), as well as for the F-statistic value and degrees of freedom ($F_{(df)Cal}$ and $F_{(df)Val}$), and the root mean square error ($RMSE_{Cal}$ and $RMSE_{Val}$) were assigned. The ratio of performance to deviation (RPD_{Val}) and the interquartile range ($RPIQ_{Val}$) for the validation set was also calculated. Properties with significant prediction values ($RPIQ_{Val} \geq 3$, $RPD_{Val} \geq 2$, and $R^2_{adjVal} \geq 0.7$) were examined for variable importance in projection (VIP) wavebands, upscaled to the image extent, and were assigned R^2 and RMSE (R^2_{Pred} and $RMSE_{Pred}$). Model constraints and optimization parameters' cost (C), epsilon (ϵ), and gamma (γ) are noted.

Soil properties	R^2_{adjCal}	R^2_{adjVal}	$RPIQ_{Val}$	RPD_{Val}	SVs	C	ϵ	γ	$F_{(df)Cal}$	$F_{(df)Val}$	$RMSE_{Cal}$	$RMSE_{Val}$	VIP bands (nm)	$R^2_{adjPred}$	$RMSE_{Pred}$
AWC (%)	0.844	0.776	2.671	2.005	245	275	3.2	6	3108 _(1,552)	844.1 _(1,222)	3.005	3.673	881.78, 1493.44, 1593.95, 1731.94, 2099.81 2351.07	0.417	4.127
Fractional Sand	0.913	0.817	3.681	2.528	198	200	0.045	1.3	5946 _(1,568)	1017 _(1,235)	0.035	0.044	999.77, 1493.44, 1537.43, 1769.52, 2265.92, 2351.07, 2405.36	0.854	0.047
Fractional Silt	0.901	0.810	3.491	2.218	214	300	0.04	1	5094 _(1,563)	1018 _(1,237)	0.032	0.045	881.78, 1537.43, 1593.95, 2180.05, 2417.37, 2471.15	0.494	0.061
Fractional Clay	0.903	0.785	3.245	2.313	205	200	0.019	0.4	5210 _(1,561)	861 _(1,234)	0.017	0.022	871.45, 1285.57, 2124.54, 2223.06, 2357.12, 2417.37	0.707	0.024
NO_3^- (\log_{10})	0.924	0.875	4.545	2.685	248	340	0.16	1.1	6638 _(1,547)	1548 _(1,220)	0.157	0.206	898.97, 1493.44, 1593.95, 1706.87, 1763.26, 2375.25, 2417.37	0.520	0.422
SOM (%)	0.925	0.848	3.718	2.625	220	150	0.42	3	6747 _(1,544)	1218 _(1,217)	0.355	0.458	681.91, 1493.44, 2124.54, 2357.12, 2447.30	0.723	0.434
pH	0.923	0.851	4.043	2.569	258	125	0.12	3.2	6745 _(1,563)	1277 _(1,223)	0.101	0.136	493.43, 599.39, 681.91, 1018.96, 1593.95, 2112.18, 2417.37	0.733	0.136
EC (\log_{10})	0.899	0.837	4.213	2.473	220	250	0.25	2.2	4909 _(1,550)	1174 _(1,227)	0.208	0.254	688.88, 1025.35, 1493.44, 1537.43, 1593.95, 2167.73	0.843	0.319
SAR (\log_{10})	0.902	0.842	3.573	2.637	219	175	0.15	1.1	5166 _(1,560)	1208 _(1,225)	0.136	0.158	737.04, 1706.87, 2204.65, 2278.13, 2453.27	0.783	0.170
P (\log_{10})	0.944	0.862	4.119	3.191	245	275	0.11	1.5	9221 _(1,542)	1378 _(1,220)	0.098	0.119	602.83, 737.04, 905.85, 1203.38, 1493.44, 2345.02, 2417.37	0.733	0.101
K (\log_{10})	0.948	0.841	4.490	2.555	226	350	0.21	3.3	10220 _(1,562)	1179 _(1,221)	0.166	0.231	837.02, 1493.44, 2112.18, 2235.32, 2411.37	0.338	0.450
Overall SQI	0.901	0.867	4.085	2.602	186	250	0.034	0.6	5118 _(1,560)	1484 _(1,226)	0.028	0.032	520.69, 678.46, 1317.13, 1593.95, 1688.07, 1763.26, 2223.06, 2399.35-2435.35	0.779	0.036

AWC: available water content, NO_3^- : nitrate, SOM: soil organic matter, EC: electrical conductivity, SAR: sodium adsorption ratio, P: phosphorus, K: potassium, and SQI: soil quality index.

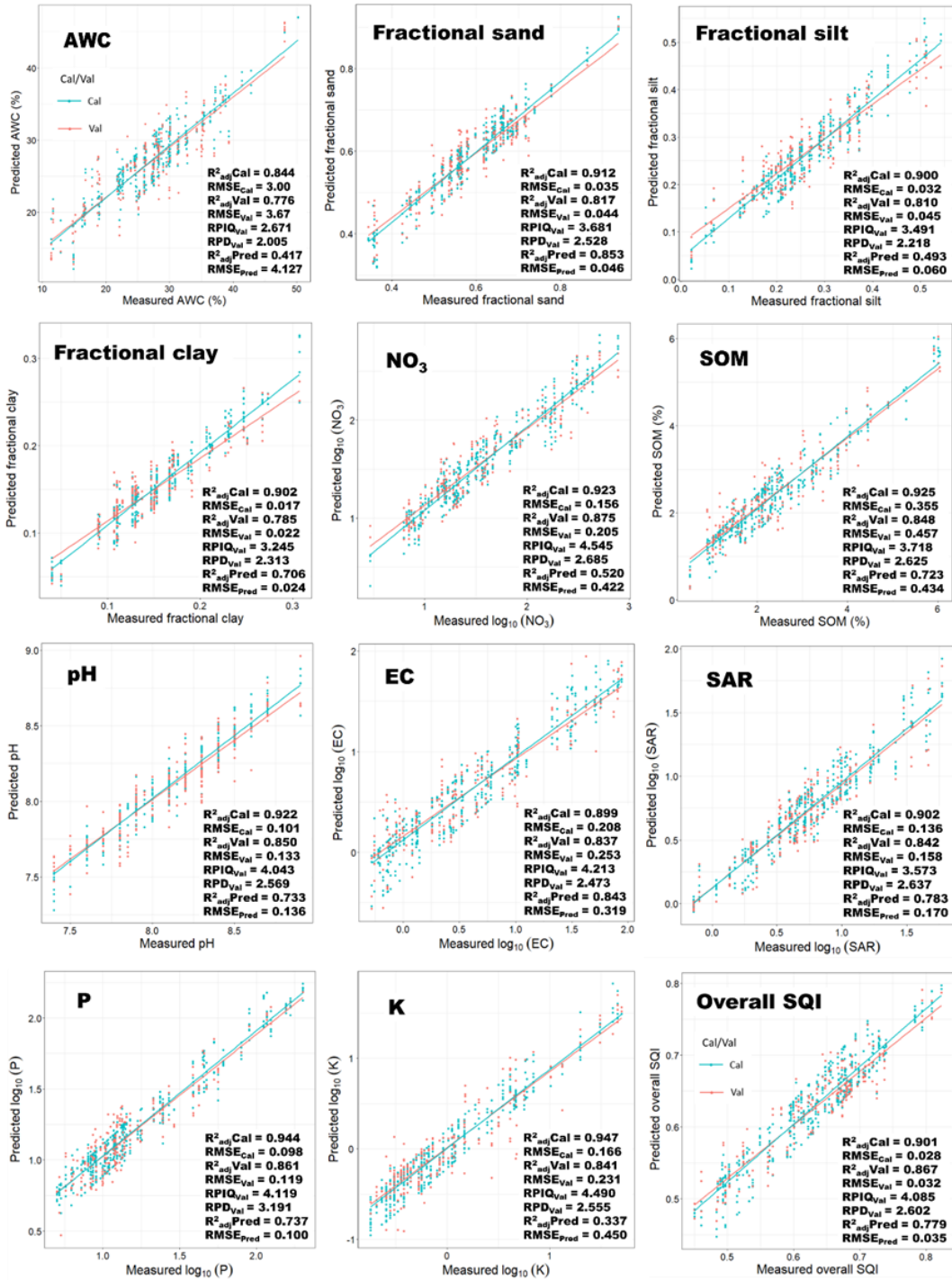
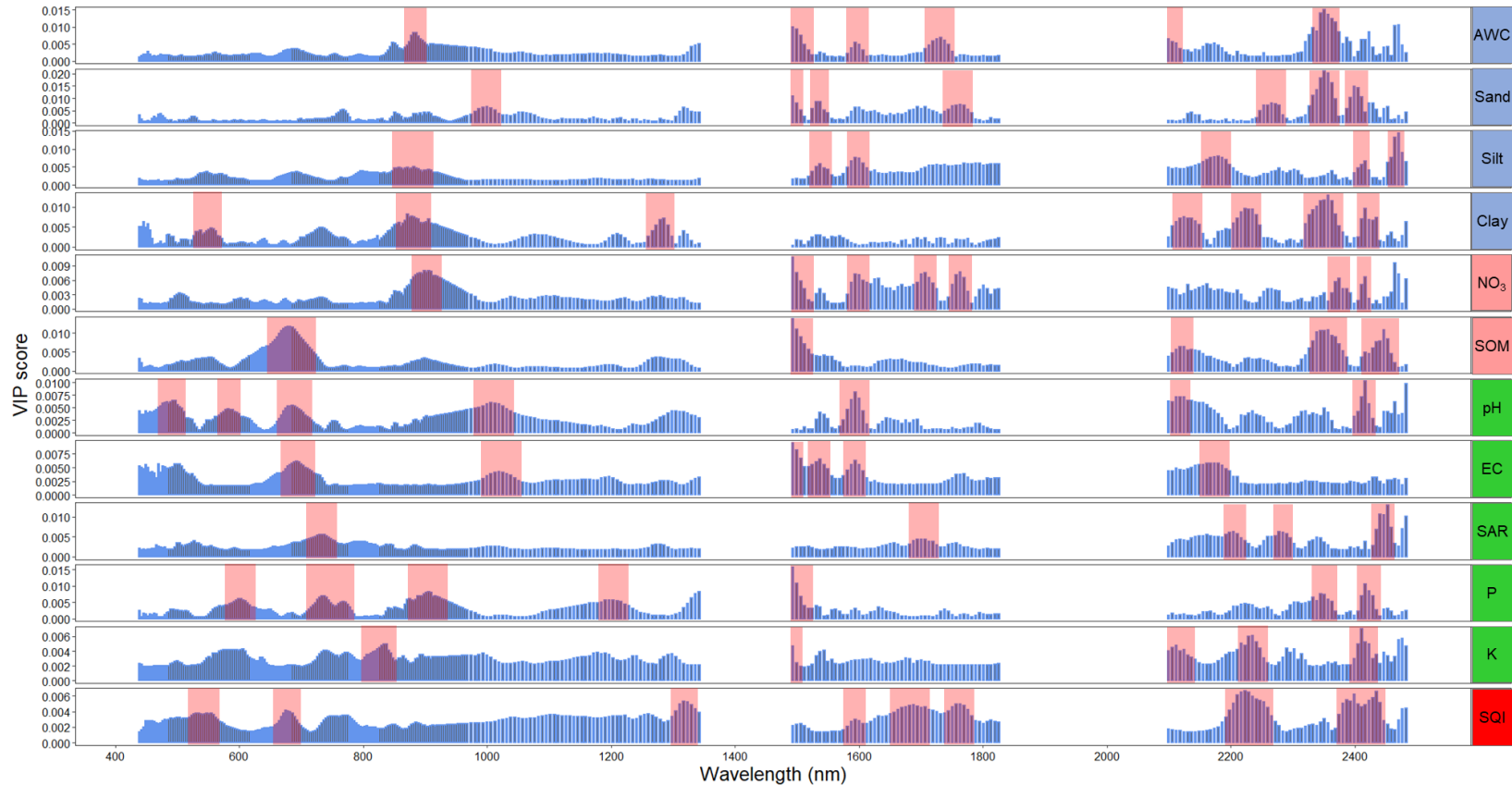


Figure 9: Support vector machine-regression (SVM-R) scatterplots and main results for the correlated soil properties and the overall soil quality index (SQI), between the measured calibration (Cal) and the validation (Val) datasets, and also the results of the upscaled image prediction maps (Pred). RMSE: root mean square error; RPIQ: ratio of performance to interquartile range; RPD: ratio of performance to deviation; AWC: available water content, NO_3^- : nitrate, SOM: soil organic matter, EC: electrical conductivity, SAR: sodium adsorption ratio, P: phosphorus, and K: potassium.



Figure

10: Variable importance in projection (VIP) plot of the physical (blue), biological (pink), and chemical (green) soil properties in the Avdat region. Each bar represents the importance score of a particular hyperspectral image waveband in the support vector machine regression (SVM-R) analysis. The red sections highlight spectral regions with significant VIP peaks. AWC: available water content, EC: electrical conductivity, Cl: chlorine, Na: sodium, Ca + Mg: calcium and magnesium, SAR: sodium adsorption ratio, NO₃⁻: nitrate, P: phosphorus, and SQI: soil quality index.

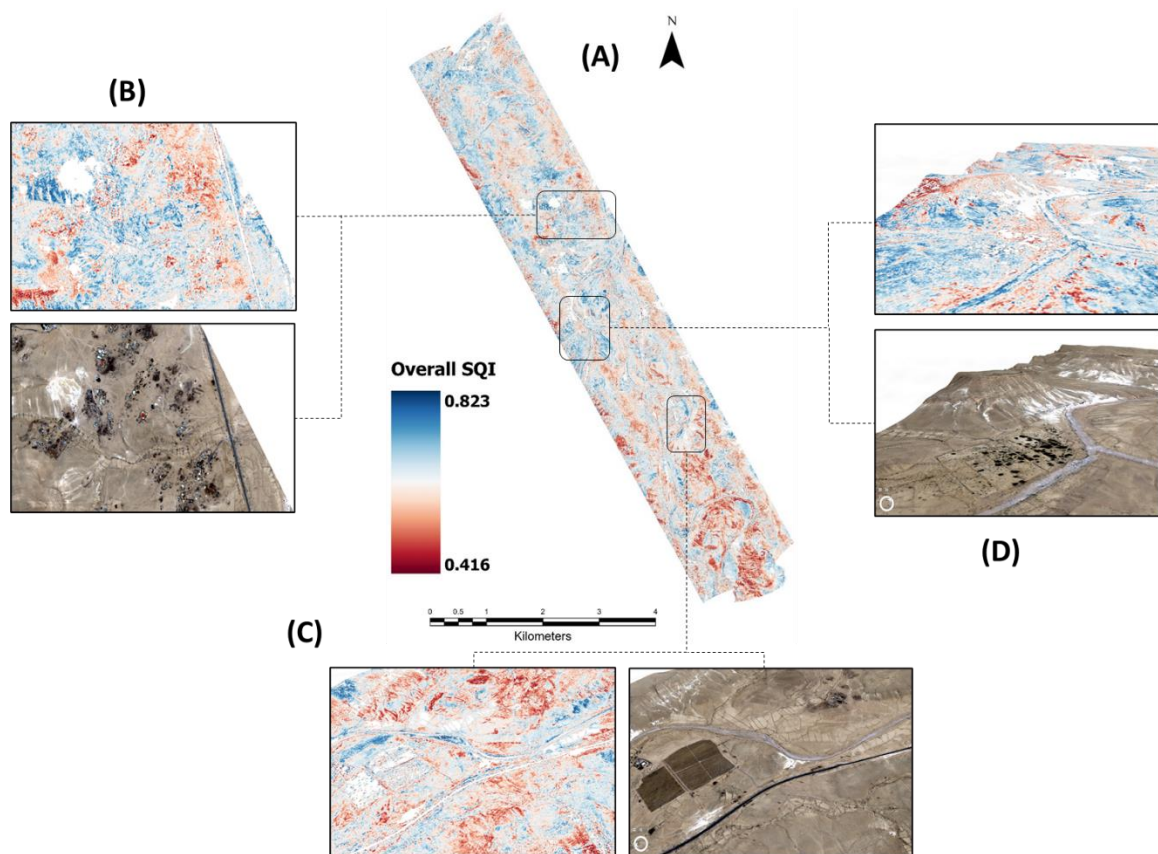


Figure 11: (A) Final upscaled prediction map for the overall soil quality index (SQI) over the Avdat region, affected by various LU features, including (B) grazing LU and highly eroded bright chalky soil around an unrecognized Bedouin village; (C) agricultural fields (on the left edge of the image), stone-wall terraces (on the right), and the Zin Stream (in the center); and (D) a *liman* runoff-harvesting system (RHS) and degraded soil in response to steep and barren topography.

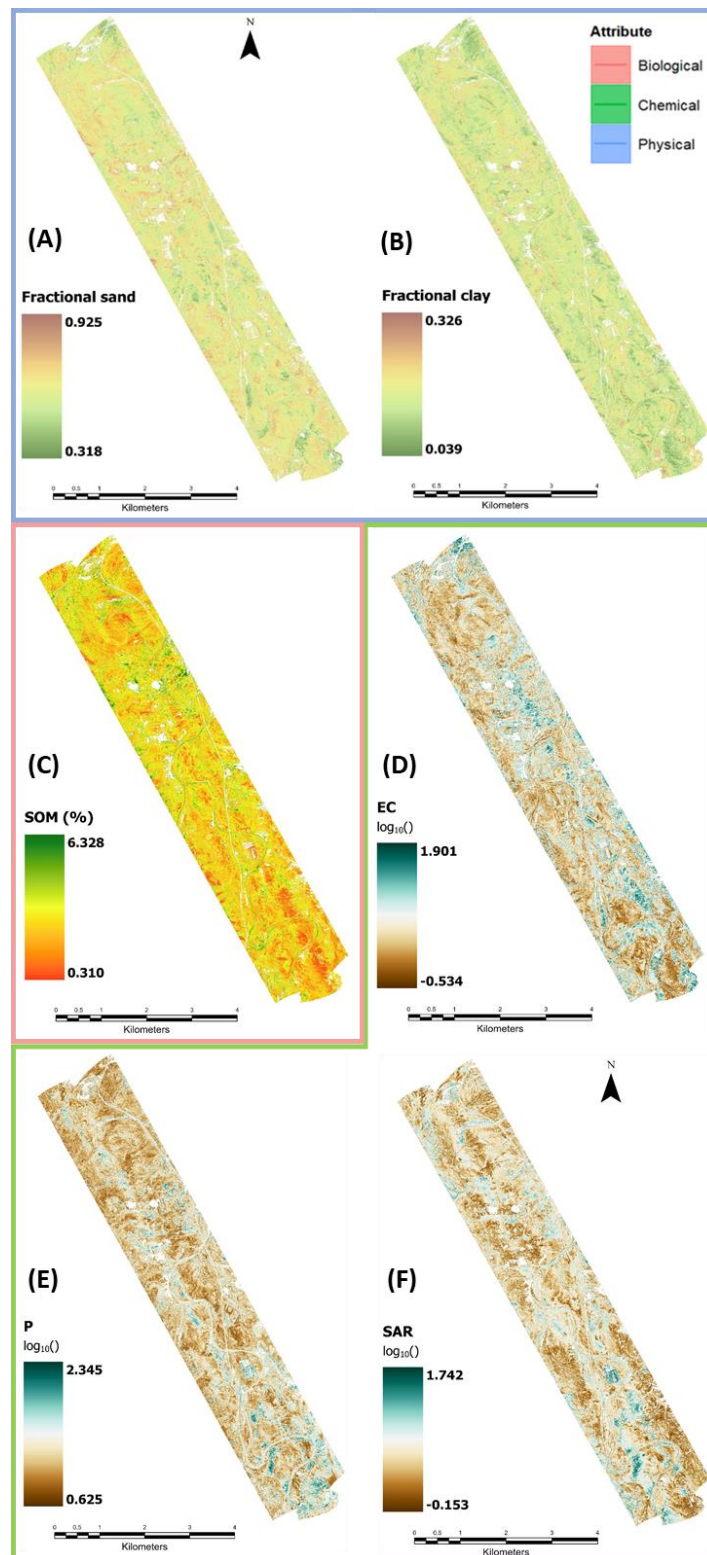


Figure 12: Final upscaled prediction maps for the individual soil properties over the Avdat region: (A) fractional sand, (B) fractional silt, (C) soil organic matter (SOM), (D) electrical conductivity (EC), (E) phosphorous (P), and (F) sodium adsorption ratio (SAR). The colored frames represent the associated physical, biological, and chemical components of the soil indicators.

4 Discussion

The current study demonstrated the capability of airborne IS for continuous surface mapping of multiple soil properties and the integrated SQI over the entire study area. The soil properties and

overall quality were tested by combining conventional laboratory surveys and the contribution of the spectral dimension to the regression-based prediction capabilities of IS. The incorporation of the laboratory soil analyses of 12 physical, biological, and chemical indicators and the integrated overall SQI with the spectral data extracted from the hyperspectral image was successfully applied. The PLS-DA classification confirmed the strong existing spectral separability among the four examined LUs. The successful classification results enable differentiating between the four LU types and their natural proximity in the arid environment of the Avdat region in the Negev Desert. The prediction of the SQI was found significant for both the local point-scale ($R^2_{\text{adjVal}} = 0.87$, $\text{RPIQ}_{\text{Val}} = 4.09$, $\text{RPD}_{\text{Val}} = 2.60$, $\text{RMSE}_{\text{Cal}} = 0.03$, and $\text{RMSE}_{\text{Val}} = 0.03$) and the large-scale regional mapping ($R^2_{\text{adjPred}} = 0.78$, $\text{RMSE}_{\text{Pred}} = 0.03$). We found high prediction ability for seven soil indicators, including fractional sand and silt, SOM, pH, EC, SAR, and P. The developed regional extent mapping enabled the recognition and monitoring of the contiguous spatial variability of different soil processes in response to both human-made practices and environmental features as one. The results provided by the IS methodology affirm its substantial advantages, effectiveness, and reproducibility capabilities for comprehensive soil quality assessment, particularly in rough and challenging arid environments, as in our case study.

4.1 Soil quality assessment

The assessment of soil quality within an ecological scope requires the selection and adjustment of a particular set of soil indicators that will best depict the function of the soil under changing LUs and management practices (Bünemann et al., 2018). The SMAF protocol (Andrews et al., 2004) was most suitable for this objective by employing chemometrics analyses of 12 physical, biological, and chemical soil indicators. As described in the previous study (Levi et al., 2020), soil indicators were selected according to the investigated arid study area and LUs. Therefore, selecting adequate soil indicators and their amount is a great challenge, especially in a resource-limited dryland environment. For instance, plant and microbiome available water, soil organic matter, nutrients, and seed banks in the soil are critically limiting factors in this climate type (Saygin, 2018). Thus, the quantification of their presence is crucial for the soil quality evaluation due to their essential role as precursors of the soil's ability to support the ecosystem's productivity and function (Lal, 2011). It is also necessary to trace soil salinization processes by measuring salinity indicators, such as EC, SAR, and other particularly saline elements (i.e., Cl, Na, and Ca + Mg). The loess-dominated aridisol soil order cannot be defined as highly alkaline in its natural state, but rather as a natric subgroup of typical soils (Singer, 2007). However, the salinity levels have shown significant fluctuations in the different LUs practiced, particularly those involved with intensive cropping and herding. Soil texture is also an important property since, in most cases, it strongly dictates other mechanisms within the soil column. Some

notable processes include water and organic matter holding capacity, drainage, permeability, fertility (Weil and Brady, 2017), and the support of developing aggregates that improve the soil's resistance and stability, which mitigate its erosion and quality degradation (Eldridge et al., 2020; Levi et al., 2021).

The potential redundancy amid the selected soil indicators in the SQI model was reduced with the exclusion of the strongly correlated salinity properties (i.e., Cl, Na, and Ca + Mg) and the descriptive soil texture, the scoring transformations, and the PCA for a better interpretation of the interrelationships between the selected indicators. The preventive measures taken have confirmed that the incorporated soil indicators were, in fact, statistically distinct and explain most of the variation in the assessment model. The PCA results were used to assign the weights to the transformed scored indicators to develop the statistically integrated SQI for a numerical and quantifiable evaluation of the soil performance in response to the different LUs and land-cover features. The significant differences found for the calculated SQI (Fig. 4) suggest that the human LU practices significantly impact the natural surroundings for the overall estimation in both improvement and degradation. The strictly regulated agricultural fields had higher SQI scores than the grazing and RHS LUs, which are more affected by sporadic processes of livestock behavior and climatic conditions, respectively, with the natural LU placed in-between. Moreover, the significant differences observed between the LUs, mainly for the biological and chemical attributes, revealed a more explicit site-specific depiction of the ongoing soil processes. The biological soil properties were significantly less abundant in the RHS and natural land than in the managed agricultural and grazing practices.

In contrast, the chemical indicators more strongly influenced the natural soils than the other three LUs. This is a direct outcome of the different agricultural, grazing, and RHS-related inputs, such as irrigation, catchment water, fertilizers, pesticides, organic matter, and livestock residues (Biagetti et al., 2021; Haynes and Naidu, 1998; Turner, 1998). These practices show that the agriculture LU is generally more affected by chemical properties related to cropping activity. At the same time, the grazing LU is more impacted by biological factors derived from livestock and herding activities. On the other hand, the RHS relies on the accumulation of transported natural resources from a severely resource-scarce environment, thus exhibiting significantly low biological properties values, similar to the natural environment.

4.2 Spectral discriminant analysis classification by LU

The described PLS-DA classification presents good visual and statistical spectral separability among the four different LU practices. The PLS-DA provides a quantitative approach to separate the cumulative probability of the soil spectral samples into statistically distinct classes, according to their respective LU. The strong classification results presented clear contrast between the different

practices, with minor confounding among parts, like grazing mixing with RHS and natural LUs. This could be explained by the fact that these practices share properties that are related to the soil condition and its management. The VIP analysis contributes an additional aspect of the differences among the four practices. While all LUs show sensitivity for shared regions across the spectral range, the particular practices accentuate specific absorption features that imply more significant soil properties. The agriculture displays more significant peaks in the SWIR region (2200-2450 nm), related to organic compounds, clay minerals, and carbonates, in comparison to spectral attributes in the VIS-NIR region (520-850 nm) that are more significantly affected by soil organic matter, nutrients, and herding activity prevailing in intensive grazing soils (Ben-Dor et al., 2015). The RHS and natural LUs show a more mixed behavior, where the natural land is less affected by SOM and organic resources due to their scarcity compared to the RHS, but also exhibits more emphasized peaks related to clay minerals (1688.07 nm) and water absorption (1285.57 and 1537.43 nm) for the natural areas (Ben-Dor, 2011).

4.3 Spectral correlations to soil indicators and the SQI

The SVM-R correlations of the measured laboratory soil indicators (i.e., raw and log-transformed) with the enriched extracted spectra from the AisaFENIX image have achieved successful validation values for the SQI ($RPIQ_{val} \geq 3$, $RPD_{val} \geq 2$, and $R^2_{adjVal} \geq 0.70$) and several soil properties (Fig. 9 and Table 3). Some showed more robust performances than others, notably EC, pH, NO_3^- , P, and K, representing variations of salinity levels and nutrient availability in the soil. The deviations in the mentioned indicators were firmly attributed to human interference originating from agriculture, grazing, and RHS activities and their effects on the SQI (Paz-kagan et al., 2016; Paz-Kagan et al., 2017). The influence of SOM and AWC is strongly related to soil texture (sand, silt, and clay fractions). Larger fractions of the finer grain-sized clay particles and minerals generally improve their retention capacity within the soil system (Marques et al., 2019). As can be seen from the mean extracted spectra by LU in Figure 6, the interrupted LU curves are less reflective than the natural ones, indicating the more significant influence and absorption of different artificial effects on the soil. Managed land cultivation increases the inputs and accumulation of vital resources such as water, nutrients, sediments, and seeds. Their increasing abundance in the soil strengthens the absorption factor in the particular spectral regions linked to these soil materials and attenuates the general spectral signature curves of the human LUs compared to the natural ones (Demattê et al., 2007; Stoner and Baumgardner, 1981).

The spectral inference indicates on strengthens of these relationships, where significant spectral features in the SQI regression VIP analysis were affiliated to particular chromophores (Fig. 10). The spectral features in the VIP were associated, regarding various molecular bonds, overtones, and

mineralogical structures, with the different soil attributes (Ben-Dor, 2011). For example, EC shows substantially important spectral features in the 1490–1590 and 2200 nm spectral regions, partially, with almost all soil indicators, including AWC, silt, clay, and SOM. These soil properties (i.e., AWC, silt, clay, and SOM) are well-known for their direct or indirect relations to hygroscopic water absorption (Ben Dor et al., 2015), hydroxyl functional O–H group minerals (Taylor, 2004), and carbonate C–O group minerals (Ben-Dor and Banin, 1995). These were mainly related to calcite and dolomite that loosely cement the sedimentary loess soil in this arid region (Shapiro, 2006). The topsoil's retention was also attributed to the soil texture and mineralogical structure and composition. Significant portions of phyllosilicate 2:1 clay and fine silt minerals (e.g., kaolinite and montmorillonite) generate greater pore area for improved water holding capacity and greater soil colloid surface for adsorption of organic matter, soil nutrients, and saline elements (Barré et al., 2008; Barton and Karathanasis, 2005). In turn, these elemental and molecular interactions regulate the exchange capacity of the mineral's electric charge that could potentially undermine the soil's aggregation stability, which eventually results in soil weathering and quality degradation (Conforti et al., 2013).

Different soil properties were acknowledged for various spectral absorption features across the entire spectral range, most notably in the SWIR region (Demattê et al., 2007). Organic matter is known for its direct absorption across the VIS-NIR region around 550–1100 nm and peaking at 675 nm, according to He et al. (2009). The SOM revealed a strong peak at 681.91 nm, along with other indicators, including EC, pH, SAR, and P. These soil indicators were related to colloid adsorption competitors that are accentuated by indirect features in the SWIR over 2300–2450 nm, where SOM moderates the salinity levels when retained in place of saline elements (Ding et al., 2020). Significant features were found within 520–600 nm that associates higher concentration of P with crop and plant residues as well as with some oxides in the soil (Morón and Cozzolino, 2007). The important peaks for K at 2112.18 and 2235.32 nm, which are more prevalent in human LUs than in natural ones, are linked to clay minerals and SOM that supply exchangeable cations (Demattê et al., 2017). The SQI regression model complies with other individual indicators' success, where significant spectral footprints affect the SQI importance analysis. These emphasized the most predominant features that imply the intercorrelation of the different soil properties (Paz-Kagan et al., 2015). They also correspond well with the acknowledged spectral features found for the PLS-DA classifications VIP analysis. However, it also seems that some unrelated VIP peaks were observed for some of the properties that could not be attributed to the known spectral absorption features of specific materials. The spectral enrichment is a possible reason for introducing particular non-elemental spectral features into the variable importance analysis. These features might originate from site-specific factors such as local topography, which might be responsible for some of the prediction models' inaccuracies.

4.4 Soil quality mapping

The final step towards a comprehensive soil quality assessment is the regional prediction based on the acquired and processed airborne AisaFENIX hyperspectral image. Integrating the extensive soil quality assessment of the physical, biological, and chemical indicators with IS allows inferring the causes of spatial variations for the SQI and soil indicators (Paz-Kagan et al., 2015). The SQI map agreed with the independent soil samples and their corresponding extracted predicted values. It managed to distinguish various clusters of pixel values in the matter of different LUs and terrain features, such as livestock pens and intensive grazing (Fig. 11B), agricultural fields, stone-wall terrace effects, stream paths (Fig. 11C), hillslopes, a *liman*, and underdeveloped soils (Fig. 11D). The spatial divergence was found significant for the SQI and seven other soil properties.

The general trend is that lower and flatter surfaces, like those around the ephemeral Zin Stream, with more developed soil systems, present higher SQI values than the more rugged and steep topography at the study area's western and southern borders. The stream channel itself displayed relatively high SQI scores, with significantly higher rates in locations of deposited fine sediments, such as point and channel bars and stream banks along the meandering stream path (Hu et al., 2017). Along with the discharged deposits, the intensive flashflood events that characterize the region carry soil, organic matter, and mineral nutrients that enrich the soil, improving soil quality (Yang et al., 2019). The RHSs located alongside the stream path showed different trends according to the type of water catchment system observed. The primary function of an RHS is to capture the water and sediment flow that would otherwise wash out of the watershed during runoff-generating rainfall events. The *liman* systems collect the runoff, sediments, and essential soil materials into small catchment areas. Studies have shown that *limans* generally exhibit better SQI score characteristics (Paz-Kagan et al., 2019, 2017). They act as sinks that prevent discharge back to the stream and significantly improve soil quality in small catchment areas (Paz-Kagan et al., 2017). The hydrological barriers of the stone-wall terraces reduce water conductivity and water leakage while increasing soil deposits and moisture on the watershed scale. A general decrease in SQI is detected as the stream attenuates northwards since the terraces effectively reduce the energy of the runoff flow. The upstream terraces dilute a significant amount of the transported soil, resulting in decreased SQI in the downstream watershed (Biagetti et al., 2021; Yizhaq et al., 2020). Studies of terraced riverbeds revealed their essential function in agricultural systems and the conservation of abandoned riverbeds to prevent soil erosion and fertility loss. Our research demonstrates that integrating human-designed water harvesting systems into nature is possible when knowledge on watershed ecology is available. This knowledge can produce a sustainable human-ecological management policy by enhancing services without modifying their inherent properties.

Within the other human-impacted LUs and their surroundings, different variabilities in SQI

scores occurred. The modern agriculture fields exhibit diverse patterns among and within plots, which vary in response to applied treatments, irrigation, fertilization, and crops (Ohana-levi et al., 2018). Like the agricultural areas, our results show that the livestock settlements impacted SQI centroids that gradually decreased with distance. These hotspots of degraded SQI scores within the grazing LU are centered mainly around livestock pens, animal waste fills, poor land cultivation, and excessive organic matter accumulation in the feeding areas (Amiri et al., 2008). In contrast, less affected in-between soils exhibited relatively good SQI values.

The overall SQI map depicts the variation in soil processes derived from its assembled individual soil indicators. The EC map accorded well with the SQI map. Higher salinity was observed in weathered and disintegrated soils (i.e., very bright chalk and marlstone) and soils in proximity to Bedouin villages, and steep exposed hillslopes correlated with poor SQI scores. Soil brightness could be an explanatory factor for the bright chalky soils, where a positive correlation was found between soil whiteness and high salinity levels (da Neto et al., 2017; Moreira et al., 2015). The highly SQI-ranked *limans* profited from the low predicted salinity levels. However, some agricultural LU and stone-wall terrace presented high predicted EC values and high SQI scores. It could be assumed that other indicators took precedence over EC in influencing the overall soil quality within these closed systems. In this regard, the SAR and P (and the poorly predicted K) maps show a similar trend of high predicted values in the agro-systems mentioned above that correlate with lower SQIs. This matching trend can refer to the PCA results (Table 2 and Appendix A), where both SAR and P were found to be the most significant properties under PC1 and showed very similar factor loadings, with EC placed only under PC2. High measured SAR values imply an excessive sodium content in irrigation water and other fertilizers that act as potential adsorptions to the soil particles, which risks causing soil sodicity. High sodicity levels in the soil can deteriorate the water infiltration rate and hydraulic conductivity, limiting the plant available water and eventually presenting hazards to the soil health (Robbins, 1984).

The SOM distribution was mainly concentrated in some of the agricultural fields and the nearby agro-pastoral settlements. Much of the soil organic compound concentration is derived from cropping and herding occurring along the Zin Stream, as seen by the precipitation of transported organic material across the streambed in the SOM predicted map. The large-scale prediction value of SOM reached an agreement of 0.723, close to the 0.71 predicted SOM mapping value presented by Ou et al. (2021) over a study area in China. For its decisive role in the hydrological properties and material retention in the soil, the soil texture was found significant for both sand and clay. The predominant sandy-loam texture of the region found a high prediction accuracy for sand abundance ($R^2_{\text{adjPred}} = 0.853$), compared to more temperate climates with loam and silt-loam soil textural classes in Germany (0.77; Kanning et al., 2016) and the Czech Republic (0.67; Žižala et al., 2017), but with a significantly

lower agreement for smaller clay fractions (0.706) compared to clay-rich soils in Brazil (0.78; Bellinaso et al., 2021).

Although most detected elements were linked to spectral features recognized by previous literature, we found that other signal interferences caused some additional peaks. These could originate from mixed pixels, surface brightness, the BRDF effect, restricted image spatial resolution, and the remnants of residual organic and non-soil material common in relatively noisy data of this kind (Ben-Dor et al., 2009; Schläpfer et al., 2015). Achieving a color-balanced multi-stripped hyperspectral image is highly challenging and assumes an inherited degree of BRDF error for such rugged terrain with multiplex viewing and illumination angles (Jia et al., 2020). A specific gradient was observed for the BRDF disruption, despite removing the image fringes. Increased interference and striping appeared in models with weaker prediction accuracy, meaning significant prediction models were robust enough to overcome the BRDF impediment to present a credible contiguous soil property representation.

Nevertheless, the quantitative capabilities of IS for large-scale soil monitoring, in general, and soil quality assessment, in particular, have proved to possess strong prediction competence. IS applications were recognized as being a comprehensive, time-efficient, non-destructive, and reproducible analytical approach. At this point, the sensors are mostly airplane-carried and restricted to a specific regional spatial extent due to the current lack of operational hyperspectral satellite platforms (Ong et al., 2019). However, this is starting to change as various soil-induced high signal-to-noise ratio spaceborne imaging spectrometer missions embark on their first steps in orbit to make their acquired imagery accessible for future studies (Chabrillat et al., 2019). Such missions include: the Italian–Israeli SHALOM (Spaceborne Hyperspectral Applicative Land and Ocean Mission) with 10-m spatial resolution and 240 spectral bands scheduled for 2024 (Feingersh & Ben-Dor, 2015); the Italian PRISMA (PRecursore IperSpettrale della Missione Applicativa) launched in March 2019 with 30 m per pixel and 238 bands (Loizzo et al., 2018); the French HypXIM provisioned for 2021 with pixel width starting from 8 m and 210 bands (Michel et al., 2011); the German EnMAP (Environmental Mapping and Analysis Program) planned for 2021 containing 30-m resolution and 228 wavebands (Guanter et al., 2015); the International Space Station (ISS) mounted NASA's HypsIRI (Hyperspectral InfraRed Imager) with 30 m pixel size and 210 bands in 2018 (Lee et al., 2015); and the Japanese HISUI (Hyperspectral Imager SUite) in December 2019 with 30-m resolution and 185 spectral bands (Matsunaga et al., 2013). The current research could stimulate potential soil studies and questions in future hyperspectral earth-observing space platforms for soil applications at regional and global scales.

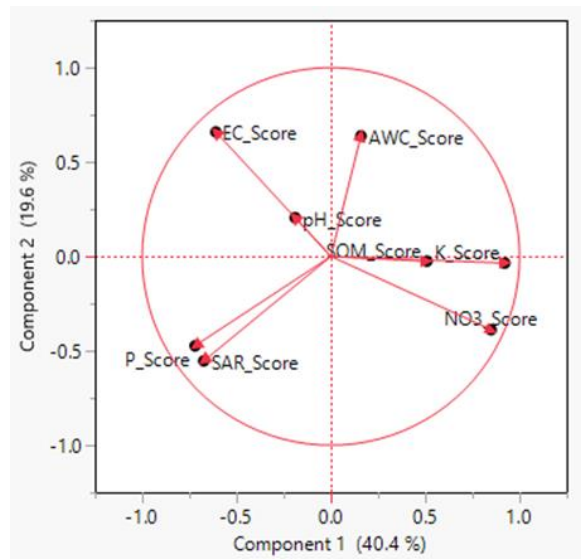
5 Conclusion

The effects of LU changes, derived from ancient and modern human activity and disturbance of the natural environment, are crucial in ecological preservation and environmental health monitoring, in general, and for soil quality assessment. The impact of these land transformations is particularly acute when they occur in harsh resource-limited arid conditions such as the Avdat region in Israel's Negev Desert. In this study, a novel approach was developed for soil quality assessment by applying the IS method for a large-scale continuous and precise mapping of the overall SQI and individual soil indicators over the entire study area, particularly under extreme arid climate conditions. The assessment was based on the regression of the measured indicators and the highly detailed spectral information collected from an acquired hyperspectral image. The image-extracted spectra were first classified to examine their inherent separability among the four tested land-uses. Then the soil properties and the overall SQI were correlated using SVM-R, which managed to predict the measured SQI well on the local point-scale and the predicted regional mapping. As a result, seven soil properties were successfully mapped over the entirety of the AisaFENIX image. The significantly predicted regional maps have depicted the most prevalent soil-forming and degrading processes causing various environmental disturbances, both natural and human-made, affecting the land and the soil quality through different mechanisms. Many challenges are associated when using IS, like adjusting the assessment model to changing types of soils, climates, scales, and land-uses, as well as overcoming limitations derived from the imaging process, such as high operational costs and the lack of continuous image acquisition over time for long-term monitoring. Despite all these, the strong quantitative capabilities of IS affirm its accuracy, time-efficiency, scalability, and reproducibility even in challenging dryland conditions. This study underscores the applicability of IS for soil function examination under a large variety of environmental conditions and scales, which could be an essential tool for sustainable and efficient land management in degraded land.

Acknowledgments

This project has received funding from the European Union's Horizon 2020 research and innovation program "European Long-Term Ecosystem, Critical Zone, and Socio-Ecological systems Research Infrastructure PLUS" (eLTER PLUS) under grant agreement no. 871128. The authors wish to thank Mr. Alexander Goldberg for soil collection, analysis, and logistical support in the field and laboratory work, Dr. Natalia Panov and Dr. Jisung Chang for hyperspectral images preprocessing, and Mr. Vladislav Dubinin for statistical and methodological advice.

Appendices



Appendix A: Principal component analysis (PCA) bi-plot demonstrating the loading factor of the different scored soil indicators for the interactions of PC1 and PC2. AWC: available water content, NO_3^- : nitrate, SOM: soil organic matter, EC: electrical conductivity, SAR: sodium adsorption ratio, P: phosphorus and, K: potassium.

Appendix B: Confusion matrix of the land-use land-cover (LULC) minimum distance classification for the AisaFENIX hyperspectral image, resampled to Landsat 8 spectral resolution (Fig. 5B).

Class	Observed					Producer accuracy (%)	User accuracy (%)	Overall agreement rate
	Very bright soil	Bright soil	Soil	Dark soil	Road/Built-up			
Very bright soil	1599	150	0	0	8	99.69	91.01	Total accuracy: 95.11%
Bright soil	5	4126	77	3	72	95.13	96.33	
Soil	0	40	12450	680	0	99.36	94.53	
Dark soil	0	16	3	3156	9	78.57	99.12	
Road/Built-up	0	0	0	147	2959	97.05	95.27	
Total	1604	4337	12530	4017	3049	100	100	
						Total		Kappa (Kc): 0.928
Area (km ²)	0.25	4.03	16.03	2.97	0.25	23.53		
% of total area	1.08	12.63	68.13	17.11	1.05	100		

Chapter 1- References

- Adeel, Z., Safriel, U., Niemeijer, D., White, R., 2005. Ecosystems and human well-being - A report of the millenium ecosystem assessment, World Health.
- Andrews, S.S., Karlen, D.L., Cambardella, C. a, 2004. The Soil Management Assessment Framework: A Quantitative Soil Quality Evaluation Method. *Soil Sci. Soc. Am. J.* 68, 1945–1962. <https://doi.org/10.2136/sssaj2009.0029>
- Andrews, S.S., Karlen, D.L., Mitchell, J.P., 2002. A comparison of soil quality indexing methods for vegetable production systems in Northern California. *Agric. Ecosyst. Environ.* 90, 25–45. [https://doi.org/Pii S0167-8809\(01\)00174-8](https://doi.org/Pii%20S0167-8809(01)00174-8) \rDoi 10.1016/S0167-8809(01)00174-8
- Awiti, A.O., Walsh, M.G., Shepherd, K.D., Kinyamario, J., 2008. Soil condition classification using infrared spectroscopy: A proposition for assessment of soil condition along a tropical forest-cropland chronosequence. *Geoderma* 143, 73–84. <https://doi.org/10.1016/j.geoderma.2007.08.021>
- Ben-dor, E., 2017. Characterization of Soil Properties Using Reflectance Spectroscopy. <https://doi.org/10.1201/b11222-31>
- Ben-Dor, E., Banin, A., 1995. Near-Infrared Analysis as a Rapid Method to Simultaneously Evaluate Several Soil Properties. *Soil Sci. Soc. Am. J.* 59, 364. <https://doi.org/10.2136/sssaj1995.03615995005900020014x>
- Ben-Dor, E., Chabrillat, S., Demattê, J.A.M., Taylor, G.R., Hill, J., Whiting, M.L., Sommer, S., 2009. Using Imaging Spectroscopy to study soil properties. *Remote Sens. Environ.* 113, S38–S55. <https://doi.org/10.1016/j.rse.2008.09.019>
- Ben Dor, E., Ong, C., Lau, I.C., 2015. Reflectance measurements of soils in the laboratory: Standards and protocols. *Geoderma* 245–246, 112–124. <https://doi.org/10.1016/j.geoderma.2015.01.002>
- Blecker, S.W., Stillings, L.L., Amacher, M.C., Ippolito, J.A., Decrappeo, N.M., 2012. Development of vegetation based soil quality indices for mineralized terrane in arid and semi-arid regions. *Ecol. Indic.* 20, 65–74. <https://doi.org/10.1016/j.ecolind.2012.02.010>
- Brady, N.C., Weil, R.R., 1999. Soil organic matter., in: *The Nature and Properties of Soils*.
- Bünemann, E.K., Bongiorno, G., Bai, Z., Creamer, R.E., De Deyn, G., de Goede, R., Fleskens, L., Geissen, V., Kuyper, T.W., Mäder, P., Pulleman, M., Sukkel, W., van Groenigen, J.W., Brussaard, L., 2018. Soil quality – A critical review. *Soil Biol. Biochem.* 120, 105–125. <https://doi.org/10.1016/j.soilbio.2018.01.030>
- Bushong, J.T., Norman, R.J., Slaton, N.A., Bushong, J.T., Norman, R.J., Slaton, N.A., Slaton, N.A., 2015. Communications in Soil Science and Plant Analysis Near-Infrared Reflectance Spectroscopy as a Method for Determining Organic Carbon Concentrations in Soil Near-Infrared Reflectance Spectroscopy as a Method for Determining Organic Carbon Concentrations in Soil. *Commun. Soil Sci. Plant Anal.* 46, 1791–1801. <https://doi.org/10.1080/00103624.2015.1048250>
- Carter, M.R., Gregorich, E.G., 2006. *Soil Sampling and Methods of Analysis, Measurement*. <https://doi.org/10.1017/S0014479708006546>
- Casida, L.E., Klein, D.A., Santoro, T., 1964. SOIL DEHYDROGENASE ACTIVITY: *Soil Sci.* 98, 371–376. <https://doi.org/10.1097/00010694-196412000-00004>
- Cécillon, L., Es, B., Gomez, C., Ertlen, D., Génot, V., Hedde, M., Stevens, A., Brun, J.-J., 2009. Assessment and monitoring of soil quality using near infrared reflectance spectroscopy (NIRS). *Eur. J. Soil Sci.* 60, 770–784. <https://doi.org/10.1111/j.1365-2389.2009.01178.x>
- Chang, C., Laird, D., Mausbach, M.J., 2001. *Near-Infrared Reflectance Spectroscopy – Principal*

- Components Regression Analyses of Soil Properties Near-Infrared Reflectance Spectroscopy – Principal Components. <https://doi.org/10.2136/sssaj2001.652480x.Rights>
- Crist, E., Mora, C., Engelman, R., 2017. and biodiversity protection 264, 260–264.
- Division, C., Nature, I., Authority, P., Shaul, G., Conservation, N., Campus, S.B., 2012. Patterns in Habitat Type , Species Richness and Community Composition At Avdat Lter , Israel 5–23.
- Doran, J.W., Parkin, T.B., 1994. Defining and assessing soil quality. *Defin. soil Qual. a Sustain. Environ.* <https://doi.org/10.2136/sssaspecpub35.c1>
- Fidêncio, P.H., Poppi, R.J., Andrade, J.C. De, 2002. Determination of organic matter in soils using radial basis function networks and near infrared spectroscopy & 453, 125–134.
- Foley, J.A., 2005. Global Consequences of Land Use. *Science* (80-.). 309, 570–574. <https://doi.org/10.1126/science.1111772>
- Fystro, G., 2002. The prediction of C and N content and their potential mineralisation in heterogeneous soil samples using Vis-NIR spectroscopy and comparative methods. *Plant Soil* 246, 139–149. <https://doi.org/10.1023/A:1020612319014>
- Groenendyk, D.G., Ferré, T.P.A., Thorp, K.R., Rice, A.K., 2015. Hydrologic-Process-Based Soil Texture Classifications for Improved Visualization of Landscape Function. <https://doi.org/10.1371/journal.pone.0131299>
- Gupta, B., Huang, B., 2014. Mechanism of Salinity Tolerance in Plants : Physiological , Biochemical , and Molecular Characterization 2014.
- Haynes, R.J., Naidu, R., 1998. Influence of lime , fertilizer and manure applications on soil organic matter content and soil physical conditions : a review 123–137.
- Hotelling, H., 1933. Analysis of a complex of statistical variables into principal components. *J. Educ. Psychol.* 24, 417–441. <https://doi.org/10.1037/h0071325>
- Idowu, O.J., Van Es, H.M., Abawi, G.S., Wolfe, D.W., Schindelbeck, R.R., Moebius-Clune, B.N., Gugino, B.K., 2009. Use of an integrative soil health test for evaluation of soil management impacts. *Renew. Agric. Food Syst.* 24, 214–224. <https://doi.org/10.1017/S1742170509990068>
- Issues, K., 2013. Mid-Infrared Spectroscopy Applications for Soil Assessment with Emphasis on Soil Organic Matter Content and Quality : , pp.1349–1362. Issues, K., 2013. Mid-Infrared Spectroscopy Applications for Soil Assessment with Emphasis on Soil Organic Matter Content and Quality : 1349–1362. <https://doi.org/10.1366/13-07288>
- Jolliffe, I.T., Cadima, J., Cadima, J., 2016. Principal component analysis : a review and recent developments Subject Areas : Author for correspondence :
- Karlen, D.L., Mausbach, M.J., Doran, J.W., Cline, R.G., Harris, R.F., Schuman, G.E., 1997. Soil Quality: A Concept, Definition, and Framework for Evaluation (A Guest Editorial). *Soil Sci. Soc. Am. J.* 61, 4. <https://doi.org/10.2136/sssaj1997.03615995006100010001x>
- Knadel, M., Katuwal, S., 2018. Visible-Near-Infrared Spectroscopy Prediction of Soil Characteristics as Affected by Soil-Water Content 1333–1346. <https://doi.org/10.2136/sssaj2018.01.0052>
- Kothari, C., 2004. Research methodology: methods and techniques, New Age International. <https://doi.org/http://196.29.172.66:8080/jspui/bitstream/123456789/2574/1/Research%20Methodology.pdf>
- Leys, C., Ley, C., Klein, O., Bernard, P., Licata, L., 2013. *Journal of Experimental Social Psychology* Detecting outliers : Do not use standard deviation around the mean , use absolute deviation around the median 4–6.
- Lima, G.C., Silva, M.L.N., Freitas, D.A.F. De, 2016. Spatialization of soil quality index in the Sub-Basin of Posses , Extrema , Minas Gerais. <https://doi.org/10.1590/1807->

- Mandal, D.K., Mandal, C., Velayutham, M., 2001. Development of a land quality index for sorghum in Indian semi-arid tropics (SAT) 70, 335–350.
- Martens, H., Høy, M., Wise, B.M., Bro, R., Brockhoff, P.B., 2003. Pre-whitening of data by covariance-weighted pre-processing. *J. Chemom.* 17, 153–165. <https://doi.org/10.1002/cem.780>
- Masto, R.E., Chhonkar, P.K., Singh, D., Patra, A.K., 2007. Soil quality response to long-term nutrient and crop management on a semi-arid Inceptisol. *Agric. Ecosyst. Environ.* 118, 130–142. <https://doi.org/10.1016/j.agee.2006.05.008>
- Mcbratney, A.B., Minasny, B., 2016. Why you don ' t need to use RPD By Budiman Minasny & Alex . McBratney University of Sydney.
- Metzger, M.J., Rounsevell, M.D.A., Acosta-Michlik, L., Leemans, R., Schröter, D., 2006. The vulnerability of ecosystem services to land use change. *Agric. Ecosyst. Environ.* <https://doi.org/10.1016/j.agee.2005.11.025>
- Moebius-Clune, B.N., Moebius-Clune, D., Gugino, B., Idowu, O., Schindelbeck, R., Ristow, A., van Es, H., Thies, J., Shayler, H., McBride, M., Wolfe, D., Abawi, G., 2016. Comprehensive Assessment of Soil Health - The Cornell Framework Manual. <https://doi.org/10.1080/00461520.2015.1125787>
- Mukherjee, A., Lal, R., 2014. Comparison of Soil Quality Index Using Three Methods. <https://doi.org/10.1371/journal.pone.0105981>
- Norman, R.J., Stucki, J.W., 1981. The Determination of Nitrate and Nitrite in Soil Extracts by Ultraviolet Spectrophotometry 1. *Soil Sci. Soc. Am. J.* 45, 347–353. <https://doi.org/10.2136/sssaj1981.03615995004500020024x>
- Ohana-levi, N., Paz-kagan, T., Panov, N., Peeters, A., Tsoar, A., Karnieli, A., Paz-kagan, T., Panov, N., Peeters, A., Tsoar, A., 2018. Time series analysis of vegetation-cover response to environmental factors and residential development in a dryland region. *GIScience Remote Sens.* 00, 1–26. <https://doi.org/10.1080/15481603.2018.1519093>
- Olsvig-whittaker, L., 1983. Vegetation pattern related to environmental factors in a Negev Desert Watershed. <https://doi.org/10.1007/BF00047104>
- Orenstein, D.E., Hamburg, S.P., 2009. To populate or preserve? Evolving political-demographic and environmental paradigms in Israeli land-use policy. *Land use policy* 26, 984–1000. <https://doi.org/10.1016/j.landusepol.2008.12.003>
- Paz-Kagan, T., Shachak, M., Zaady, E., Karnieli, A., 2014. A spectral soil quality index (SSQI) for characterizing soil function in areas of changed land use. *Geoderma* 230–231, 171–184. <https://doi.org/10.1016/j.geoderma.2014.04.003>
- Paz-Kagan, T., Zaady, E., Salbach, C., Schmidt, A., Lausch, A., Zacharias, S., Notesco, G., Ben-Dor, E., Karnieli, A., 2015. Mapping the spectral soil quality index (SSQI) using airborne imaging spectroscopy. *Remote Sens.* 7, 15748–15781. <https://doi.org/10.3390/rs71115748>
- Paz-kagan, T., Zaady, E., Shachak, M., Karnieli, A., 2016. Forest Ecology and Management Transformation of shrublands to forests : The role of woody species as ecosystem engineers and landscape modulators. *For. Ecol. Manage.* 361, 257–268. <https://doi.org/10.1016/j.foreco.2015.11.021>
- Perkins, J.S., Thomas, D.S.G., 1993. SPREADING DESERTS OR SPATIALLY CONFINED ENVIRONMENTAL IMPACTS ? LAND DEGRADATION AND CATTLE RANCHING IN THE KALAHARI DESERT OF 4, 179–194.
- Phillips, H.R.P., Newbold, T., Purvis, A., 2017. Land-use effects on local biodiversity in tropical

- forests vary between continents. *Biodivers. Conserv.* 26, 2251–2270. <https://doi.org/10.1007/s10531-017-1356-2>
- Press, A.I.N., 2007. Application of near infrared reflectance (NIR) and fluorescence spectroscopy to analysis of microbiological and chemical properties of arctic soil 39, 1664–1673. <https://doi.org/10.1016/j.soilbio.2007.01.022>
- Romsonthi, C., Tawornpruek, S., Watana, S., 2018. In situ near-infrared spectroscopy for soil organic matter prediction in paddy soil, pasak watershed, thailand. *Plant, Soil Environ.* 64, 70–75. <https://doi.org/10.17221/716/2017-PSE>
- Rozenstein, O., Paz-Kagan, T., Salbach, C., Karnieli, A., 2015. Comparing the Effect of Preprocessing Transformations on Methods of Land-Use Classification Derived from Spectral Soil Measurements. *IEEE J. Sel. Top. Appl. Earth Obs. Remote Sens.* 8, 2393–2404. <https://doi.org/10.1109/JSTARS.2014.2371920>
- Savitzky, A., Golay, M.J.E., 1964. Smoothing and Differentiation of Data by Simplified Least Squares Procedures. *Anal. Chem.* 36, 1627–1639. <https://doi.org/10.1021/ac60214a047>
- Seybold, C.A., Mausbauch, M.J., Karlen, D.L., Rogers, H.H., 1997. Quantification of soil quality. *Soil Process. Carbon Cycle* 387–404.
- Shepherd, K.D., Walsh, M.G., 2002. Development of Reflectance Spectral Libraries for Characterization of Soil Properties. *Soil Sci. Soc. Am. J.* 66, 988. <https://doi.org/10.2136/sssaj2002.9880>
- Smet, M., Ward, D., 2009. A comparison of the effects of different rangeland management systems on plant species composition , diversity and vegetation structure in a semi-arid savanna 0119. <https://doi.org/10.2989/10220110509485862>
- Smet, M.Ã., Ward, D., 2006. Soil quality gradients around water-points under different management systems in a semi-arid savanna , South Africa 64, 251–269. <https://doi.org/10.1016/j.jaridenv.2005.04.014>
- Tekin, Y., Tümsavas, Z., Mouazen, A.M., 2014. Comparing the artificial neural network with partial least squares for prediction of soil organic carbon and pH at different moisture content levels using visible and near-infrared spectroscopy 38, 1794–1804.
- Triantafyllidis, V., Kontogeorgos, A., 2018. An Assessment of the Soil Quality Index in a Mediterranean Agro Ecosystem. <https://doi.org/10.9755/ejfa.2018.v30.i12.1886>
- Tscharntke, T., Klein, A.M., Kruess, A., Steffan-Dewenter, I., Thies, C., Teja Tscharntke,* Alexandra M. Klein, Andreas Kruess, I.S.-D. and C.T., 2005. REVIEWS AND Landscape perspectives on agricultural intensification and biodiversity – ecosystem service management. *Ecol. Lett.* <https://doi.org/10.1111/j.1461-0248.2005.00782.x>
- Union, I., Pure, O.F., Chemistry, A., 1994. COMMISSION ON PHYSICAL ORGANIC CHEMISTRY * GLOSSARY OF TERMS USED IN 66, 1077–1184.
- United Nation Environment Program World atlas of desertification; UNEP and Edward Arnold Press: London, UK, 1992. - Google Search [WWW Document], n.d.
- Velasquez, E., Lavelle, P., Barrios, E., Joffre, R., Reversat, F., 2005. Evaluating soil quality in tropical agroecosystems of Colombia using NIRS. *Soil Biol. Biochem.* 37, 889–898. <https://doi.org/10.1016/j.soilbio.2004.09.009>
- Veum, K.S., Sudduth, K.A., Kremer, R.J., Kitchen, N.R., 2017. Sensor data fusion for soil health assessment. *Geoderma* 305, 53–61. <https://doi.org/10.1016/j.geoderma.2017.05.031>
- Viscarra Rossel, R.A., Walvoort, D.J.J., McBratney, A.B., Janik, L.J., Skjemstad, J.O., 2006. Visible, near infrared, mid infrared or combined diffuse reflectance spectroscopy for simultaneous

- assessment of various soil properties. *Geoderma* 131, 59–75. <https://doi.org/10.1016/j.geoderma.2005.03.007>
- Wienhold, B.J., Karlen, D.L., Andrews, S.S., Stott, D.E., 2009. Protocol for indicator scoring in the soil management assessment framework (SMAF) 24, 260–266. <https://doi.org/10.1017/S1742170509990093>
- Wise, B.M., Gallagher, N.B., Bro, R., Shaver, J.M., Windig, W., Koch, R.S., 2006. PLS_Toolbox Version 4.0 for use with MATLAB™, Eigenvector Research.
- Yair, A., Danin, A., 1980. Spatial variations in vegetation as related to the soil moisture regime over an arid limestone hillside , northern Negev , Israel. <https://doi.org/10.1007/BF00541779>
- Yong, H.E., Hai-yan, S., García, P.A., Hernández, G.A., 2015. Measurement and analysis of soil nitrogen and organic matter content using near-infrared spectroscopy techniques *. <https://doi.org/10.1631/jzus.2005.B1081>
- Ziv, B., Saaroni, H., Pargament, R., Harpaz, T., Alpert, P., 2014. Trends in rainfall regime over Israel, 1975–2010, and their relationship to large-scale variability. *Reg. Environ. Chang.* 14, 1751–1764. <https://doi.org/10.1007/s10113-013-0414-x>

Chapter 2- References

- Albert, K.M., 2015. Role of revegetation in restoring fertility of degraded mined soils in Ghana: A review. *Int. J. Biodivers. Conserv.* 7, 57–80. <https://doi.org/10.5897/ijbc2014.0775>
- Andrés, P., Mateos, E., 2006. Soil mesofaunal responses to post-mining restoration treatments. *Appl. Soil Ecol.* 33, 67–78.
- Andrews, S.S., Mitchell, J.P., Mancinelli, R., Karlen, D.L., Hartz, T.K., Horwath, W.R., Pettygrove, G.S., Scow, K.M., Munk, D.S., 2002. On-farm assessment of soil quality in California's Central Valley, in: *Agronomy Journal*. pp. 12–23.
- Armenise, E., Redmile-Gordon, M.A., Stellacci, A.M., Ciccicarese, A., Rubino, P., 2013. Developing a soil quality index to compare soil fitness for agricultural use under different managements in the mediterranean environment. *Soil Tillage Res.* 130, 91–98. <https://doi.org/10.1016/j.still.2013.02.013>
- Aronson, J., Floret, C., Floch, E.L., C, O., R, P., 1993. Restoration and rehabilitation of Degraded Ecosystems in Arid and Semi-Arid Lands. *Restor. Ecol.* 1, 9–17.
- Asensio, V., Covelo, E.F., Kandeler, E., 2013a. Soil management of copper mine tailing soils - Sludge amendment and tree vegetation could improve biological soil quality. *Sci. Total Environ.* 456–457, 82–90. <https://doi.org/10.1016/j.scitotenv.2013.03.061>
- Asensio, V., Guala, S.D., Vega, F.A., Covelo, E.F., 2013b. A soil quality index for reclaimed mine soils. *Environ. Toxicol. Chem.* 32, 2240–2248. <https://doi.org/10.1002/etc.2315>
- Bandyopadhyay, S., Maiti, S.K., 2019. Evaluation of ecological restoration success in mining-degraded lands. *Environ. Qual. Manag.* 29, 89–100.
- Bastida, F., Zsolnay, A., Hernández, T., García, C., 2008. Past, present and future of soil quality indices: A biological perspective. *Geoderma*. <https://doi.org/10.1016/j.geoderma.2008.08.007>
- Belnap, J., 2006. The potential roles of biological soil crusts in dryland hydrologic cycles. *Hydrol. Process.* 3159–3178. <https://doi.org/10.1002/hyp.6325>
- Belnap, J., Eldridge, D., 2001. *Disturbance and Recovery of Biological Soil Crusts*. Springer-Verlag, Berlin. https://doi.org/10.1007/978-3-642-56475-8_27
- Ben-David, E.A., Zaady, E., Sher, Y., Nejidat, A., 2011. Assessment of the spatial distribution of soil microbial communities in patchy arid and semi-arid landscapes of the Negev Desert using combined PLFA and DGGE analyses. *FEMS Microbiol. Ecol.* 76, 492–503.
- Beniston, J.W., Lal, R., Mercer, K.L., 2016. Assessing and Managing Soil Quality for Urban Agriculture in a Degraded Vacant Lot Soil. *L. Degrad. Dev.* 27, 996–1006. <https://doi.org/10.1002/ldr.2342>

- Blecker, S.W., Stillings, L.L., Amacher, M.C., Ippolito, J.A., Decrappeo, N.M., 2012. Development of vegetation based soil quality indices for mineralized terrane in arid and semi-arid regions. *Ecol. Indic.* 20, 65–74. <https://doi.org/10.1016/j.ecolind.2012.02.010>
- Bodlák, L., Křováková, K., Kobesová, M., Brom, J., Šťastný, J., Pecharová, E., 2012. SOC content—An appropriate tool for evaluating the soil quality in a reclaimed post-mining landscape. *Ecol. Eng.* 43, 53–59.
- Borges, S.R., Santos, R.S., Oliveira, D.M.S., Souza, I.F., Verburg, E.E.J., Pimentel, L.G., Cruz, R.S., Silva, I.R., 2019. Practices for rehabilitating bauxite-mined areas and an integrative approach to monitor soil quality. *L. Degrad. Dev.* 30, 866–877. <https://doi.org/10.1002/ldr.3273>
- Borůvka, L., Kozák, J., Mühlhanslová, M., Donátová, H., Nikodem, A., Němeček, K., Drábek, O., 2012. Effect of covering with natural topsoil as a reclamation measure on brown-coal mining dumpsites. *J. Geochemical Explor.* 113, 118–123. <https://doi.org/10.1016/j.gexplo.2011.11.004>
- Bowker, M.A., Belnap, J., Davidson, D.W., Phillips, S.L., 2005. Evidence for Micronutrient Limitation of Biological Soil Crusts: Importance to Arid-Lands Restoration, Source: Ecological Applications.
- Bowker, M.A., Reed, S.C., Maestre, F.T., Eldridge, D.J., 2018. Biocrusts: the living skin of the earth. *Plant Soil.* <https://doi.org/10.1007/s11104-018-3735-1>
- Bradshaw, A., 1997. Restoration of mined lands-using natural processes, *Ecological Engineering*.
- Brady, N.C., Weil, R.R., 1999. Soil organic matter., in: *The Nature and Properties of Soils*.
- Bünemann, E.K., Bongiorno, G., Bai, Z., Creamer, R.E., De Deyn, G., de Goede, R., Fleskens, L., Geissen, V., Kuyper, T.W., Mäder, P., Pulleman, M., Sukkel, W., van Groenigen, J.W., Brussaard, L., 2018. Soil quality – A critical review. *Soil Biol. Biochem.* 120, 105–125. <https://doi.org/10.1016/j.soilbio.2018.01.030>
- Casida, L.E., Klein, D.A., Santoro, T., 1964. SOIL DEHYDROGENASE ACTIVITY: *Soil Sci.* 98, 371–376. <https://doi.org/10.1097/00010694-196412000-00004>
- Chamizo, S., Adessi, A., Mugnai, G., Simiani, A., De Philippis, R., 2019. Soil Type and Cyanobacteria Species Influence the Macromolecular and Chemical Characteristics of the Polysaccharidic Matrix in Induced Biocrusts. *Microb. Ecol.* 78, 482–493. <https://doi.org/10.1007/s00248-018-1305-y>
- Chamizo, S., Cantón, Y., Rodríguez-Caballero, E., Domingo, F., 2016. Biocrusts positively affect the soil water balance in semiarid ecosystems. *Ecohydrology* 9, 1208–1221. <https://doi.org/10.1002/eco.1719>
- Chaudhuri, S., McDonald, L.M., Skousen, J., Pena-Yewtukhiw, E.M., 2015. Soil organic carbon molecular properties: effects of time since reclamation in a minesoil chronosequence. *L. Degrad. Dev.* 26, 237–248.
- Conover, W.J., Iman, R.L., 1981. Rank transformations as a bridge between parametric and nonparametric statistics. *Am. Stat.* 35, 124–128. <https://doi.org/10.1080/00031305.1981.10479327>
- Costantini, E.A.C., Branquinho, C., Nunes, A., Schwilch, G., Stavi, I., Valdecantos, A., Zucca, C., 2016. Soil indicators to assess the effectiveness of restoration strategies in dryland ecosystems. *Solid Earth* 7, 397–414. <https://doi.org/10.5194/se-7-397-2016>
- Dangi, S.R., Stahl, P.D., Wick, A.F., Ingram, L.J., Buyer, J.S., 2012. Soil microbial community recovery in reclaimed soils on a surface coal mine site. *Soil Sci. Soc. Am. J.* 76, 915–924.
- Dische, Z., 1955. New Color Reactions for Determination of Sugars in Polysaccharides. John Wiley & Sons, Ltd, pp. 313–358. <https://doi.org/10.1002/9780470110188.ch11>
- Dixon, j. c., 2009. *Geomorphology of desert environments*, 2nd ed, Aridic soils, Patterned Ground, and Desert Pavements. Springer. <https://doi.org/10.1007/978-1-4020-5719-9>
- Doran and Zeiss, M.R., 2000. Soil health: Managing the biotic component of soil quality - Introduction. *Appl. Soil Ecol.* 15, 3–11. [https://doi.org/10.1016/S0929-1393\(00\)00066-4](https://doi.org/10.1016/S0929-1393(00)00066-4)
- Drinkwater, L.E., Cambardella, C.A., Reeder, J.D., Rice, C.W., 2015. Potentially Mineralizable Nitrogen as an Indicator of Biologically Active Soil Nitrogen. John Wiley & Sons, Ltd, pp. 217–229. <https://doi.org/10.2136/sssaspepub49.c13>

- Dumedah, G., Coulibaly, P., 2011. Evaluation of statistical methods for infilling missing values in high-resolution soil moisture data. *J. Hydrol.* 400, 95–102. <https://doi.org/10.1016/j.jhydrol.2011.01.028>
- Dungait, J.A.J., Kemmitt, S.J., Michallon, L., Guo, S., Wen, Q., Brookes, P.C., Evershed, R.P., 2011. Variable responses of the soil microbial biomass to trace concentrations of ¹³C-labelled glucose, using ¹³C-PLFA analysis. *Eur. J. Soil Sci.* 62, 117–126.
- Dunger, W., Voigtländer, K., 2005. Assessment of biological soil quality in wooded reclaimed mine sites, in: *Geoderma*. pp. 32–44. <https://doi.org/10.1016/j.geoderma.2004.12.028>
- Elbert, W., Weber, B., Burrows, S., Steinkamp, J., Büdel, B., Andreae, M.O., Pöschl, U., 2012. Contribution of cryptogamic covers to the global cycles of carbon and nitrogen. *Nat. Geosci.* 5, 459–462. <https://doi.org/10.1038/ngeo1486>
- Eldridge, D.J., Reed, S., Travers, S.K., Bowker, M.A., Maestre, F.T., Ding, J., Havrilla, C., Rodriguez-Caballero, E., Barger, N., Weber, B., 2020. The pervasive and multifaceted influence of biocrusts on water in the world’s drylands. *Glob. Chang. Biol.* 26, 6003–6014.
- Farrick, K.K., Wuddivira, M.N., Martin, O., 2019. Estimation of soil texture from permanent wilting point measured with a chilled-mirror dewpoint technique. *J. Plant Nutr. Soil Sci.* 182, 119–125. <https://doi.org/10.1002/jpln.201700573>
- Feng, Y., Wang, J., Bai, Z., Reading, L., 2019. Effects of surface coal mining and land reclamation on soil properties: A review. *Earth-science Rev.*
- Ferrenberg, S., Reed, S.C., Belnap, J., Schlesinger, W.H., 2015. Climate change and physical disturbance cause similar community shifts in biological soil crusts. *Proc. Natl. Acad. Sci. U. S. A.* 112, 12116–12121. <https://doi.org/10.1073/pnas.1509150112>
- Golos, P.J., Dixon, K.W., Erickson, T.E., 2016. Plant recruitment from the soil seed bank depends on topsoil stockpile age, height, and storage history in an arid environment. *Restor. Ecol.* 24, S53–S61.
- Gómez-Sagasti, M.T., Alkorta, I., Becerril, J.M., Epelde, L., Anza, M., Garbisu, C., 2012. Microbial monitoring of the recovery of soil quality during heavy metal phytoremediation. *Water. Air. Soil Pollut.* 223, 3249–3262. <https://doi.org/10.1007/s11270-012-1106-8>
- Jolliffe, I.T., Cadima, J., Cadima, J., 2016. Principal component analysis : a review and recent developments Subject Areas : Author for correspondence :
- Jones, C.G., Lawton, J.H., Shachak, M., 1997. POSITIVE AND NEGATIVE EFFECTS OF ORGANISMS AS PHYSICAL ECOSYSTEM ENGINEERS. *Ecology* 78, 1946–1957. [https://doi.org/10.1890/0012-9658\(1997\)078\[1946:PANEOO\]2.0.CO;2](https://doi.org/10.1890/0012-9658(1997)078[1946:PANEOO]2.0.CO;2)
- Kaiser, H.F., 1958. The varimax criterion for analytic rotation in factor analysis. *Psychometrika* 23, 187–200. <https://doi.org/10.1007/bf02289233>
- Karlen, D.L., Ditzler, C.A., Andrews, S.S., 2003. Soil quality: why and how? *Geoderma* 114, 145–156.
- Karlen, D.L., Mausbach, M.J., Doran, J.W., Cline, R.G., Harris, R.F., Schuman, G.E., 1997. Soil Quality: A Concept, Definition, and Framework for Evaluation (A Guest Editorial). *Soil Sci. Soc. Am. J.* 61, 4. <https://doi.org/10.2136/sssaj1997.03615995006100010001x>
- Karnieli, A., Kidron, G.J., Glaesser, C., Ben-Dor, E., 1999. Spectral characteristics of cyanobacteria soil crust in semiarid environments. *Remote Sens. Environ.* 69, 67–75.
- Kuske, C.R., Yeager, C.M., Johnson, S., Ticknor, L.O., Belnap, J., 2012. Response and resilience of soil biocrust bacterial communities to chronic physical disturbance in arid shrublands. *ISME J.* 6, 886–897. <https://doi.org/10.1038/ismej.2011.153>
- Lal, R., 2015. Restoring Soil Quality to Mitigate Soil Degradation. *Sustainability* 7, 5875.
- Lal, R., 2011. Soil health and climate change: an overview, in: *Soil Health and Climate Change*. Springer, pp. 3–24.
- Levi, N., Karnieli, A., Paz-kagan, T., 2020. Using reflectance spectroscopy for detecting land-use effects on soil quality in drylands. *Soil Tillage Res.* 199, 104571. <https://doi.org/10.1016/j.still.2020.104571>
- Leys, C., Ley, C., Klein, O., Bernard, P., Licata, L., 2013. *Journal of Experimental Social Psychology*

Detecting outliers : Do not use standard deviation around the mean , use absolute deviation around the median 4–6.

- Lowry, O.H., Rosebrough, N.J., Farr, A.L., Randall, R.J., 1951. Protein measurement with the Folin phenol reagent. *J. Biol. Chem.* 193, 265–275.
- Madsen, M.D., Chandler, D.G., 2007. Automation and Use of Mini Disk Infiltrimeters. *Soil Sci. Soc. Am. J.* 71, 1469–1472. <https://doi.org/10.2136/sssaj2007.0009n>
- Mager, D.M., Thomas, A.D., 2011. Extracellular polysaccharides from cyanobacterial soil crusts: a review of their role in dryland soil processes. *J. Arid Environ.* 75, 91–97.
- Maiti, S.K., 2012. *Ecorestoration of the coalmine degraded lands*. Springer Science & Business Media.
- Maiti, S.K., Ahirwal, J., 2019. Ecological Restoration of Coal Mine Degraded Lands: Topsoil Management, Pedogenesis, Carbon Sequestration, and Mine Pit Limnology, in: *Phytomanagement of Polluted Sites*. Elsevier, pp. 83–111.
- Martins, W.B.R., Lima, M.D.R., Junior, U. de O.B., Amorim, L.S.V.-B., de Assis Oliveira, F., Schwartz, G., 2020. Ecological methods and indicators for recovering and monitoring ecosystems after mining: A global literature review. *Ecol. Eng.* 145, 105707.
- Masto, R. E., Chhonkar, P.K., Purakayastha, T.J., Patra, A.K., Singh, D., 2008. Soil quality indices for evaluation of long-term land use and soil management practices in semi-arid sub-tropical India. *L. Degrad. Dev.* 19, 516–529. <https://doi.org/10.1002/ldr.857>
- Masto, R E, Chhonkar, P.K., Purakayastha, T.J., Patra, A.K., Singh, D., 2008. Soil quality indices for evaluation of long-term land use and soil management practices in semi-arid sub-tropical India. *L. Degrad. Dev.* 19, 516–529.
- Mazor, G., Kidron, G.J., Vonshak, A., Abeliovich, A., 1996. The role of cyanobacterial exopolysaccharides in structuring desert microbial crusts. *FEMS Microbiol. Ecol.* 21, 121–130. <https://doi.org/10.1111/j.1574-6941.1996.tb00339.x>
- McGinnies and Nicholas, P.J., 1980. Effects of topsoil thickness and nitrogen fertilizer on the revegetation of coal mine spoils. *J. Environ. Qual.* Vol. 9, 681–685.
- Melgar-Ramírez, R., González, V., Sánchez, J.A., García, I., 2012. Effects of application of organic and inorganic wastes for restoration of sulphur-mine soil. *Water. Air. Soil Pollut.* 223, 6123–6131. <https://doi.org/10.1007/s11270-012-1345-8>
- Mendez, M.O., Maier, R.M., 2008. Phytoremediation of mine tailings in temperate and arid environments. *Rev. Environ. Sci. Biotechnol.* <https://doi.org/10.1007/s11157-007-9125-4>
- Mendoza-Aguilar, D., Cortina, J., Pando-Moreno, M., 2014. Biological soil crust influence on germination and rooting of two key species in a *Stipa tenacissima* steppe. *Plant Soil* 375, 267–274. <https://doi.org/10.1007/s11104-013-1958-8>
- Mensah, A.K., 2015. Role of revegetation in restoring fertility of degraded mined soils in Ghana: A review. *Int. J. Biodivers. Conserv.* 7, 57–80.
- Menta, C., Conti, F.D., Pinto, S., Leoni, A., Lozano-Fondón, C., 2014. Monitoring soil restoration in an open-pit mine in northern Italy. *Appl. Soil Ecol.* 83, 22–29. <https://doi.org/10.1016/j.apsoil.2013.07.013>
- Moebius-Clune, B.N., 2017. *Comprehensive Assessment of Soil Health*.
- Mukhopadhyay, S., George, J., Masto, R.E., 2017. Changes in polycyclic aromatic hydrocarbons (PAHs) and soil biological parameters in a revegetated coal mine spoil. *L. Degrad. Dev.* 28, 1047–1055.
- Mukhopadhyay, S., Maiti, S.K., Masto, R.E., 2014. Development of mine soil quality index (MSQI) for evaluation of reclamation success: A chronosequence study. *Ecol. Eng.* 71, 10–20. <https://doi.org/10.1016/j.ecoleng.2014.07.001>
- Muñoz-Rojas, M., 2018. Soil quality indicators: critical tools in ecosystem restoration. *Curr. Opin. Environ. Sci. Heal.* <https://doi.org/10.1016/j.coesh.2018.04.007>
- Muñoz-Rojas, M., Erickson, T.E., Dixon, K.W., Merritt, D.J., 2016. Soil quality indicators to assess functionality of restored soils in degraded semiarid ecosystems. *Restor. Ecol.* 24, S43–S52.
- Nathan, Y., Soudry, D., Levy, Y., Shitrit, D., Dorfman, E., 1997. Geochemistry of cadmium in the

Negev phosphorites 142, 87–107.

- Paz-Kagan, T., Ohana-Levi, N., Shachak, M., Zaady, E., Karnieli, A., 2017. Ecosystem effects of integrating human-made runoff-harvesting systems into natural dryland watersheds. *J. Arid Environ.* <https://doi.org/10.1016/j.jaridenv.2017.07.015>
- Paz-Kagan, T., Zaady, E., Salbach, C., Schmidt, A., Lausch, A., Zacharias, S., Notesco, G., Ben-Dor, E., Karnieli, A., 2015. Mapping the spectral soil quality index (SSQI) using airborne imaging spectroscopy. *Remote Sens.* 7, 15748–15781. <https://doi.org/10.3390/rs71115748>
- Pietrzykowski, M., 2014. Soil quality index as a tool for Scots pine (*Pinus sylvestris*) monoculture conversion planning on afforested, reclaimed mine land. *J. For. Res.* 25, 63–74. <https://doi.org/10.1007/s11676-013-0418-x>
- Puglisi, E., Del Re, A.A.M., Rao, M.A., Gianfreda, L., 2006. Development and validation of numerical indexes integrating enzyme activities of soils. *Soil Biol. Biochem.* 38, 1673–1681. <https://doi.org/10.1016/j.soilbio.2005.11.021>
- Rezaei, S.A., Gilkes, R.J., Andrews, S.S., 2006. A minimum data set for assessing soil quality in rangelands. *Geoderma* 136, 229–234. <https://doi.org/http://dx.doi.org/10.1016/j.geoderma.2006.03.021>
- Schielzeth, H., Nakagawa, S., 2013. Nested by design: model fitting and interpretation in a mixed model era. *Methods Ecol. Evol.* 4, 14–24. <https://doi.org/10.1111/j.2041-210x.2012.00251.x>
- Schindelbeck, R.R., van Es, H.M., Abawi, G.S., Wolfe, D.W., Whitlow, T.L., Gugino, B.K., Idowu, O.J., Moebius-Clune, B.N., 2008. Comprehensive assessment of soil quality for landscape and urban management. *Landsc. Urban Plan.* 88, 73–80. <https://doi.org/http://dx.doi.org/10.1016/j.landurbplan.2008.08.006>
- Schulte, E.E., 1995. Recommended Soil Organic Matter Tests. *Recomm. Soil Test. Proced. North East. USA. Northeast. Reg. Publ. No. 493.* Agricultural Exp. Stn. Univ. Delaware, Newark.
- Sharma, K.L., Mandal, U.K., Srinivas, K., Vittal, K.P.R., Mandal, B., Grace, J.K., Ramesh, V., 2005. Long-term soil management effects on crop yields and soil quality in a dryland Alfisol. *Soil Tillage Res.* 83, 246–259. <https://doi.org/10.1016/j.still.2004.08.002>
- Sheoran, V., Sheoran, A.S., Poonia, P., 2010. Soil reclamation of abandoned mine land by revegetation: a review. *Int. J. Soil, Sediment Water* 3, 13.
- Shukla, M.K., Lal, R., Ebinger, M., 2006. Determining soil quality indicators by factor analysis. *Soil Tillage Res.* 87, 194–204. <https://doi.org/10.1016/j.still.2005.03.011>
- Soudry, D., 1992. Primary bedded phosphorites in the Campanian Mishash Formation, Negev, southern Israel, *Sedimentary Geology*.
- Toktar, M., Lo Papa, G., Kozybayeva, F.E., Dazzi, C., 2016. Ecological restoration in contaminated soils of Kokdzhon phosphate mining area (Zhambyl region, Kazakhstan). *Ecol. Eng.* 86, 1–4. <https://doi.org/10.1016/j.ecoleng.2015.09.080>
- Ushey, K., Allaire, J.J., Tang, Y., 2020. *reticulate: Interface to “Python.”*
- Visser, S., Fujikawa, J., Griffiths, C.L., Parkinson, D., 1984. Effect of topsoil storage on microbial activity, primary production and decomposition potential, *Hant and Soil*.
- Wang, H., Zhang, B., Bai, X., Shi, L., 2018. A novel environmental restoration method for an abandoned limestone quarry with a deep open pit and steep palisades: a case study. *R. Soc. open Sci.* 5, 180365.
- Wetschoreck, F., Krabel, T., Krishnamurthy, S., 2020. 8080Labs/Ppscore: Zenodo Release. <https://doi.org/10.5281/ZENODO.4091345>
- Wong, M.H., 2003. Ecological restoration of mine degraded soils, with emphasis on metal contaminated soils. *Chemosphere.* [https://doi.org/10.1016/S0045-6535\(02\)00232-1](https://doi.org/10.1016/S0045-6535(02)00232-1)
- Yirdaw, E., Tigabu, M., Monge, A., 2017. Rehabilitation of degraded dryland ecosystems—review. *Silva Fenn.* 51, 1673.
- Zaady, E., Ben-David, E.A., Sher, Y., Tzirkin, R., Nejdat, A., 2010. Inferring biological soil crust successional stage using combined PLFA, DGGE, physical and biophysiological analyses. *Soil Biol. Biochem.* 42, 842–849.
- Zaady, E., Eldridge, D.J., Bowker, M.A., 2016. Effects of local-scale disturbance on biocrusts, in:

- Biological Soil Crusts: An Organizing Principle in Drylands. Springer, pp. 429–449.
- Zavarella, L., 2020. Using The Predictive Power Score in R. Medium.
- Zou, H., 2019. Study on soil ecological environment restoration strategy of abandoned mining area. *Arab. J. Geosci.* 12, 717.

Chapter 3- References

- Alewell, C., Borrelli, P., Meusburger, K., Panagos, P., 2019. Using the USLE: Chances, challenges and limitations of soil erosion modelling. *Int. Soil Water Conserv. Res.* <https://doi.org/10.1016/j.iswcr.2019.05.004>
- Andrews, S.S., Karlen, D.L., Cambardella, C. a, 2004. The Soil Management Assessment Framework: A Quantitative Soil Quality Evaluation Method. *Soil Sci. Soc. Am. J.* 68, 1945–1962. <https://doi.org/10.2136/sssaj2009.0029>
- Andrews, S.S., Mitchell, J.P., Mancinelli, R., Karlen, D.L., Hartz, T.K., Horwath, W.R., Pettygrove, G.S., Scow, K.M., Munk, D.S., 2002. On-farm assessment of soil quality in California's Central Valley, in: *Agronomy Journal*. pp. 12–23.
- Askari, M.S., O'Rourke, S.M., Holden, N.M., 2015. Evaluation of soil quality for agricultural production using visible–near-infrared spectroscopy. *Geoderma* 243–244, 80–91. <https://doi.org/10.1016/J.GEODERMA.2014.12.012>
- Ayoubi, S., Pilehvar, A., Mokhtari, P., L., K., 2011. Application of Artificial Neural Network (ANN) to Predict Soil Organic Matter Using Remote Sensing Data in Two Ecosystems, in: *Biomass and Remote Sensing of Biomass*. InTech. <https://doi.org/10.5772/18956>
- Ballabio, C., Lugato, E., Fernández-Ugalde, O., Orgiazzi, A., Jones, A., Borrelli, P., Montanarella, L., Panagos, P., 2019. Mapping LUCAS topsoil chemical properties at European scale using Gaussian process regression. *Geoderma* 355, 113912. <https://doi.org/10.1016/J.GEODERMA.2019.113912>
- Barré, P., Velde, B., Fontaine, C., Catel, N., Abbadie, L., 2008. Which 2:1 clay minerals are involved in the soil potassium reservoir? Insights from potassium addition or removal experiments on three temperate grassland soil clay assemblages. *Geoderma* 146, 216–223. <https://doi.org/10.1016/J.GEODERMA.2008.05.022>
- Barsi, J., Lee, K., Kvaran, G., Markham, B., Pedelty, J., 2014. The Spectral Response of the Landsat-8 Operational Land Imager. *Remote Sens.* 6, 10232–10251. <https://doi.org/10.3390/rs61010232>
- Barton, C., Karathanasis, A., 2005. Clay Minerals. *Encycl. Soil Sci.* Second Ed. <https://doi.org/10.1201/noe0849338304.ch57>
- Beckers, B., Berking, J., Schütt, B., 2013. Ancient Water Harvesting Methods in the Drylands of the Mediterranean and Western Asia. *eTopoi. J. Anc. Stud.* 0, 145–164.
- Bellinaso, H., Silvero, N.E.Q., Ruiz, L.F.C., Accorsi Amorim, M.T., Rosin, N.A., Mendes, W. de S., Sousa, G.P.B. de, Sepulveda, L.M.A., Queiroz, L.G. de, Nanni, M.R., Demattê, J.A.M., 2021. Clay content prediction using spectra data collected from the ground to space platforms in a smallholder tropical area. *Geoderma* 399, 115116. <https://doi.org/10.1016/j.geoderma.2021.115116>
- Bellon-Maurel, V., Fernandez-Ahumada, E., Palagos, B., Roger, J.M., McBratney, A., 2010. Critical review of chemometric indicators commonly used for assessing the quality of the prediction of soil attributes by NIR spectroscopy. *TrAC - Trends Anal. Chem.* <https://doi.org/10.1016/j.trac.2010.05.006>
- Ben-Dor, E., 2011. Characterization of Soil Properties Using Reflectance Spectroscopy, in: *Hyperspectral Remote Sensing of Vegetation*. CRC Press, pp. 513–558. <https://doi.org/10.1201/b11222-31>
- Ben-Dor, E., Banin, A., 1995. Near-Infrared Analysis as a Rapid Method to Simultaneously Evaluate Several Soil Properties. *Soil Sci. Soc. Am. J.* 59, 364. <https://doi.org/10.2136/sssaj1995.03615995005900020014x>
- Ben-Dor, E., Chabrillat, S., Demattê, J.A.M., Taylor, G.R., Hill, J., Whiting, M.L., Sommer, S., 2009.

- Using Imaging Spectroscopy to study soil properties. *Remote Sens. Environ.* 113, S38–S55. <https://doi.org/10.1016/j.rse.2008.09.019>
- Ben-Dor¹, E., Patkin¹, K., Banin², A., Karnieli³, A., 2002. Mapping of several soil properties using DAIS-7915 hyperspectral scanner data—a case study over clayey soils in Israel. *int. j. Remote Sens.* 23, 1043–1062. <https://doi.org/10.1080/01431160010006962>
- Ben Dor, E., Ong, C., Lau, I.C., 2015. Reflectance measurements of soils in the laboratory: Standards and protocols. *Geoderma* 245–246, 112–124. <https://doi.org/10.1016/j.geoderma.2015.01.002>
- Biagetti, S., Alcaina-Mateos, J., Ruiz-Giralt, A., Lancelotti, C., Groenewald, P., Ibañez-Insa, J., Gur-Arie, S., Morton, F., Merlo, S., 2021. Identifying anthropogenic features at Seoke (Botswana) using pXRF: Expanding the record of southern African Stone Walled Sites. *PLoS One* 16, e0250776. <https://doi.org/10.1371/JOURNAL.PONE.0250776>
- Bogrekci, I., Lee, W.S., 2005. Spectral phosphorus mapping using diffuse reflectance of soils and grass. *Biosyst. Eng.* 91, 305–312.
- Brady, N.C., Weil, R.R., 1999. Soil organic matter., in: *The Nature and Properties of Soils*.
- Brook, A., Ben-Dor, E., 2015. Supervised Vicarious Calibration (SVC) of Multi-Source Hyperspectral Remote-Sensing Data. *Remote Sens.* 7, 6196–6223. <https://doi.org/10.3390/rs70506196>
- Bünemann, E.K., Bongiorno, G., Bai, Z., Creamer, R.E., De Deyn, G., de Goede, R., Fleskens, L., Geissen, V., Kuyper, T.W., Mäder, P., Pulleman, M., Sukkel, W., van Groenigen, J.W., Brussaard, L., 2018. Soil quality – A critical review. *Soil Biol. Biochem.* 120, 105–125. <https://doi.org/10.1016/j.soilbio.2018.01.030>
- Casida, L.E., Klein, D.A., Santoro, T., 1964. SOIL DEHYDROGENASE ACTIVITY: *Soil Sci.* 98, 371–376. <https://doi.org/10.1097/00010694-196412000-00004>
- Cécillon, L., Cassagne, N., Czarnes, S., Gros, R., Brun, J.J., 2008. Variable selection in near infrared spectra for the biological characterization of soil and earthworm casts. *Soil Biol. Biochem.* 40, 1975–1979. <https://doi.org/10.1016/j.soilbio.2008.03.016>
- Cécillon, L., Es, B., Gomez, C., Ertlen, D., Génot, V., Hedde, M., Stevens, A., Brun, J.-J., 2009. Assessment and monitoring of soil quality using near infrared reflectance spectroscopy (NIRS). *Eur. J. Soil Sci.* 60, 770–784. <https://doi.org/10.1111/j.1365-2389.2009.01178.x>
- Chabrillat, S., Ben-Dor, E., Cierniewski, J., Gomez, C., Schmid, T., Van Wesemael, B., 2019. *Imaging Spectroscopy for Soil Mapping and Monitoring* 40, 361–399. <https://doi.org/10.1007/s10712-019-09524-0>
- Chabrillat, Sabine, Gholizadeh, A., Neumann, C., Berger, D., Milewski, R., Ogen, Y., Ben-Dor, E., 2019. Preparing a soil spectral library using the Internal Soil Standard (ISS) method: Influence of extreme different humidity laboratory conditions. *Geoderma* 355, 113855. <https://doi.org/10.1016/j.geoderma.2019.07.013>
- Chang, C., Laird, D., Mausbach, M.J., 2001. Near-Infrared Reflectance Spectroscopy – Principal Components Regression Analyses of Soil Properties Near-Infrared Reflectance Spectroscopy – Principal Components. <https://doi.org/10.2136/sssaj2001.652480x.Rights>
- Chen, L., Ren, C., Li, Lin, Wang, Y., Zhang, B., Wang, Z., Li, Linfeng, 2019. A Comparative Assessment of Geostatistical, Machine Learning, and Hybrid Approaches for Mapping Topsoil Organic Carbon Content. *ISPRS Int. J. Geo-Inf* 8, 174. <https://doi.org/10.3390/ijgi8040174>
- Chesworth, W., 2008. *Encyclopedia of soil science / edited by Ward Chesworth., Encyclopedia of soil science, Encyclopedia of earth sciences.* Springer, Dordrecht.
- Cohen, M.J., Dabral, S., Graham, W.D., Prenger, J.P., Debusk, W.F., 2006. Evaluating ecological condition using soil biogeochemical parameters and near infrared reflectance spectra. *Environ. Monit. Assess.* 116, 427–457. <https://doi.org/10.1007/s10661-006-7664-8>
- Conforti, M., Buttafuoco, G., Leone, A.P., Aucelli, P.P.C., Robustelli, G., Scarciglia, F., 2013. Studying the relationship between water-induced soil erosion and soil organic matter using Vis-NIR spectroscopy and geomorphological analysis: A case study in southern Italy. *Catena* 110, 44–58. <https://doi.org/10.1016/j.catena.2013.06.013>
- Crist, E., Mora, C., Engelman, R., 2017. The interaction of human population, food production, and

- biodiversity protection. *Science* (80-.). <https://doi.org/10.1126/science.aal2011>
- da Neto, O.C.R., dos Teixeira, A.S., de Leão, R.A.O., Moreira, L.C.J., Galvão, L.S., 2017. Hyperspectral remote sensing for detecting soil salinization using ProSpecTIR-VS aerial imagery and sensor simulation. *Remote Sens.* 9. <https://doi.org/10.3390/rs9010042>
- Davies, G.E., Calvin, W.M., 2017. Mapping acidic mine waste with seasonal airborne hyperspectral imagery at varying spatial scales. *Environ. Earth Sci.* 76, 1–14. <https://doi.org/10.1007/s12665-017-6763-x>
- de Santana, F.B., Otani, S.K., de Souza, A.M., Poppi, R.J., 2021. Comparison of PLS and SVM models for soil organic matter and particle size using vis-NIR spectral libraries. *Geoderma Reg.* 27, e00436. <https://doi.org/10.1016/J.GEODRS.2021.E00436>
- Deiss, L., Margenot, A.J., Culman, S.W., Demyan, M.S., 2020. Tuning support vector machines regression models improves prediction accuracy of soil properties in MIR spectroscopy. *Geoderma* 365, 114227. <https://doi.org/10.1016/j.geoderma.2020.114227>
- Demattê, J.A.M., Dotto, A.C., Paiva, A.F.S., Sato, M. V., Dalmolin, R.S.D., de Araújo, M. do S.B., da Silva, E.B., Nanni, M.R., ten Caten, A., Noronha, N.C., Lacerda, M.P.C., de Araújo Filho, J.C., Rizzo, R., Bellinaso, H., Francelino, M.R., Schaefer, C.E.G.R., Vicente, L.E., dos Santos, U.J., de Sá Barretto Sampaio, E. V., Menezes, R.S.C., de Souza, J.J.L.L., Abrahão, W.A.P., Coelho, R.M., Grego, C.R., Lani, J.L., Fernandes, A.R., Gonçalves, D.A.M., Silva, S.H.G., de Menezes, M.D., Curi, N., Couto, E.G., dos Anjos, L.H.C., Ceddia, M.B., Pinheiro, É.F.M., Grunwald, S., Vasques, G.M., Marques Júnior, J., da Silva, A.J., Barreto, M.C. de V., Nóbrega, G.N., da Silva, M.Z., de Souza, S.F., Valladares, G.S., Viana, J.H.M., da Silva Terra, F., Horák-Terra, I., Fiorio, P.R., da Silva, R.C., Frade Júnior, E.F., Lima, R.H.C., Alba, J.M.F., de Souza Junior, V.S., Brefin, M.D.L.M.S., Ruivo, M.D.L.P., Ferreira, T.O., Brait, M.A., Caetano, N.R., Bringhenti, I., de Sousa Mendes, W., Safanelli, J.L., Guimarães, C.C.B., Poppiel, R.R., e Souza, A.B., Quesada, C.A., do Couto, H.T.Z., 2019. The Brazilian Soil Spectral Library (BSSL): A general view, application and challenges. *Geoderma* 354, 113793. <https://doi.org/10.1016/j.geoderma.2019.05.043>
- Demattê, J.A.M., Nanni, M.R., Formaggio, A.R., Epiphanyo, J.C.N., 2007. Spectral reflectance for the mineralogical evaluation of Brazilian low clay activity soils. *Int. J. Remote Sens.* 28, 4537–4559. <https://doi.org/10.1080/01431160701250408>
- Demattê, J.A.M., Ramirez-Lopez, L., Marques, K.P.P., Rodella, A.A., 2017. Chemometric soil analysis on the determination of specific bands for the detection of magnesium and potassium by spectroscopy. *Geoderma* 288, 8–22. <https://doi.org/10.1016/j.geoderma.2016.11.013>
- Diek, S., Schaepman, M., de Jong, R., 2016. Creating Multi-Temporal Composites of Airborne Imaging Spectroscopy Data in Support of Digital Soil Mapping. *Remote Sens.* 8, 906. <https://doi.org/10.3390/rs8110906>
- Ding, Z., Kheir, A.M.S., Ali, M.G.M., Ali, O.A.M., Abdelaal, A.I.N., Lin, X., Zhou, Z., Wang, B., Liu, B., He, Z., 2020. The integrated effect of salinity, organic amendments, phosphorus fertilizers, and deficit irrigation on soil properties, phosphorus fractionation and wheat productivity. *Sci. Rep.* 10, 1–13. <https://doi.org/10.1038/s41598-020-59650-8>
- Doran, J.W., Parkin, T.B., 1994. Defining and assessing soil quality. *Defin. soil Qual. a Sustain. Environ.* <https://doi.org/10.2136/sssaspecpub35.c1>
- Drucker, H., Burges, C.J.C., Kaufman, L., Smola, A.J., Vapnik, V., 1997. Support Vector Regression Machines, in: Mozer, M.C., Jordan, M.I., Petsche, T. (Eds.), *Advances in Neural Information Processing Systems* 9. MIT Press, pp. 155–161.
- Eldridge, D.J., Reed, S., Travers, S.K., Bowker, M.A., Maestre, F.T., Ding, J., Havrilla, C., Rodriguez-Caballero, E., Barger, N., Weber, B., 2020. The pervasive and multifaceted influence of biocrusts on water in the world’s drylands. *Glob. Chang. Biol.* 26, 6003–6014.
- FAO, 2019. *The State of Food and Agriculture 2019, The State of Food and Agriculture 2019. Food and Agriculture Organization of the United Nations, Rome.* <https://doi.org/10.4060/ca6030en>
- Feingersh, T., Dor, E. Ben, 2015. SHALOM - A Commercial Hyperspectral Space Mission, in: *Optical Payloads for Space Missions.* John Wiley & Sons, Ltd, Chichester, UK, pp. 247–263.

<https://doi.org/10.1002/9781118945179.ch11>

- Foley, J.A., 2005. Global Consequences of Land Use. *Science* (80-). 309, 570–574. <https://doi.org/10.1126/science.1111772>
- Freschet, G.T., Barthès, B.G., Brunet, D., Hien, E., Masse, D., 2011. Use of Near Infrared Reflectance Spectroscopy (NIRS) for Predicting Soil Fertility and Historical Management. *Commun. Soil Sci. Plant Anal.* 42, 1692–1705. <https://doi.org/10.1080/00103624.2011.584597>
- Gholizadeh, A., Borůvka, L., Saberioon, M., Vašát, R., 2013. Visible, near-infrared, and mid-infrared spectroscopy applications for soil assessment with emphasis on soil organic matter content and quality: State-of-the-art and key issues. *Appl. Spectrosc.* 67, 1349–1362.
- Goetz, A.F.H., Vane, G., Solomon, J.E., Rock, B.N., 1985. Imaging spectrometry for earth remote sensing. *Science* (80-). 228, 1147–1153. <https://doi.org/10.1126/science.228.4704.1147>
- Groenendyk, D.G., Ferré, T.P.A., Thorp, K.R., Rice, A.K., 2015. Hydrologic-Process-Based Soil Texture Classifications for Improved Visualization of Landscape Function. *PLoS One* 10, e0131299. <https://doi.org/10.1371/journal.pone.0131299>
- Guanter, L., Kaufmann, H., Segl, K., Foerster, S., Rogass, C., Chabrillat, S., Kuester, T., Hollstein, A., Rossner, G., Chlebek, C., Straif, C., Fischer, S., Schrader, S., Storch, T., Heiden, U., Mueller, A., Bachmann, M., Mühle, H., Müller, R., Habermeyer, M., Ohndorf, A., Hill, J., Buddenbaum, H., Hostert, P., van der Linden, S., Leitão, P., Rabe, A., Doerffer, R., Krasemann, H., Xi, H., Mauser, W., Hank, T., Locherer, M., Rast, M., Staenz, K., Sang, B., 2015. The EnMAP Spaceborne Imaging Spectroscopy Mission for Earth Observation. *Remote Sens.* 7, 8830–8857. <https://doi.org/10.3390/rs70708830>
- Haynes, R.J., Naidu, R., 1998. Influence of lime , fertilizer and manure applications on soil organic matter content and soil physical conditions : a review 123–137.
- He, T., Wang, J., Lin, Z., Cheng, Y., 2009. Spectral features of soil organic matter. *Geo-Spatial Inf. Sci.* 12, 33–40. <https://doi.org/10.1007/s11806-009-0160-x>
- Hotelling, H., 1933. Analysis of a complex of statistical variables into principal components. *J. Educ. Psychol.* 24, 417–441. <https://doi.org/10.1037/h0071325>
- Hu, G.M., Ding, R.X., Li, Y.B., Shan, J.F., Yu, X.T., Feng, W., 2017. Role of flood discharge in shaping stream geometry: Analysis of a small modern stream in the Uinta Basin, USA. *J. Palaeogeogr.* 6, 84–95. <https://doi.org/10.1016/J.JOP.2016.10.001>
- Idowu, O.J., van Es, H.M., Abawi, G.S., Wolfe, D.W., Ball, J.I., Gugino, B.K., Moebius, B.N., Schindelbeck, R.R., Bilgili, A. V, 2008. Farmer-oriented assessment of soil quality using field, laboratory, and VNIR spectroscopy methods. *Plant Soil* 307, 243–253. <https://doi.org/10.1007/s11104-007-9521-0>
- Idowu, O.J., Van Es, H.M., Abawi, G.S., Wolfe, D.W., Schindelbeck, R.R., Moebius-Clune, B.N., Gugino, B.K., 2009. Use of an integrative soil health test for evaluation of soil management impacts. *Renew. Agric. Food Syst.* 24, 214–224. <https://doi.org/10.1017/S1742170509990068>
- Iglewicz, B., 2011. Summarizing Data with Boxplots, in: *International Encyclopedia of Statistical Science*. Springer Berlin Heidelberg, pp. 1572–1575. https://doi.org/10.1007/978-3-642-04898-2_582
- Jia, W., Pang, Y., Tortini, R., Schläpfer, D., Li, Z., Roujean, J.L., 2020. A kernel-driven BRDF approach to correct airborne hyperspectral imagery over forested areas with rugged topography. *Remote Sens.* 12, 432. <https://doi.org/10.3390/rs12030432>
- Johnston, R.M., Barry, S.J., Bleys, E., Bui, E.N., Moran, K.C.J., Simon, D.A.P., Carlile, P., McKenzie, N.J., Henderson, B.L., Chapman, G., Imhoff, M., Maschmedt, D., Howe, D., Grose, C., Schoknecht, N., Powell, B., Grundy, M., 2003. ASRIS: the database. *Soil Res.* 41, 1021–1036. <https://doi.org/10.1071/SR02033>
- Jolliffe, I.T., Cadima, J., Cadima, J., 2016. Principal component analysis : a review and recent developments Subject Areas : Author for correspondence :
- Kanning, M., Siegmann, B., Jarmer, T., 2016. Regionalization of uncovered agricultural soils based on organic carbon and soil texture estimations. *Remote Sens.* 8. <https://doi.org/10.3390/rs8110927>

- Karlen, D.L., Ditzler, C.A., Andrews, S.S., 2003. Soil quality: why and how? *Geoderma* 114, 145–156.
- Karlen, D.L., Mausbach, M.J., Doran, J.W., Cline, R.G., Harris, R.F., Schuman, G.E., 1997. Soil Quality: A Concept, Definition, and Framework for Evaluation (A Guest Editorial). *Soil Sci. Soc. Am. J.* 61, 4. <https://doi.org/10.2136/sssaj1997.03615995006100010001x>
- Kettler, T.A., Doran, J.W., Gilbert, T.L., 2001. Simplified Method for Soil Particle-Size Determination to Accompany Soil-Quality Analyses. *Soil Sci. Soc. Am. J.* 65, 849–852. <https://doi.org/10.2136/sssaj2001.653849x>
- Kinoshita, R., Moebius-Clune, B.N., van Es, H.M., Hively, W.D., Bilgili, A.V., 2012. Strategies for Soil Quality Assessment Using Visible and Near-Infrared Reflectance Spectroscopy in a Western Kenya Chronosequence. *Soil Sci. Soc. Am. J.* 76, 1776. <https://doi.org/10.2136/sssaj2011.0307>
- Kothari, C., 2004. Research methodology: methods and techniques, New Age International. <https://doi.org/http://196.29.172.66:8080/jspui/bitstream/123456789/2574/1/Research%20Methodology.pdf>
- Kuhn, M., 2020. caret: Classification and Regression Training.
- Lal, R., 2011. Soil health and climate change: an overview, in: *Soil Health and Climate Change*. Springer, pp. 3–24.
- Lal, R., 1997. Degradation and resilience of soils. *Philos. Trans. R. Soc. B Biol. Sci.* 352, 997–1010. <https://doi.org/10.1098/rstb.1997.0078>
- Lee, C.M., Cable, M.L., Hook, S.J., Green, R.O., Ustin, S.L., Mandl, D.J., Middleton, E.M., 2015. An introduction to the NASA Hyperspectral InfraRed Imager (HyspIRI) mission and preparatory activities. *Remote Sens. Environ.* 167, 6–19. <https://doi.org/10.1016/j.rse.2015.06.012>
- Levi, N., Hillel, N., Zaady, E., Rotem, G., Ziv, Y., Karnieli, A., Paz-Kagan, T., 2021. Soil quality index for assessing phosphate mining restoration in a hyper-arid environment. *Ecol. Indic.* 125, 107571. <https://doi.org/10.1016/j.ecolind.2021.107571>
- Levi, N., Karnieli, A., Paz-Kagan, T., 2020. Using reflectance spectroscopy for detecting land-use effects on soil quality in drylands. *Soil Tillage Res.* 199, 104571. <https://doi.org/10.1016/j.still.2020.104571>
- Leys, C., Ley, C., Klein, O., Bernard, P., Licata, L., 2013. *Journal of Experimental Social Psychology* Detecting outliers : Do not use standard deviation around the mean , use absolute deviation around the median 4–6.
- Li, Z., 2020. Selenium-enriched soil mapping using airborne SASI images. *Geoderma* 363, 114133. <https://doi.org/10.1016/j.geoderma.2019.114133>
- Lima, G.C., Silva, M.L.N., Freitas, D.A.F. De, 2016. Spatialization of soil quality index in the Sub-Basin of Posses , Extrema , Minas Gerais. <https://doi.org/10.1590/1807-1929/agriambi.v20n1p78-84>
- Loizzo, R., Guarini, R., Longo, F., Scopa, T., Formaro, R., Facchinetti, C., Varacalli, G., 2018. Prisma: The Italian hyperspectral mission, in: *International Geoscience and Remote Sensing Symposium (IGARSS)*. Institute of Electrical and Electronics Engineers Inc., pp. 175–178. <https://doi.org/10.1109/IGARSS.2018.8518512>
- Lugassi, R., Goldshleger, N., Chudnovsky, A., 2017. Studying Vegetation Salinity : From the Field View to a Satellite-Based Perspective 1–16. <https://doi.org/10.3390/rs9020122>
- Marques, K.P., Rizzo, R., Carneletto Dotto, A., Souza, A.B. e, Mello, F.A., Neto, L.G., Anjos, L.H.C. dos, Demattê, J.A., 2019. How qualitative spectral information can improve soil profile classification? *J. Near Infrared Spectrosc.* 27, 156–174. <https://doi.org/10.1177/0967033518821965>
- Masto, R.E., Chhonkar, P.K., Purakayastha, T.J., Patra, A.K., Singh, D., 2008. Soil quality indices for evaluation of long-term land use and soil management practices in semi-arid sub-tropical India. *L. Degrad. Dev.* 19, 516–529.
- Masto, R.E., Chhonkar, P.K., Singh, D., Patra, A.K., 2007. Soil quality response to long-term nutrient

- and crop management on a semi-arid Inceptisol. *Agric. Ecosyst. Environ.* 118, 130–142. <https://doi.org/10.1016/j.agee.2006.05.008>
- Matsunaga, T., Iwasaki, A., Tsuchida, S., Tanii, J., Kashimura, O., Nakamura, R., Yamamoto, H., Tachikawa, T., Rokugawa, S., 2013. Current status of Hyperspectral Imager Suite (HISUI), in: *International Geoscience and Remote Sensing Symposium (IGARSS)*. pp. 3510–3513. <https://doi.org/10.1109/IGARSS.2013.6723586>
- Mcbratney, A.B., Minasny, B., 2016. Why you don ' t need to use RPD By Budiman Minasny & Alex . McBratney University of Sydney.
- Metzger, M.J., Rounsevell, M.D.A., Acosta-Michlik, L., Leemans, R., Schröter, D., 2006. The vulnerability of ecosystem services to land use change. *Agric. Ecosyst. Environ.* <https://doi.org/10.1016/j.agee.2005.11.025>
- Meyer, D., Dimitriadou, E., Hornik, K., Weingessel, A., Leisch, F., 2019. e1071: Misc Functions of the Department of Statistics, Probability Theory Group (Formerly: E1071), TU Wien.
- Michel, S., Gamet, P., Lefevre-Fonollosa, M.J., 2011. HYPXIM A hyperspectral satellite defined for science, security and defence users, in: *Workshop on Hyperspectral Image and Signal Processing, Evolution in Remote Sensing*. <https://doi.org/10.1109/WHISPERS.2011.6080864>
- Miles, J., 2005. R-Squared, Adjusted R-Squared. *Encycl. Stat. Behav. Sci.* <https://doi.org/10.1002/0470013192.BSA526>
- Moebius-Clune, B.N., 2017. *Comprehensive Assessment of Soil Health*.
- Moebius-Clune, B.N., Moebius-Clune, D., Gugino, B., Idowu, O., Schindelbeck, R., Ristow, A., van Es, H., Thies, J., Shayler, H., McBride, M., Wolfe, D., Abawi, G., 2016. *Comprehensive Assessment of Soil Health - The Cornell Framework Manual*. <https://doi.org/10.1080/00461520.2015.1125787>
- Moreira, L.C.J., Teixeira, A.D.S., Galvão, L.S., 2015. Potential of multispectral and hyperspectral data to detect saline-exposed soils in Brazil. *GIScience Remote Sens.* 52, 416–436. <https://doi.org/10.1080/15481603.2015.1040227>
- Morón, A., Cozzolino, D., 2007. Measurement of Phosphorus in Soils by Near Infrared Reflectance Spectroscopy: Effect of Reference Method on Calibration. *38*, 1965–1974. <https://doi.org/10.1080/00103620701548498>
- Mourad, M., Bertrand-Krajewski, J.L., Chebbo, G., 2005. Calibration and validation of multiple regression models for stormwater quality prediction: Data partitioning, effect of dataset size and characteristics, *Water Science and Technology*. <https://doi.org/10.2166/wst.2005.0060>
- Norman, R.J., Stucki, J.W., 1981. The Determination of Nitrate and Nitrite in Soil Extracts by Ultraviolet Spectrophotometry 1. *Soil Sci. Soc. Am. J.* 45, 347–353. <https://doi.org/10.2136/sssaj1981.03615995004500020024x>
- Ohana-levi, N., Paz-kagan, T., Panov, N., Peeters, A., Tsoar, A., Karnieli, A., Paz-kagan, T., Panov, N., Peeters, A., Tsoar, A., 2018. Time series analysis of vegetation-cover response to environmental factors and residential development in a dryland region. *GIScience Remote Sens.* 00, 1–26. <https://doi.org/10.1080/15481603.2018.1519093>
- Olsvig-Whittaker, L., Walczak, M., Jobse, D., Boeken, B., 2012. Patterns in Habitat Type, Species Richness and Community Composition at Avdat Lter, Israel. *J. Landsc. Ecol.* 5, 5–23. <https://doi.org/10.2478/v10285-012-0056-6>
- Ong, C., Carrère, · V, Chabrilat, · S, Clark, · R, Hoefen, · T, Kokaly, · R, Marion, · R, Souza Filho, · C R, Swayze, · G, Thompson, · D R, 2019. Imaging Spectroscopy for the Detection, Assessment and Monitoring of Natural and Anthropogenic Hazards 40, 431–470. <https://doi.org/10.1007/s10712-019-09523-1>
- Orgiazzi, A., Ballabio, C., Panagos, P., Jones, A., Fernández-Ugalde, O., 2018. LUCAS Soil, the largest expandable soil dataset for Europe: a review. *Eur. J. Soil Sci.* <https://doi.org/10.1111/ejss.12499>
- Padarian, J., Minasny, B., McBratney, A.B., 2019. Using deep learning to predict soil properties from regional spectral data. *Geoderma Reg.* 16, e00198.

<https://doi.org/10.1016/j.geodrs.2018.e00198>

- Pansu, M., Gautheyrou, J., 2006. Organic Forms of Nitrogen, Mineralizable Nitrogen (and Carbon), in: *Handbook of Soil Analysis*. Springer Berlin Heidelberg, pp. 497–547. https://doi.org/10.1007/978-3-540-31211-6_14
- Paz-Kagan, T., DeMalach, N., Zaady, E., Shachak, M., 2019. Resource redistribution effects on annual plant communities in a runoff harvesting system in dryland. *J. Arid Environ.* 171, 103984. <https://doi.org/10.1016/J.JARIDENV.2019.05.012>
- Paz-kagan, T., Ohana-levi, N., Herrmann, I., Zaady, E., Henkin, Z., Karnieli, A., 2016. Catena Grazing intensity effects on soil quality : A spatial analysis of a Mediterranean grassland. *Catena* 146, 100–110. <https://doi.org/10.1016/j.catena.2016.04.020>
- Paz-Kagan, T., Ohana-Levi, N., Shachak, M., Zaady, E., Karnieli, A., 2017. Ecosystem effects of integrating human-made runoff-harvesting systems into natural dryland watersheds. *J. Arid Environ.* 147, 133–143. <https://doi.org/10.1016/j.jaridenv.2017.07.015>
- Paz-Kagan, Tarin, Shachak, M., Zaady, E., Karnieli, A., 2014. A spectral soil quality index (SSQI) for characterizing soil function in areas of changed land use. *Geoderma* 230–231, 171–184. <https://doi.org/10.1016/j.geoderma.2014.04.003>
- Paz-Kagan, T., Shachak, M., Zaady, E., Karnieli, A., 2014. A spectral soil quality index (SSQI) for characterizing soil function in areas of changed land use. *Geoderma* 230–231. <https://doi.org/10.1016/j.geoderma.2014.04.003>
- Paz-Kagan, T., Zaady, E., Salbach, C., Schmidt, A., Lausch, A., Zacharias, S., Notesco, G., Ben-Dor, E., Karnieli, A., 2015. Mapping the spectral soil quality index (SSQI) using airborne imaging spectroscopy. *Remote Sens.* 7, 15748–15781. <https://doi.org/10.3390/rs71115748>
- Pelta, R., Carmon, N., Ben-Dor, E., 2019. A machine learning approach to detect crude oil contamination in a real scenario using hyperspectral remote sensing. *Int. J. Appl. Earth Obs. Geoinf.* 82, 101901. <https://doi.org/10.1016/j.jag.2019.101901>
- Rahimi, H., Pazira, E., Tajik, F., 2000. Effect of soil organic matter, electrical conductivity and sodium adsorption ratio on tensile strength of aggregates. *Soil Tillage Res.* 54, 145–153. [https://doi.org/10.1016/S0167-1987\(00\)00086-6](https://doi.org/10.1016/S0167-1987(00)00086-6)
- Rinot, O., Levy, G.J., Steinberger, Y., Svoray, T., Eshel, G., 2019. Soil health assessment: A critical review of current methodologies and a proposed new approach. *Sci. Total Environ.* 648, 1484–1491. <https://doi.org/10.1016/J.SCITOTENV.2018.08.259>
- Roades, J.D., 1982. Soluble salts, in: *Methods of Soil Analysis, Part 2, Chemical and Microbiological Properties*, 2nd Ed. ASA-SSSA, Agronomy monograph 9, pp. 137–179.
- Robbins, C.W., 1984. Sodium adsorption ratio-exchangeable sodium percentage relationships in a high potassium saline-sodic soil. *Irrig. Sci.* 5, 173–179. <https://doi.org/10.1007/BF00264606>
- Romsonthi, C., Tawornpruek, S., Watana, S., 2018. In situ near-infrared spectroscopy for soil organic matter prediction in paddy soil, pasak watershed, thailand. *Plant, Soil Environ.* 64, 70–75. <https://doi.org/10.17221/716/2017-PSE>
- Rosero-Vlasova , O.A., Pérez-Cabello, F., Montorio Llovería, R., Vlassova, L., 2016. Assessment of laboratory VIS-NIR-SWIR setups with different spectroscopy accessories for characterisation of soils from wildfire burns. *Biosyst. Eng.* 152, 51–67. <https://doi.org/10.1016/j.biosystemseng.2016.06.011>
- Rossel, R.A.V., Behrens, T., 2010. Using data mining to model and interpret soil diffuse reflectance spectra. *Geoderma* 158, 46–54. <https://doi.org/10.1016/j.geoderma.2009.12.025>
- Saygin, S.D., 2018. Strategies to Enhance Sustainability of Land Resources in Arid Regions, in: *Arid Environments and Sustainability*. InTech. <https://doi.org/10.5772/intechopen.72492>
- Schindelbeck, R.R., van Es, H.M., Abawi, G.S., Wolfe, D.W., Whitlow, T.L., Gugino, B.K., Idowu, O.J., Moebius-Clune, B.N., 2008. Comprehensive assessment of soil quality for landscape and urban management. *Landsc. Urban Plan.* 88, 73–80. <https://doi.org/http://dx.doi.org/10.1016/j.landurbplan.2008.08.006>
- Schläpfer, D., Richter, R., Feingersh, T., 2015. Operational BRDF effects correction for wide-field-of-view optical scanners (BREFCOR). *IEEE Trans. Geosci. Remote Sens-ing* 53, 1855–1864.

<https://doi.org/10.1109/tgrs.2014.2349946>

- Schmid, T., Koch, M., Gumuzzio, J., Medel, I., 2005. FIELD AND IMAGING SPECTROSCOPY TO DETERMINE SOIL DEGRADATION STAGES IN SEMI-ARID TERRESTRIAL ECOSYSTEMS.
- Schmid, Thomas, Rodríguez-Rastrero, Manuel, Escribano, P., Palacios-Orueta, A., Ben-Dor, E., Plaza, A., Milewski, R., Huesca, M., Bracken, A., Cicuéndez, V., Pelayo, Marta, Chabrillat, S., Schmid, T., Rodríguez-Rastrero, M., Pelayo, M., 2016. Characterization of Soil Erosion Indicators Using Hyperspectral Data From a Mediterranean Rainfed Cultivated Region. *IEEE J. Sel. Top. Appl. EARTH Obs. Remote Sens.* 9, 845. <https://doi.org/10.1109/JSTARS.2015.2462125>
- Scrimgeour, C., 2008. *Soil Sampling and Methods of Analysis (Second Edition)*. Edited by M. R. Carter and E. G. Gregorich. Boca Raton, FL, USA: CRC Press (2008), pp. 1224, £85.00. ISBN-13: 978-0-8593-3586-0. *Exp. Agric.* 44, 437–437. <https://doi.org/10.1017/s0014479708006546>
- Shapiro, M.B., 2006. Soils of Israel. *Eurasian Soil Sci.* 39, 1170–1175. <https://doi.org/10.1134/S1064229306110032>
- Shi, P., Castaldi, F., van Wesemael, B., Van Oost, K., 2020. Large-Scale, High-Resolution Mapping of Soil Aggregate Stability in Croplands Using APEX Hyperspectral Imagery. *Remote Sens.* 12, 666. <https://doi.org/10.3390/rs12040666>
- Shi, Q., Niu, G., Lin, Q., Xu, T., Li, F., Duan, Y., 2015. Quantitative analysis of sedimentary rocks using laser-induced breakdown spectroscopy: Comparison of support vector regression and partial least squares regression chemometric methods. *J. Anal. At. Spectrom.* 30, 2384–2393. <https://doi.org/10.1039/c5ja00255a>
- Shi, Z., Wang, Q.L., Peng, J., Ji, W.J., Liu, H.J., Li, X., Viscarra Rossel, R.A., 2014. Development of a national VNIR soil-spectral library for soil classification and prediction of organic matter concentrations. *Sci. China Earth Sci.* 57, 1671–1680. <https://doi.org/10.1007/s11430-013-4808-x>
- Singer, A., 2007. *The soils of Israel, The Soils of Israel*. Springer Berlin Heidelberg. <https://doi.org/10.1007/978-3-540-71734-8>
- Singh, K.P., Malik, A., Mohan, D., Sinha, S., Singh, V.K., 2005. Chemometric data analysis of pollutants in wastewater—a case study. *Anal. Chim. Acta* 532, 15–25. <https://doi.org/10.1016/J.ACA.2004.10.043>
- Singh, S., Kasana, S.S., 2019. Estimation of soil properties from the EU spectral library using long short-term memory networks. *Geoderma Reg.* 18, e00233. <https://doi.org/10.1016/j.geodrs.2019.e00233>
- Srivastava, N., Hinton, G., Krizhevsky, A., Sutskever, I., Salakhutdinov, R., 2014. Dropout: A simple way to prevent neural networks from overfitting. *J. Mach. Learn. Res.* 15, 1929–1958.
- Stafford, A.D., Kusumo, B.H., Jeyakumar, P., Hedley, M.J., Anderson, C.W.N., 2018. Cadmium in soils under pasture predicted by soil spectral reflectance on two dairy farms in New Zealand. *Geoderma Reg.* 13, 26–34. <https://doi.org/10.1016/j.geodrs.2018.03.001>
- Stevens, A., Van Wesemael, B., Goire Vandenschrick, G., Touré, S., Tychon, B., n.d. Detection of Carbon Stock Change in Agricultural Soils Using Spectroscopic Techniques. <https://doi.org/10.2136/sssaj2005.0025>
- Stoner, E.R., Baumgardner, M.F., 1981. Characteristic Variations in Reflectance of Surface Soils. *Soil Sci. Soc. Am. J.* 45, 1161–1165. <https://doi.org/10.2136/SSSAJ1981.03615995004500060031X>
- Svoray, T., Hassid, I., Atkinson, P.M., Moebius-Clune, B.N., Es, H.M. van, 2015. Mapping Soil Health over Large Agriculturally Important Areas. *Soil Sci. Soc. Am. J.* 79, 1420–1434. <https://doi.org/10.2136/SSSAJ2014.09.0371>
- Taylor, G.R., 2004. Field and image spectrometry for soil mapping, in: 12th Australian Remote Sensing Conference, Fremantle, WA, Australia.
- Thissen, U., Pepers, M., Üstün, B., Melssen, W.J., Buydens, L.M.C., 2004. Comparing support vector machines to PLS for spectral regression applications. *Chemom. Intell. Lab. Syst.* 73, 169–179. <https://doi.org/10.1016/j.chemolab.2004.01.002>

- Tsakiridis, N.L., Chadoulos, C.G., Theocharis, J.B., Ben-Dor, E., C. Zalidis, G., 2020. A three-level Multiple-Kernel Learning approach for soil spectral analysis. *Neurocomputing* 389, 27–41. <https://doi.org/10.1016/j.neucom.2020.01.008>
- Tscharntke, T., Klein, A.M., Kruess, A., Steffan-Dewenter, I., Thies, C., Teja Tscharntke,* Alexandra M. Klein, Andreas Kruess, I.S.-D. and C.T., 2005. REVIEWS AND Landscape perspectives on agricultural intensification and biodiversity – ecosystem service management. *Ecol. Lett.* <https://doi.org/10.1111/j.1461-0248.2005.00782.x>
- Tucker, C.J., 1979. Red and Photographic Infrared Linear Combinations for Monitoring Vegetation, REMOTE SENSING OF ENVIRONMENT.
- Turner, M.D., 1998. Long-term effects of daily grazing orbits on nutrient availability in Sahelian West Africa: I. Gradients in the chemical composition of rangeland soils and vegetation. *J. Biogeogr.* 25, 669–682. <https://doi.org/10.1046/j.1365-2699.1998.2540669.x>
- Tziolas, N., Tsakiridis, N., Ogen, Y., Kalopesa, E., Ben-Dor, E., Theocharis, J., Zalidis, G., 2020. An integrated methodology using open soil spectral libraries and Earth Observation data for soil organic carbon estimations in support of soil-related SDGs. *Remote Sens. Environ.* 244, 111793. <https://doi.org/10.1016/j.rse.2020.111793>
- UN-WPP, 2020. World Population Prospects 2019 - Volume II: Demographic Profiles, World Population Prospects 2019 - Volume II: Demographic Profiles. <https://doi.org/10.18356/7707d011-en>
- Ushey, K., Allaire, J.J., Tang, Y., 2020. reticulate: Interface to “Python.”
- Vågen, T.G., Shepherd, K.D., Walsh, M.G., 2006. Sensing landscape level change in soil fertility following deforestation and conversion in the highlands of Madagascar using Vis-NIR spectroscopy. *Geoderma* 133, 281–294. <https://doi.org/10.1016/j.geoderma.2005.07.014>
- Vanschoenwinkel, B., Manderick, B., 2005. Appropriate kernel functions for support vector machine learning with sequences of symbolic data, in: *Lecture Notes in Computer Science (Including Subseries Lecture Notes in Artificial Intelligence and Lecture Notes in Bioinformatics)*. Springer, Berlin, Heidelberg, pp. 256–280. https://doi.org/10.1007/11559887_16
- Veum, K.S., Sudduth, K.A., Kremer, R.J., Kitchen, N.R., 2017. Sensor data fusion for soil health assessment. *Geoderma* 305, 53–61. <https://doi.org/10.1016/j.geoderma.2017.05.031>
- Veum, K.S., Sudduth, K.A., Kremer, R.J., Kitchen, N.R., 2015. Estimating a Soil Quality Index with VNIR Reflectance Spectroscopy. *Soil Sci. Soc. Am. J.* 79, 637–649. <https://doi.org/10.2136/sssaj2014.09.0390>
- Viscarra Rossel, R.A., Behrens, T., Ben-Dor, E., Brown, D.J., Demattê, J.A.M., Shepherd, K.D., Shi, Z., Stenberg, B., Stevens, A., Adamchuk, V., Aichi, H., Barthès, B.G., Bartholomeus, H.M., Bayer, A.D., Bernoux, M., Böttcher, K., Brodský, L., Du, C.W., Chappell, A., Fouad, Y., Genot, V., Gomez, C., Grunwald, S., Gubler, A., Guerrero, C., Hedley, C.B., Knadel, M., Morrás, H.J.M., Nocita, M., Ramirez-Lopez, L., Roudier, P., Campos, E.M.R., Sanborn, P., Sellitto, V.M., Sudduth, K.A., Rawlins, B.G., Walter, C., Winowiecki, L.A., Hong, S.Y., Ji, W., 2016. A global spectral library to characterize the world’s soil. *Earth-Science Rev.* <https://doi.org/10.1016/j.earscirev.2016.01.012>
- Viscarra Rossel, R.A., Walvoort, D.J.J., McBratney, A.B., Janik, L.J., Skjemstad, J.O., 2006. Visible, near infrared, mid infrared or combined diffuse reflectance spectroscopy for simultaneous assessment of various soil properties. *Geoderma* 131, 59–75. <https://doi.org/10.1016/j.geoderma.2005.03.007>
- von Lützw, M., Kögel-Knabner, I., Ekschmitt, K., Flessa, H., Guggenberger, G., Matzner, E., Marschner, B., 2007. SOM fractionation methods: Relevance to functional pools and to stabilization mechanisms. *Soil Biol. Biochem.* <https://doi.org/10.1016/j.soilbio.2007.03.007>
- Wacker, A., Landgrebe, D., 1972. Minimum Distance Classification in Remote Sensing. LARS Tech. Reports.
- Wang, C.Y., Wang, N., Wang, S., 2000. Regression Analysis When Covariates Are Regression Parameters of a Random Effects Model for Observed Longitudinal Measurements. *Biometrics* 56, 487–495. <https://doi.org/10.1111/j.0006-341X.2000.00487.x>

- Wang, J., Peng, J., Li, H., Yin, C., Liu, W., Wang, T., Zhang, H., 2021. Soil salinity mapping using machine learning algorithms with the sentinel-2 MSI in arid areas, China. *Remote Sens.* 13, 1–14. <https://doi.org/10.3390/rs13020305>
- Weil, R., Brady, N., 2017. *The Nature and Properties of Soils*. 15th edition.
- Wetschoreck, F., Krabel, T., Krishnamurthy, S., 2020. 8080Labs/Ppscore: Zenodo Release. <https://doi.org/10.5281/ZENODO.4091345>
- Wienhold, B.J., Karlen, D.L., Andrews, S.S., Stott, D.E., 2009. Protocol for indicator scoring in the soil management assessment framework (SMAF). *Renew. Agric. Food Syst.* 24, 260–266. <https://doi.org/10.1017/S1742170509990093>
- Wise, B.M., Gallagher, N.B., Bro, R., Shaver, J.M., Windig, W., Koch, R.S., 2006. PLS_Toolbox Version 4.0 for use with MATLAB™, Eigenvector Research.
- Xuemei, L., Jianshe, L., 2013. Measurement of soil properties using visible and short wave-near infrared spectroscopy and multivariate calibration. *Measurement* 46, 3808–3814. <https://doi.org/10.1016/J.MEASUREMENT.2013.07.007>
- Yair, A., Danin, A., 1980. Spatial variations in vegetation as related to the soil moisture regime over an arid limestone hillside, northern Negev, Israel. <https://doi.org/10.1007/BF00541779>
- Yang, X.-D., Wang, J., Xu, M.-S., Ali, A., Xu, Y., Lamb, D., Duan, L.-C., Yan, K.-H., Yang, S.-T., 2019. Effects of the ephemeral stream on plant species diversity and distribution in an alluvial fan of arid desert region: An application of a low altitude UAV. *PLoS One* 14. <https://doi.org/10.1371/JOURNAL.PONE.0212057>
- Yizhaq, H., Shachak, M., Meron, E., 2020. A model study of terraced riverbeds as novel ecosystems. *Sci. Reports* 2020 101 10, 1–10. <https://doi.org/10.1038/s41598-020-60706-y>
- Yuan, Q., Shen, H., Li, T., Li, Z., Li, S., Jiang, Y., Xu, H., Tan, W., Yang, Q., Wang, J., Gao, J., Zhang, L., 2020. Deep learning in environmental remote sensing: Achievements and challenges. *Remote Sens. Environ.* 241, 111716. <https://doi.org/10.1016/j.rse.2020.111716>
- Zavarella, L., 2020. Using The Predictive Power Score in R. *Medium*.
- Zhang, C., Mishra, D.R., Pennings, S.C., 2019. Mapping salt marsh soil properties using imaging spectroscopy. *ISPRS J. Photogramm. Remote Sens.* 148, 221–234. <https://doi.org/10.1016/j.isprsjprs.2019.01.006>
- Ziv, B., Saaroni, H., Pargament, R., Harpaz, T., Alpert, P., 2014. Trends in rainfall regime over Israel, 1975–2010, and their relationship to large-scale variability. *Reg. Environ. Chang.* 14, 1751–1764. <https://doi.org/10.1007/s10113-013-0414-x>
- Žížala, D., Zádorová, T., Kapička, J., 2017. Assessment of Soil Degradation by Erosion Based on Analysis of Soil Properties Using Aerial Hyperspectral Images and Ancillary Data, Czech Republic. *Remote Sens.* 9, 28. <https://doi.org/10.3390/rs9010028>

שימוש בחישה מרחוק היפרספקטרלית לזיהוי ומיפוי איכות קרקע בשימושי קרקע
שונים באקלים מדברי

מחקר לשם מילוי חלקי של הדרישות לקבלת תואר "דוקטור לפילוסופיה"

מאת

לוי נתן

הוגש לסינאט אוניברסיטת בן גוריון בנגב

י"ח בכסלו תשפ"ג

6 בדצמבר 2022

באר שבע



שימוש בחישה מרחוק היפרספקטרלית לזיהוי ומיפוי איכות קרקע בשימושי קרקע
שונים באקלים מדברי

מחקר לשם מילוי חלקי של הדרישות לקבלת תואר "דוקטור לפילוסופיה"

מאת

לוי נתן

הוגש לסינאט אוניברסיטת בן גוריון בנגב

אישור המנחים:

פרופ' ארנון קרניאלי
דר טרין פז כגן

פרופ' ירון זיו

אישור דיקן בית הספר ללימודי מחקר מתקדמים ע"ש קרייטמן

י"ח בכסלו תשפ"ג

6 בדצמבר 2022

באר שבע

העבודה נעשתה בהדרכת

ד"ר טרין פז כגן, פרופ' ארנון קרניאלי, פרופ' ירון זיו
במחלקה המכונים לחקר המדבר, אוניברסיטת בן גוריון בנגב,

הצהרת תלמיד המחקר עם הגשת עבודת הדוקטור לשיפוט

אני החתום מטה מצהיר/ה בזאת: (אנא סמן):

____ חיברתי את חיבורי בעצמי, להוציא עזרת ההדרכה שקיבלתי מאת מנחה/ים.

____ החומר המדעי הנכלל בעבודה זו הינו פרי מחקרי מתקופת היותי תלמיד/ת מחקר.

____ בעבודה נכלל חומר מחקרי שהוא פרי שיתוף עם אחרים, למעט עזרה טכנית שאינה כוללת ניתוח תוצאות, הנהוגה בעבודה ניסיונית. לפי כך מצורפת בזאת הצהרה על תרומתי ותרומת שותפי למחקר, שאושרה על ידם ומוגשת בהסכמתם.

____ תזה במתכונת אסופת מאמרים, כוללת מאמרים בהם אני מחבר ראשון משותף (equal contribution). במקרה זה, נא לצרף הצהרה של המחבר השותף על חלקו בפרסום, ואישורו לכך, שמאמר זה לא יוכל להיכלל בתזת מאמרים נוספת, שהוא יגיש.

תאריך _____ שם התלמיד/ה _____ חתימה _____

תקציר: גידול האוכלוסייה העולמי הביא לשינויים משמעותיים בשימושי קרקע (LU) וגרם להפיכת מערכות אקולוגיות טבעיות רבות למערכות הנשלטות על ידי האדם. התמרה של מערכות אקולוגיות טבעיות למערכות מנוהלות אדם, הביאה לעיתים להידלדלות בתנאי הסביבה המשפיעים על מדדי איכות קרקע רבים. דינמיקה כזו של שינוי בשימושי קרקע דורשת ניצול רב יותר של משאבים, מה שגורם בדרך כלל לתנאים סביבתיים מדולדלים המשפיעים על מרכיבי הקרקע השונים ועל בריאות הקרקע הכוללת, והשירותים שהיא מספקת לאדם. תופעת הידלדלות קרקע מחריפה אף יותר בסביבות צחיחות בהם המשאבים מוגבלים כמו שטחים מדבר. לפיכך, יש צורך בפיתוח גישות מתאימות להערכת איכות הקרקע ותפקוד הקרקע באזורים יובשניים, מאחר והקרקעות באזורים אלה בדרך כלל לא מפותחות ובעלות תכולת חומר אורגני נמוך יחסית, זמינות המים בהם נמוכה וכן הפעילות המיקרוביולית בקרקע מוגבלת. השימוש באינדקסים להערכת איכות הקרקע (SQI) הוכחה היטב כיעילה בסביבות צחיחות ונמצא כי שימושי קרקע שונים משפיעים על מדדי טיב הקרקע. הערכת טיב קרקע מתייחסת לשילוב של המדדים הכימיים ביולוגיים ופיזיקאליים של הקרקע לכדי מדד כולל המעיד על מידת תיפקודה. במחקר זה נעשה שימוש בגישות מבוססות חישה מרחוק היפר-ספקטראלית, ממדידות נקודתיות ועד לקנה מידה אזורי ע"י שימוש בחיישנים מוטסים היפר-ספקטראליים. שימוש בספקטרוסקופיה מאפשר למדוד הבדלים במדדי איכות קרקע מקנה מידה נקודתי ועד אזורי ע"י זיהוי החזר בתחום הנראה (VIS), אינפרה אדום קרוב (NIR) והרחוק (SWIR), הכוללת טווח ספקטראלי בין 400-2500 ננומטר. שימוש בחישה מרחוק היפר-ספקטראלית מסייע בהערכת תכונות קרקע פיזיות, ביולוגיות וכימיות על סמך הבדלים ספקטראליים בין קרקעות טבעיות וקרקעות שעברו שינוי עקב פעילות אנושית (למשל, חקלאות, מרעה וכריה). בעבודת הדוקטורט הזאת נבחנה הישימות של מודל הערכת איכות הקרקע בסביבות יבשות שעברו השפעות אנתרופוגניות שונות ע"י כלים שונים של חישה מרחוק היפר-ספקטראלית. התזה מחולקת לשלושה פרקים מרכזיים.

הפרק הראשון התמקד בפיתוח מדד להערכת איכות קרקע המשלב כ-14 מאפייני קרקע לשלושה שימושי קרקע שונים (חקלאות מודרנית וקדומה, מרעה, ושטח טבעי לייחוס) ע"י ספקטרוסקופיה בקנה מידה אזורי באזור עבדת במרכז הנגב, ישראל. מטרת המחקר הייתה ליישם, למדוד ולהעריך את תכונות הקרקע בהתבסס אך ורק על ההבדלים הספקטראליים בין שימושי הקרקע השונים המנוהלות על ידי האדם בסביבת צחיחה של מרכז הנגב. מטרה זו הושגה באמצעות פיתוח והטמעה של טכניקות כימוטריות שנוצרו מספקטרוסקופיה שנמדוד במעבדה. פותח אינדקס להערכת איכות הקרקע (SQI), המבוססים על 14 תכונות קרקע פיזיקליות, ביולוגיות וכימיות, ונבחנו ההבדלים במדדי הטיב בשימושי הקרקע השונים. נאספו מדגם קרקעות ובוצעו מדידות ספקטראליות במעבדה של דגימות קרקע שהושווה למידות מעבדה המקובלות. ממדידות אילו פותח אינדקס המשלב את כלל המדדים להערכת הטיב הכולל של הקרקע. נמצאו הבדלים משמעותיים בערכי SQI בין יחידות הגיאוגרפיות השונות ושימושי הקרקע. השיטות הסטטיסטיות והמתטיות להערכת ההבדלים הספקטראליים של מאפייני הקרקע כללו אנליזה של (PCA), ומודל רגרסיה רב משתנים (PLS-R) וניתוח מיון של מאפייני הקרקע בשימושי הקרקע השונים (PLS-DA). מתאמים בין ערכי המדידות הספקטראליות חזויים ותכונות קרקע שנמדדו ו-SQI חושבו באמצעות PLS-R והוערכו לפי מקדם (R^2), שגיאת ה-Cross-Validation (RMSEC ו-RMSECV), והיחס של ביצועים לסטייה (RPD). ה-PLS-R יצר ערכי חיזוי "מצוינים" ו"טובים" עבור חלק ממאפייני הקרקע, כולל מדדי קרקע EC, Cl, Na, Ca + Mg, SAR, NO₃, P ו-SOM. התוצאות של מודל PLS-R עבור SQI גם הן הראו מתאמים גבוהים וטעות קטנה $R^2 = 0.90$, $RPD = 2.46$, $RMSEC = 0.034$ ו-RMSECV = 0.057. סיווג על בסיס מודל ה-PLS-DA של החתימות הספקטראליות של הקרקעות, הראה ערכי דיוק גבוהים במיון הקרקעות על בסיס שימושי הקרקע. לעומת זאת, מיון הקרקעות באתרי הדיגום השונים הראו יכולת הפרדה

נמוכה יחסית ($Acc = 0.82$) וערכי דיוק ($Kc = 0.80$). המסקנה המרכזית מפרק זה היא שניתן להגיע להערכה מדויקת בין תכונות קרקע פיזיות, ביולוגיות וכימיות, על סמך ההבדלים הספקטראליים שלהן. כמין כן נמצא, כי שימושי הקרקע השונים משפיעים על המידע הספקטראלי, וניתן לחזות את האיכות הכוללת של הקרקע ע"י ספקטרוסקופיה ולאפיין תהליכי שונים בקרקע בגישה אינטגרטיבית. התוצאות מוכיחות שניתן להעריך בהצלחה את איכות הקרקע ואת תכונות הקרקע באמצעות ספקטרוסקופיה כדרך עקיפה לשיטות המעבדה המוקבלות, גישה שהיא אינה הרסנית, חסכונית בזמן ובעלות.

פרק השני עסק בהערכת השפעות של שיקום כרייה על איכות הקרקע ככלי להערכת הצלחת השיקום. המחקר שואף להעריך את ההשפעה של שיטות שיקום (כלומר, שיקום קרקע עליונה) על מאפייני איכות הקרקע בהשוואה לשיטות טבעיים סמוכים במכרה פוספט פתוח באזור צחיח בישראל. הכרייה תורמת משמעותית לפיתוח הכלכלי, אך היא טומנת בחובה נזקים סביבתיים נרחבים, כגון הרס קרקע וזיהום מים ואוויר. פעילות הכרייה משפיעה על איכות הקרקע, ולעתים קרובות היא אינה מסוגלת לתמוך בתפקוד ובמבנה של המערכת האקולוגית. מטרת המחקר הנוכחי היא ליישם את גישת הערכת איכות הקרקע (SQI) כמתודולוגיה לכימות מצב שיקום הקרקע במכרה פוספט פתוח בסביבה צחיחה בישראל. בהתאם לכך, המטרה הראשונית שלנו הייתה לקבוע האם שיטת שימור הקרקע העליונה דומה לאזור הטבעי הסמוך מבחינת תכונות הקרקע ואיכות הקרקע הכוללת, למרות תנאי הסביבה והאקלים הקיצוניים של אזור צחיח זה. המטרה השנייה שלנו הייתה להעריך את הצלחת השיקום בהתבסס על גישת להערכת טיב קרקע כפונקציה של זמן על ידי השוואת שלבי השיקום השונים המיושמים באתרים שונים שאזור המכרה. לכן, ההשערה של המחקר היא ששיטת שיקום הקרקע ע"י שמירה על שכבת הקרקע העליונה והשבתה לאחר תהליך הכרייה במכרות פוספט, תשפר את איכות הקרקע והשיקום הכולל, כאשר טווח הזמן מאז השיקום ישפיע גם על התהליכים השיקום עקב התפתחות האיטית יחסית של קרקעות בסביבה כה צחיחה. בהקשר זה, בחנו שיטות שיקום אקולוגית הכוללת השבה של הקרקע העליונה לאחר כרייה בהשוואה למערכת הטבעית הבלתי מופרעת הסמוכה, תוך שימוש במדדי הקרקע שעברו טרנספורמציה ע"י בחינה של כ- 11 תכונות קרקע פיזיות, ביולוגיות וכימיות. פיתחנו מודל סטטיסטי המאפשר לשכלל את איכות הקרקע הכוללת באתרי השיקום השונים. התוצאות שלנו חשפו הבדלים משמעותיים בין אזורי השיקום לבין האזורים הטבעיים הסמוכים, עם ערך איכות קרקע גבוה יותר באתרים ששוקמו מוקדם יותר. במחקר נמצא כי שיטת שיקום ע"י השבת הקרקע העליונה משפיעה בעיקר על המדדים ביולוגיים בקרקע, כגון חומר אורגני בקרקע, חלבוני קרקע ופוליסקרידים הקשורים להתפתחות קרומים ביולוגיה בקרקע מדברית, ובמידה פחותה, הייתה השפעה של מדדי הקרקע הפיזיקליים (בעיקר קצב החדירה, ואחריו AWC). מאפייני השיקום של השבת שכבת הקרקע העליונה מעודדים את התפתחות של קרום ביולוגי, החיוני לייצוב פני הקרקע ומשפיע על קצב חדירת המים וזמינות חומרי הזנה. מאידך, האינדיקטורים הכימיים לא הראו הבדלים משמעותיים בין רוב האתרים לאיכות הקרקע הכוללת ולכן והשפעתם פחותה. לסיכום, ישנה חשיבות בהערכה של מרכבי הקרקע הביולוגיים והפיזיקליים, שלהם השפעה על מידת הצלחת השיקום והשבת הקרקע למצבה הקודם, כדי לכמת ולהעריך שיטות שיקום במערכות אקולוגיות צחיחה.

הפרק השלישי, התמקד בהערכת ההשפעות של פעילויות אנושיות (כלומר, שימושי קרקע כגון מרעה, חקלאות מודרנית ומערכות קציר נגר) על איכות הקרקע באמצעות חישה היפר ספקטראלית מוטסת באזור המחקר של אזור עבדת. בהתבסס על ההשפעה המשמעותית שיש לשימושי קרקע על קרקעות בסביבה צחיחה. המטרה העיקרית של מחקר זה היא להעריך ולמפות את ההשפעות של שימוש קרקע על מרכבי הקרקע השונים ואיכות הקרקע הכוללת אמצעות יישומי חישה מרחוק היפר-ספקטראליים. המטרות כוללות (1) הדגמת היכולת של חישה היפר ספקטראלית למיפוי רציף של מאפייני קרקע השונים ומדד איכות הקרקע הכולל על פני כל אזור המחקר; (2) בחינת השילוב בין מדידות מעבדה כימית קונבנציונלית

לקרקע לבין תרומת הממד הספקטראלי ליכולות הניבוי מבוססות רגרסיה של מידע מהדמאות היפר ספקטראליות; וכן (3) הערכת ההשפעה של שינוי בשימושי הקרקע על דפוסי בריאות הקרקע באזורים צחיחים הכוללים מערכות חקלאות, מרעה וערכת קציר נגר (RHSs) למטרות חקלאות וייעור ביחס לקרקע הטבעית. לשם כך נבחרו 12 מאפייני קרקע פיזיקליים, ביולוגיים וכימיים ששולבו יחד למדד איכות הקרקע (SQI) כשיטה להערכת ההשפעות המשמעותיות של שינויים בשימושי הקרקע באזור צחיח בדרום ישראל. הוטס החיפוש ההיפר ספקטראלי AisaFENIX ששימש לפיתוח מודל חיזוי עבור הערכת טיב הקרקע בקנה מידה אזורי. החתימות הספקטראליות, שהופקו מהתמונה ההיפר-ספקטראלית עצמה, הראו יכולת הפרדה טובה בין ארבעת שימושי הקרקע באמצעות מודל PLS-DA ($OA = 95.31\%$, $Kc = 0.90$). המתאם בוצע באמצעות מודלים רב משתנים המבוססים על למידת מכונה (SVM-R) לבחינת הקשר בין הנתונים הספקטראליים ומדדי הקרקע השונים ומדד איכות הקרקע הכולל. המודלים של SVM-R היו בקורלציה מובהקת עבור מספר מאפייני קרקע, כולל מדד איכות הקרקע הכולל ($R2adjVal = 0.87$), עם חיזוי מוצלח של מיפוי טיב קרקע אזוריות ($R2adjPred = 0.78$). שבעה מאפייני קרקע נוספים נמצאו בקורלציות גבוהות בניהם, כולל מדדי טקסטורת הקרקע (חול, חרסית וסילט) SOM, pH, EC, SAR, שימשו בהצלחה לפיתוח מפות חיזוי. יישום חישה היפר ספקטראלית ושיטות סטטיסטיות אינטגרטיביות להערכות של איכות הקרקע מאפשר לשפר את דיוק הניבוי ולאפיון של בריאות הקרקע והערכת תהליכי הידלדלות בסביבות צחיחות בקנה מידה אזורי. מחקר זה מבסס כלי מדויק לניהול בר קיימא של קרקעות ויכול להוות דוגמה למשימות חלל עתידיות ומציג את הפוטנציאל למחקרים ויישומים של הערכת איכות קרקע בקנה מידה עולמי.